AN INVESTIGATION OF ALTERNATIVE METHODS FOR MEASURING STATIC PRESSURE OF UNITARY AIR CONDITIONERS AND HEAT PUMPS

A Thesis

by

GRANT BENSON WHEELER

Submitted to the Office of Graduate Studies of
Texas A&M University
in partial fulfillment of the requirements for the degree of

MASTER OF SCIENCE

Chair of Committee,	Michael Pate
Committee Members,	Andrew Duggleby
	Edward White
Head of Department,	Andreas Polycarpou

August 2013

Major Subject: Mechanical Engineering

ABSTRACT

This project was created to address an important issue currently faced by test facilities measuring static pressure for air-conditioning and heat pumps. Specifically, ASHRAE Standard 37, the industry standard for test setup, requires an outlet duct of a certain length, based on the unit outlet geometry, and this ducting added to the unit height may result in a test apparatus height that exceeds psychometric test room dimensions. This project attempted to alter the outlet duct in a way that reduces the test apparatus height while maintaining the reliability of the ASHRAE Standard 37 testing setup. The investigation was done in two scenarios, the first, which altered the direction of the flow after the unit with an elbow and measured static pressure downstream of the elbow, and the second which inserted a passive resistive piece in the flow to decrease the required distance between the unit and the static pressure measurement. Three air handling units were used in Scenario 1 and Scenario 2 testing, with the two smallest units additionally being tested in Scenario 1 with an over-sized duct. The scenario tests were required to be within 5% power and 2.5% airflow of a baseline test following ASHRAE Standard 37.

The results for Scenario 1 have shown that ASHRAE Standard 37 can be modified to reduce testing height restrictions by using a square elbow with turning vanes, provided it is oriented in a specific way in relation to the blower. Furthermore, additional Scenario 1 testing on the over-sized outlet duct shows that possibilities exist for using a single over-sized duct to successfully meet ASHRAE Standard 37 testing conditions when testing a variety of units. Finally, the results of Scenario 2 have shown that the height constraints of the outlet duct can be reduced by installing a passive resistive device consisting of a mesh at the outlet; however, this approach applies only to those units with the heat exchanger located downstream of the blower. As a result of specific issues or problems that were encountered during the project that were beyond the scope, eleven case studies were presented and recommended for future work.

ACKNOWLEDGEMENTS

I would like to thank my committee chair, Dr. Michael Pate, and my committee members, Dr. Andrew Duggleby and Dr. Edward White for their guidance and support throughout the course of this research.

To the project monitoring subcommittee from ASHRAE Technical Committee 8.11, I would like to give my gratitude for all their work in creating the project and for advising and reviewing my work throughout the project.

I want send my thanks to all the undergraduate and graduate staff at Riverside who worked so hard to help me finish this project, as well as the permanent staff at Riverside, Kathy, Jim, and Josh, who have continually lent their support and knowledge.

Finally, thanks to my entire family for their encouragement and to my girlfriend for her patience and love.

NOMENCLATURE

A	Area [in^2]
a,b	Cross-sectional Dimension [in]
AHRI	Air-Conditioning, Heating, and Refrigeration Institute
ASHRAE	American Society of Heating, Refrigerating and Air-conditioning Engineers
C	Discharge Coefficient
CFD	Computational Fluid Dynamics
CFR	Code of Federal Regulations
D	Diameter [in]
DAQ	Data Acquisition
ECM	Electronically Commutated Motor
f	Friction Factor
I	Current [A]
K	Local Pressure Loss Coefficient
L	Length [in]
P	Pressure [in. of water]
P	Power [Watts]
PF	Power Factor [radians]
Pws	Saturation Pressure
Q	Airflow [$ft^3\ min^{-1}$, cfm]
R	Relay Switch

Re	Reynolds Number
RFP	Request for Proposal
RSS	Root of the Sum of Squares
s	Sample standard deviation
S	Solenoid
SEER	Seasonal Energy Efficiency Ratio
T	Temperature [Fahrenheit]
v	Specific Volume [ft^3 lbm^{-1}]
V	Velocity [Ft s^{-1}]
V	Voltage [V]
$\bar{V}$	Mean Velocity [Ft s^{-1}]
VAF	Variable Assist Fan
W	Humidity Ratio
Wxs	Saturation Humidity Ratio
$\bar{x}$	Sample Mean

Greek Symbols

β	Orthogonal Porosity
β'	Sinusoidal Porosity
ε	Roughness Factor [in]
φ	Phase Angle [radians]
ρ	Density [lbm ft^{-3}]

μ	Dynamic Viscosity [lbm ft^{-1} s^{-1}]

Subscript

A	ASHRAE 37 Standard Pressure Location
B	Baseline
DB	Dry Bulb
L	Largest Duct
n	Nozzle
r	Rankine
s	Standardized
v	Velocity
WB	Wet Bulb

TABLE OF CONTENTS

Page

ABSTRACT ii

ACKNOWLEDGEMENTS iii

NOMENCLATURE iv

TABLE OF CONTENTS vii

LIST OF FIGURES x

LIST OF TABLES xiv

INTRODUCTION 1

- Overview 1
- Project Objective 1
- Scope of Work 2

EXPERIMENTAL TEST CONSIDERATIONS 4

- Air Handling Unit Specifications 4
- ASHRAE Standard 37 Description 5
- Pressure Theory, Instrumentation and Test Standards 8
- Pressure Drop Across Elbows 12
- Airflow Measurement 16
- Steady Flow through Screens 17
- Velocity Profile Design and Measurement 21
- Propagation of Uncertainties 23

EXPERIMENTAL TEST DESIGN AND SETUP 24

- Unit Specifications 24
- Static Pressure Measurement 24
- Baseline Test Setup Description 25
- Scenario 1 Test Setup Description 27
- Scenario 2 Test Setup Description 30
- Data Acquisition and Instrumentation 36

TEST PROCEDURES AND METHODOLOGIES 42

- Scenario 1 Test Procedure 42

Scenario 2 Test Procedure 43
Standard Airflow and Pressure Calculation 44
Power Calculation 47
Instrumentation Uncertainty 47
Statistical Analysis for Pressure and Airflow Measurements 48

RESULTS 52

Scenario 1 Results 52
Scenario 1 Results Set Pressure 56
Scenario 2 Results 57
Scenario 2 Results Set Pressure 61

ANALYSIS 64

Comparison of Baseline Tests 64
Comparison of Scenario 1 Tests 65
Comparison of Scenario 2 Tests 71

VELOCITY DATA AND ANALYSIS 75

Velocity Profile Data 75
Velocity Profile Observations 75
Scenario 2 Velocity Profile Observations 78
Velocity Profile Analysis 78

CASE STUDIES 80

CS-1: ASHRAE Standard 37 Static Pressure Measurement Position Validation 80
CS-2: Elbow Static Pressure Location Validation 86
CS-3: Calculation of Loss Coefficients for the Baseline Tests 90
CS-4: Draw-Through versus Blow-Through Air Handler Units 95
CS-5: Effects of Using an Inlet Damper-Box and Skirt Configuration 98
CS-6: Test Parameter: Airflow versus Static Pressure 100
CS-7: Theoretical versus Experimental Pressure Profile Curves Downstream of the Unit 102
CS-8: Pressure Measurement Accuracy and Pressure Ring Approaches 108
CS-9: Minimum Distance Limitation for Mounting an Elbow Downstream of the Static Pressure Measurement Point 111
CS-10: Positive Static Pressure Error for Scenario 1 Elbow Tests 114
CS-11: Baseline Test Results for Different Downstream Elbow Types and Orientations 116

CONCLUSIONS AND RECOMMENDATIONS 118

Conclusion 118
Recommendations for Future Work 121

REFERENCES 129

APPENDIX A 133

A.1 Damper-Box Dimensions 133
A.2 Skirt Dimensions 134

APPENDIX B 135

B.1 Uncertainty Propagation 135
B.2 Sample Calculations for Standardized Airflow and Static Pressure 136
B.3 Calculating ASHRAE Straight Duct Height 140

APPENDIX C 142

C.1 Passive Resistive Pieces for the 2 Ton Unit 142
C.2 Passive Resistive Pieces for the 3 Ton Unit 145
C.3 Passive Resistive Pieces for the 5 Ton Unit 147

APPENDIX D 151

D.1 Scenario 2 Raw Data 151
D.2 Scenario 1 Velocity Profile Figures 156
D.3 Scenario 2 Velocity Profile Figures 163
D.4 Set Pressure Velocity Profiles 166

LIST OF FIGURES

Page

Figure 1 ASHRAE Standard 37 test setup for measuring static pressure (ASHRAE 2005). 6

Figure 2 Air handling with a skirt and damper-box configuration. 7

Figure 3 Pressure drop estimation within the test apparatus following ASHRAE Standard 37. 8

Figure 4 Dimensions for pressure taps. 10

Figure 5 (Left) Conventional and (Right) "Triple T" pressure ring configurations (ASHRAE 2005). 11

Figure 6 Blast area and outlet area of air handling unit. 13

Figure 7 ASHRAE Standard 37 specifications for a nozzle chamber. 17

Figure 8 Dimensions for interwoven mesh. 18

Figure 9 Pitot tube array dimensions. 22

Figure 10 Scenario 1 baseline test setup. 25

Figure 11 Nozzle chamber test setup. 27

Figure 12 Scenario 1 elbow test setup. 28

Figure 13 (Left) Square elbow, (center) square elbow with turning vanes, and (right) curved elbow. 29

Figure 14 Elbow orientations 1-4. 30

Figure 15 Scenario 2 test setup. 32

Figure 16 Dimensions [in] for Scenario 2 duct after the 2 ton unit. 33

Figure 17 Scenario 2 dimensions [in] for the 3 ton unit. 35

Figure 18 Scenario 2 dimensions [in] for the 5 ton unit. 35

Figure 19 Electronic diagram of DAQ. 36

Figure 20 Ladder diagram for solenoid activation. 37

Figure 21 Solenoid valve configuration. 38

Figure 22 Instrument connections for the velocity profile. 39

Figure 23 Electronic wiring of electronic instruments. 40

Figure 24 Pressure versus airflow distribution. 49

Figure 25 Gaussian distributions for airflow and static pressure. 50

Figure 26 Gaussian distribution for a sample size of 300. 51

Figure 27 Gaussian distribution for a sample size of 30. 51

Figure 28 Pressure curves for the 2 ton unit passive resistive pieces. 59

Figure 29 Pressure drop of 4 passive resistive pieces and the baseline test for the 3 ton unit. 60

Figure 30 Pressure drop of 5 passive resistive pieces and the baseline test for the 5 ton unit. 61

Figure 31 2 ton unit metal mesh performance for set pressure and airflow. 62

Figure 32 Comparison of metal and plastic mesh performances for the 3 ton unit. 63

Figure 33 Percent error of the pressure drop along the outlet duct. 72

Figure 34 Percent error of the 3 ton unit for Scenario 2. 73

Figure 35 Percent error of the 5 ton unit compared to the AHRI rating point. 74

Figure 36 Example of horseshoe shaped velocity profile for the 2 ton unit. 78

Figure 37 Blower outlet dimensions at the unit outlet. 81

Figure 38 Velocity profile directly after the unit. 82

Figure 39 Pressure along the outlet duct after the unit. 83

Figure 40 ASHRAE Standard 37 static pressure measurement verification. 84

Figure 41 Measured pressure of the 3 ton unit with a long straight outlet. 85

Figure 42 Pressure change after the elbow for the 2 ton unit. 88

Figure 43 Pressure change after the elbow for the 3 ton unit. 89

Figure 44 Pressure change after the elbow for the 5 ton unit. 90

Figure 45 Test setup of the 5 ton unit with a long inlet duct. 99

Figure 46 Baseline versus theoretical pressure drop along the outlet duct for the 2 ton unit. 104

Figure 47 Baseline and theoretical pressure drop along the outlet duct for the 3 ton unit. 104

Figure 48 Baseline and theoretical pressure drop along the outlet duct for the 5 ton unit. 106

Figure 49 Normalized pressure versus normalized length of the 2, 3, and 5 ton units. 107

Figure 50 Pressure drop for baseline and elbow tests. 114

Figure 51 Dimensions of damper-box. 133

Figure 52 Dimensions of skirt. 134

Figure 53 Metal mesh passive resistive piece for the 2 ton unit. 142

Figure 54 Plastic mesh passive resistive piece for the 2 ton unit. 143

Figure 55 Half plastic mesh passive resistive piece for the 2 ton unit. 143

Figure 56 Single bar passive resistive piece for the 2 ton unit. 144

Figure 57 Parallel rods passive resistive piece for the 2 ton unit. 144

Figure 58 Metal mesh for the 3 ton unit. 145

Figure 59 Plastic mesh for the 3 ton unit. 146

Figure 60 Half plastic mesh for the 3 ton unit. 146

Figure 61 Double strip mesh for the 3 ton unit. 147

Figure 62 Metal mesh for the 5 ton unit. 148

Figure 63 Parallel rod for the 5 ton unit. 148

Figure 64 Large mesh for the 5 ton unit. 149

Figure 65 Frame for the 5 ton unit. 149
Figure 66 Metal mesh with a metal frame for the 5 ton unit. 150
Figure 67 Velocity profiles for the baseline 2 ton unit. 157
Figure 68 Velocity profiles for the 2 ton unit. 158
Figure 69 Velocity profiles for the 3 ton unit. 159
Figure 70 Velocity profiles for the 5 ton unit. 160
Figure 71 Velocity profile for the 2 ton unit with the oversized duct. 161
Figure 72 Velocity profiles for the 3 ton unit with the oversized duct. 162
Figure 73 Scenario 2 velocity profiles for the 2 ton unit. 163
Figure 74 Scenario 2 velocity profiles for the 3 ton unit. 164
Figure 75 Scenario 2 velocity profiles for the 5 ton unit. 165
Figure 76 Set pressure velocity profiles for the 2 ton unit. 166
Figure 77 Set pressure velocity profiles for the 3 ton unit. 166
Figure 78 Set pressure velocity profile for the 5 ton unit. 166

LIST OF TABLES

Page

Table 1 AHRI Standard 210 static pressure rating points (AHRI 2008). 12

Table 2 ASHRAE loss coefficients and pressure loss values for the three units (ASHRAE 2009b). 14

Table 3 Pressure drop for different areas for a loss coefficient of 2.8. 19

Table 4 Dimensions for 3 air handling units. 24

Table 5 Passive resistive pieces for the 2, 3, and 5 ton unit. 31

Table 6 Locations of pressure taps $P3$-P_A. 34

Table 7 Solenoid activation table. 37

Table 8 List of instruments and accuracy. 41

Table 9 Test matrix for Scenario 1. 43

Table 10 Test matrix for Scenario 2. 44

Table 11 Uncertainty analysis of instrumentation. 48

Table 12 Estimated sample size for various confidence intervals. 50

Table 13 Scenario 1 data for the 2 ton unit. 53

Table 14 Scenario 1 data for the 3 ton unit. 54

Table 15 Scenario 1 raw data for the 5 ton unit. 54

Table 16 Scenario 1 data for the 2 ton unit with the largest duct. 55

Table 17 Scenario 1 data for the 3 ton unit with the largest duct. 56

Table 18 Data for the best elbow test with airflow as the variable. 56

Table 19 Scenario 2 baseline tests. 58

Table 20 Average airflow and power for baseline tests for all units and scenarios. 64

Table 21 Normalized baseline test airflow and power for Scenario 1 with the largest duct and Scenario 2 with respect to Scenario 1 baseline. 64

Table 22 Comparison of baseline and elbow tests for the 2 ton unit. 66

Table 23 Comparison of baseline and elbow tests of the 3 ton unit. 67

Table 24 Comparison of baseline and elbow tests for the 5 ton unit. 67

Table 25 Comparison of baseline and elbow tests for the 2 ton with the largest duct. 68

Table 26 Comparison of baseline and elbow tests for the 3 ton unit with the largest duct. 69

Table 27 Comparison of baseline and elbow test with set static pressure. 69

Table 28 Percent error of the static pressure measurement for the complete elbow tests. 70

Table 29 Pressure percent error of the square elbow with turning vanes for Scenario 1. 71

Table 30 Aspect ratios of all three units related to elbow orientation. 77

Table 31 Locations of pressure rings for baseline verification case study. 85

Table 32 CS-2 pressure ring locations. 87

Table 33 Experimental and ASHRAE loss coefficients for baseline tests. 92

Table 34 Orientation dependence of the elbow loss coefficients (ASHRAE 2009b). 94

Table 35 Comparison of test parameters for the 2, 3 and 5 ton units 101

Table 36 Baseline tests for the 2 ton unit. 116

Table 37 Measurements for power uncertainty calculation. 135

Table 38 Sample parameters for standardized airflow and pressure calculations. 137

Table 39 Data for the 2 ton unit. 152

Table 40 Scenario 2 data for the 3 ton unit. 154

Table 41 Scenario 2 data for the 5 ton unit.. 155

INTRODUCTION

Overview

The American Society of Heating, Refrigerating, and Air Conditioning Engineers (ASHRAE) describes the current procedure for testing residential units in ASHRAE Standard 37, *Methods of Testing for Rating Electrically Driven Unitary Air-Conditioning and Heat Pump Equipment* (ASHRAE 2005). This standard describes the outlet duct required and the inlet duct recommended in order to accurately measure the static pressure across a unit. According to TRP-1581, the test apparatus height can reach 16 feet because of equipment placed at the inlet and outlet. As the industry moves towards more efficient designs, units are becoming larger so as to reduce mean velocity and pressure drop, which in turn requires even more vertical space to test the unit following ASHRAE Standard 37. Current test facilities are left with two options for testing newer units: reductions in the test apparatus height or else expensive and time intensive adjustments to the facility. Furthermore, the ASHRAE *Handbook Fundamentals* (2009) mentions that poor fan performance can be attributed to inlet and outlet conditions of the blower. If the inlet or outlet ducts are compromised due to space requirements, the blower could be negatively affected simply due to the test apparatus. This reduces the reliability of test facilities utilizing ASHRAE Standard 37 due to the variations in test setup.

Project Objective

The objective of this project is to develop and standardize alternate testing methods for unitary air-conditioning and heat pump equipment, which cannot be tested according to ASHRAE Standard 37 because of height restrictions, by reducing the overall height of the vertical testing apparatus. This project addresses two potential modifications to ASHRAE Standard 37. Namely, shortening the vertical outlet duct test section to a horizontal position by use of an elbow (Scenario 1) and allowing for the installation of a passive resistive device at the unit outlet to reduce the measurement height (Scenario 2).

Both modifications must be within 5% power and 2.5% airflow of a baseline that adheres to ASHRAE Standard 37 outlet ductwork.

Scope of Work

To accomplish the project objective, three units were tested that represent a range of sizes typical for residential applications (2, 3, and 5 tons). These three units were tested for two scenarios, namely Scenario 1 and Scenario 2. For Scenario 1, an elbow was installed at the unit outlet so that the static pressure section was moved to a horizontal position. The static pressure was measured after the elbow at a specified distance from the elbow junction. Three elbow configurations, a square elbow, a curved elbow, and a square elbow with turning vanes, were tested. To investigate possible directional effects, each unit was tested for four elbow orientations by rotating the unit 90 degrees each test. In addition, the two smaller units (2 and 3 tons) were tested with the duct that was sized for the 5 ton unit. In total, it was necessary to manufacture from sheet metal three outlet duct and elbow test sections to accommodate the three sizes, three elbow configurations, and four orientations.

In Scenario 2, several passive resistive pieces were individually designed, manufactured, and inserted into the flow at the unit outlet with several additional pressure taps along the duct to ascertain the minimum pressure drop distance. Therefore, the minimum distance between the passive resistive piece and static measurement position was found.

All Scenario 1 and Scenario 2 tests were compared to a series of control tests, or baseline tests, which followed ASHRAE Standard 37 for a straight duct of a specified length after the unit. Each Scenario 1 and Scenario 2 test was required to have power measurements within 5% and airflow measurements within 2.5% of the baseline tests. Velocity profiles for each test were also collected downstream of the static pressure measurement position for comparison to the baseline and for verification of flow straightening.

The data were analyzed and recommendations were provided to ASHRAE for modifying ASHRAE Standard 37 so as to reduce required height restrictions by use of alternate geometries.

EXPERIMENTAL TEST CONSIDERATIONS

Air Handling Unit Specifications

An air handling unit as defined by TRP-1581 must include a heat exchanger and a blower. These parts can be configured in two ways, namely, blow-through air handlers where the heat exchanger is placed downstream of the blower, or draw-through air handlers where the heat exchanger is upstream of the blower. Regardless of air handler type they are all given an airflow and a capacity rating. The capacity is the amount of energy the air handling unit can put into either cooling or heating an environment. It is often defined by the unit of tons, which is equivalent to 12,000 BTU/hr. Residential air handlers typically range from two to five tons in capacity. In order to encompass the residential air handlers, a 2, 3 and 5 ton unit were asked for in the project scope.

For this project the most important part of the unit is the blower as airflow and pressure are the measurements of interest. A blower consists of two parts, the motor and the fan. There are two common types of motors used in air handlers, permanent split capacitance motors (PSC) or electronically commutating motors (ECM). PSC motors are asynchronous ac motors that slightly lag behind the incoming ac frequency. The stator's magnetic field is created by the incoming ac power. The rotor creates an opposing magnetic field, which causes it to rotate. PSC motors are the most common in HVAC applications (King et al. 2012). ECM motors require a transformer due to their need for dc power. They also require electronic controls to commutate the stator to create the same effect as an ac magnetic field. ECM's provide variable speed capabilities, as the voltage is proportional to the rotational speed of the blower (Roth et al. 2004).

The motor, whether it be PSC or ECM, is connected to a fan, which is the actual component that moves air across the heat exchanger in order to cool or heat the environment. Fan configurations often refer to the orientation of the blade in regards to the rotation of the fan such as backward curving, radial, and forward curving fans. The three units that were donated for this project coincidently all had the same fan type with forward curving fans. It is very important to understand the issues that occur with the fan

as these problems directly relate to the performance of the air handling unit. The ASHRAE *Handbook Fundamentals* (ASHRAE 2009a) states,

"The most common causes of deficient performance of the fan/system combination are improper outlet connections, non-uniform inlet flow, and swirl at the fan inlet."

Non-uniform inlet itself can be a major concern as mentioned in research by Bayomi et al. (2006) where it was successfully shown that an inlet straightener, which created uniform flow, could increase airflow by up to 12% for radial and backward blades compared to a free inlet. Unlike backward curving and radial fans, forward curving fans do not seem to increase in airflow or efficiency with inlet straighteners suggesting they are less sensitive to inlet conditions (Bayomi et al. 2006). The work of Kwon and Cho (2001) expand this conclusion, that forward curving fans were not greatly affected by operating conditions for the inlet, yet they showed that the exit of the fan was very sensitive to fan operating conditions. In order to reduce the poor performance issues related to various different fan types and motors, ASHRAE Standard 37 contains certain requirements for testing.

ASHRAE Standard 37 Description

Testing air handling units requires accurate and reliable measurements of static pressure and airflow that are independent of the different configurations of air handling units that were mentioned previously. As seen in Figure 1, the lengths of ductwork on either side of the unit are specified in order to accurately measure static pressure and reduce the issues that affect fan performance (adopted from ASHRAE Standard 37).

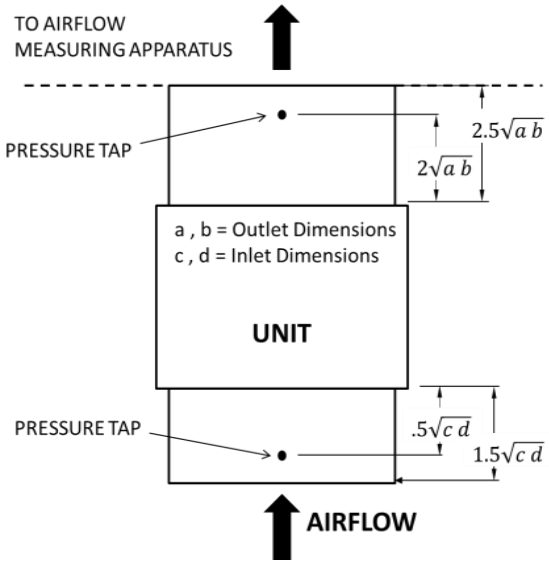

Figure 1: ASHRAE Standard 37 test setup for measuring static pressure (ASHRAE 2005).

In Figure 1, specifications are given of the straight ducts for the unit inlet and outlet used to measure static pressure. The inlet section is specifically mentioned in section 6.4.2.2 of ASHRAE Standard 37 (ASHRAE 2005). It states,

"If space within the test room permits, an inlet duct connection should be installed. If used, the inlet duct shall have cross-sectional dimensions equal to those of equipment and should otherwise be fabricated as shown by the [setup] given in [Figure 1]."

In practice, 6.4.2.2 is not used, instead a damper-box with a small skirt is used to measure the inlet pressure as illustrated in Figure 2. This inlet configuration is not used to reduce test apparatus height, rather to install a damper system at the inlet for cyclic testing following AHRI Standard 210 (AHRI 2008). In Figure 2, the unit is mounted directly above the skirt, which is 6 inches tall and has four pressure taps located in the center of each side. The ASHRAE Project Monitoring Subcommittee decided the skirt dimensions for this project. The damper-box is below the skirt (white) with a horizontal inlet. Following the Department of Energy (DOE) guidelines on inlet damper-box manufacturing (DOE 2013), the damper-box opening must be equal to or greater than

the unit. The dimensional drawings of the damper-box and skirt are found in Appendix A.

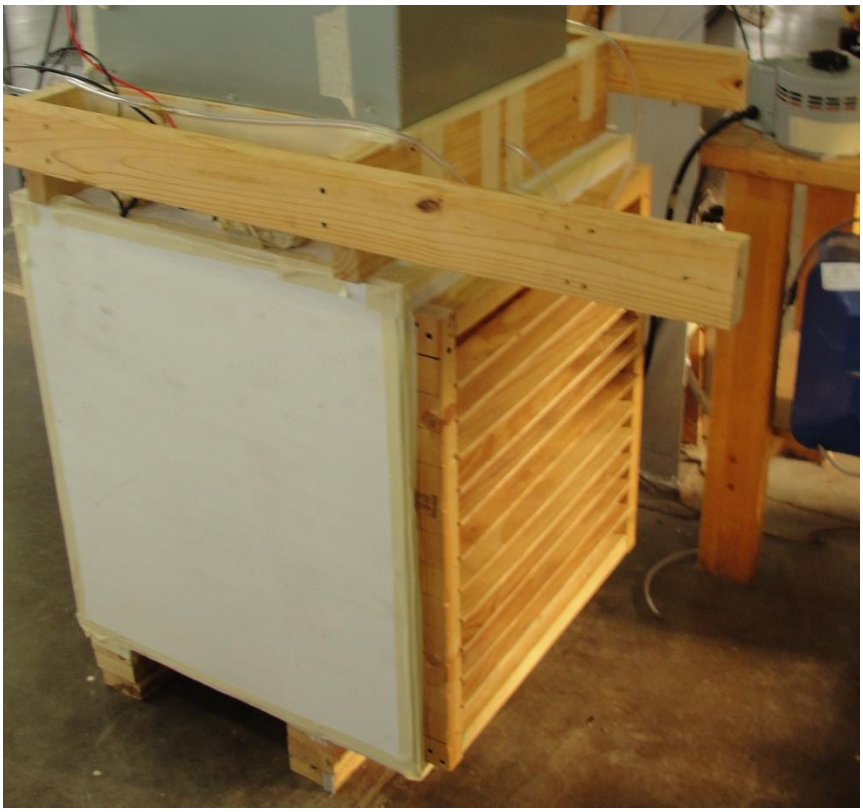

Figure 2: Air handling with a skirt and damper-box configuration.

The damper-box and skirt inlet configuration could potentially affect the fan performance and is an important consideration, yet the scope of this project is limited to studying the effect of changing the outlet conditions, therefore this project does not address poor inlet conditions, as the damper-box and skirt are standard practice in industry and are accepted by ASHRAE Standard 37. Additional testing outside the scope of the project was performed to look at different inlet conditions and is presented in the Case Studies chapter.

Pressure Theory, Instrumentation and Test Standards

Pressure is one of the three important parameters for this project. In the following section several important topics are covered which relate to pressure drop for HVAC applications.

Theoretical Pressure Drop

In a straight section of duct with fluid movement, it has been proven that there is apparent friction between the boundaries and the moving fluid (Moody 1944). This friction is caused by the no slip condition, which must be met at the boundary. Figure 3 illustrates how the theoretical pressure changes through the test apparatus for a baseline test following the ASHRAE 37 requirements with an outlet duct and also shows pressure measurements that are recorded.

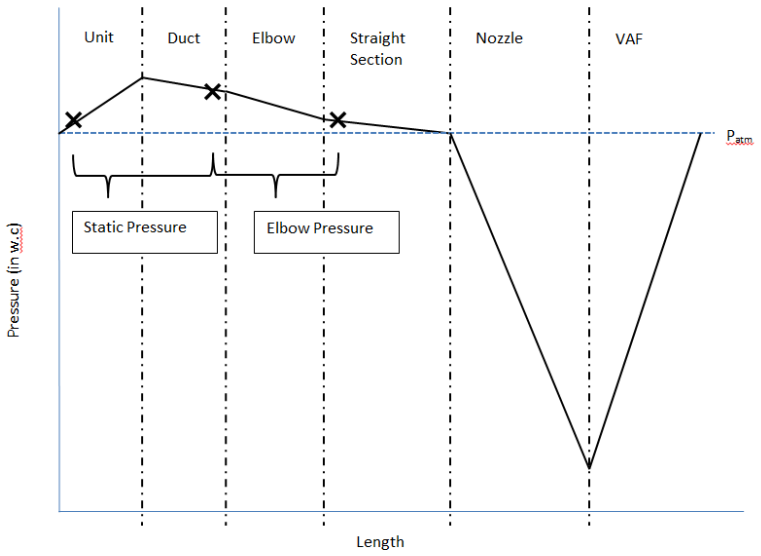

Figure 3: Pressure drop estimation within the test apparatus following ASHRAE Standard 37.

Figure 3 is a simple model of the pressure change in the test apparatus. The blower increases the pressure similar to a pump for water and as the air moves through the duct work, the pressure drops due to frictional losses. Figure 3 estimates the pressure changes to be linear, which neglects the complexity of the blower and the local dynamic effects of junctions and transitions. A simple linear relationship between pressure drop and axial length can be realistic for fluid moving through a straight duct (Moody 1944). The friction factor is defined as the slope or rate of change of the pressure drop compared to the flow direction. Churchill (1977) developed a relation, which finds the friction factor for all Reynolds numbers using Equations 1-6.

$$f = 8\left[\left(\frac{8}{Re_D}\right)^{12} + \frac{1}{(A+B)^{1.5}}\right]^{\frac{1}{12}} \tag{1}$$

Equation 1 calculates the friction factor, *f*, given the Reynolds number and the parameters A and B, which are functions of the Reynolds number, the effective roughness, and the diameter. The parameter, A, can be found by Equation 2.

$$A = \left[2.457\ \ln\left(\frac{1}{\left(\frac{7}{Re_D}\right)^{0.9} + \left(0.27\frac{\epsilon}{D}\right)}\right)\right]^{16} \tag{2}$$

B is found by Equation 3.

$$B = \left(\frac{37{,}530}{Re_D}\right)^{16} \tag{3}$$

The Reynolds number is calculated by Equation 4.

$$Re_D = \frac{Q\ D_h\ \rho}{720\ \mu} \tag{4}$$

For rectangular ducts the hydraulic diameter is used, which is found by Equation 5.

$$D_h = \frac{4A}{P} \tag{5}$$

Huebscher (1948) has shown that the use of the hydraulic diameter is appropriate for ducts with aspect ratios less than 8 with no appreciable difference of the friction factor

between pipe flow and rectangular flow. The pressure drop can then be estimated for a rectangular duct by applying the Darcy equation given in Equation 6 (ASHRAE 2009a).

$$\Delta P = \frac{fL}{D_h}\,\rho\left(\frac{144\,Q}{1097\,A}\right)^2 \tag{6}$$

The ASHRAE *Handbook Fundamentals* (ASHRAE 2009a) states that the friction factor tends to be between 0.016 and 0.05 for HVAC applications.

Figure 3 also showed the measured values including the static pressure. This value is measured with instruments that are defined in the next section.

Pressure Tap and Ring Dimensions

Static pressure is most often measured using pressure taps in the ducts specified by ASHRAE Standard 37 as were shown in Figure 1. An illustration of a pressure tap with important dimensions is shown below in Figure 4.

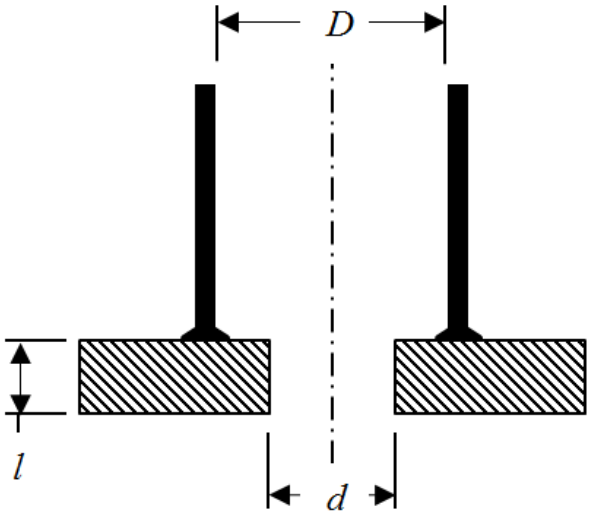

Figure 4: Dimensions for pressure taps.

ASHRAE Standard 37 specifies the recommendations for the diameter of the hole, *d*, as 0.04 inches and the larger diameter, *D*, as 0.25 inches. Shaw (1960) provides detailed work on the parameters of interest, *d*, *D*, and *l*, for static pressure measurement.

ASHRAE Standard 51 (ASHRAE 2007) also provides specifications for the three parameters which sometimes contrast to the conclusions presented by Shaw (1960). What is agreed upon is that the hole diameter, *d*, should be kept small to reduce pressure reading error. More comparisons of the literature for pressure taps can be found in the Case Studies chapter (CS-5).

For rectangular duct, four pressure taps are placed in the center of each face and connected in one of two ways as seen in Figure 5 to create a pressure ring. No preference is given by ASHRAE Standard 37 for measuring pressure between the two configurations shown in Figure 5.

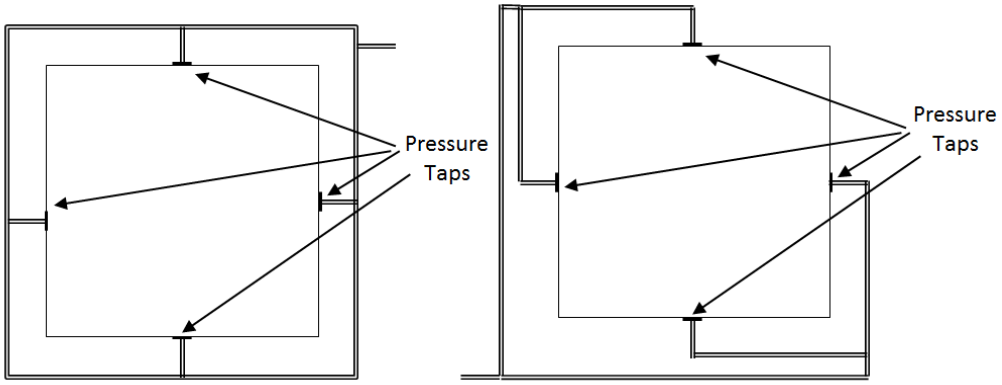

Figure 5: (Left) Conventional and (Right) "Triple T" pressure ring configurations (ASHRAE 2005).

AHRI Static Pressure Rating Points

AHRI Standard 210 (AHRI 2008) is the industry standard for rating air conditioners and heat pump equipment. Standard test procedures dictate that the static pressure must be set using the pressure rings as defined previously. The standard static pressure rating points for each of the units as per AHRI Standard 210 are shown in Table 1. These values are based on capacity of the air handling unit.

Table 1: AHRI Standard 210 static pressure rating points (AHRI 2008).

Unit Tonnage	Static Pressure (in w.c)
2	0.1
3	0.15
5	0.20

Pressure Drop Across Elbows

Of importance in finding a possible alternative for ASHRAE Standard 37 is determining the effect of the elbow on the static pressure measurement, as it is the main difference between the static pressure measurement for the baseline tests and the elbow tests for Scenario 1 (refer to Figure 10 and Figure 12). In order for the baseline tests and elbow tests to be comparable in power, airflow, and static pressure, as is required to satisfactorily change ASHRAE Standard 37, the elbow influence must be negligible. The effect of the elbow can be estimated by calculating the pressure drop of the three elbows using the loss coefficient, K_o.

The Loss Coefficient for Elbows

The loss coefficient relates the pressure drop with the mean velocity of the flow by Equation 7.

$$K_o = \frac{\Delta P}{\rho \left(\frac{V}{1097}\right)^2} \tag{7}$$

Loss coefficients for curved, square, and square elbows with turning vanes are well established as can be seen in the ASHRAE *Handbook Fundamentals* (2009b). Depending on the elbow, the loss coefficient can be a function of aspect ratio, blast or blowout area compared to outlet area, or even elbow orientation. It is important to define the aspect ratio now, as it will be used extensively. For this project the aspect ratio, $\frac{a}{b}$, will be defined as the height of the horizontal section of the elbow (also known as bending length) over the width. The aspect ratio will also be used for the straight duct

and will similarly be defined as the height divided by width. The blast and outlet area can best be seen in Figure 6.

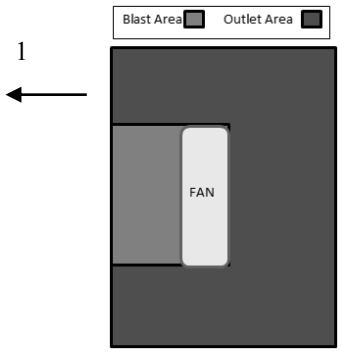

Figure 6: Blast area and outlet area of air handling unit.

The blast area is the throat area of the blower whereas the outlet area is the exit dimensions of the unit (always larger). The orientations will be numbered 1-4 with each number representing a rotation of 90 degrees. This is further explained later on (refer to Figure 14) although elbow orientation 1 is illustrated in Figure 6 for reference. Table 2 summarizes the local pressure loss coefficient, K_0, and the calculated pressure drop expected for curved, square, and square elbows with turning vanes for similar geometry and airflow as those found with the three units (ASHRAE 2009b).

Table 2: ASHRAE loss coefficients and pressure loss values for the three units (ASHRAE 2009b).

		K_0	Q	A	V	ΔP
	Units		CFM	in^2	FPM	in water
2 Ton Unit	Curved Elbow 1	1.40	727	208	503	0.02
	Curved Elbow 2	1.25				0.02
	Curved Elbow 3	0.80				0.01
	Curved Elbow 4	1.20				0.02
	Square Elbow a/b=1	1.15				0.02
	Square Elbow a/b=1	1.15				0.02
	Single Turning Vanes	0.33				0.01
	Double Turning Vanes	0.25				0.00
3 Ton Unit	Curved Elbow 1	3.80	1123	266	608	0.09
	Curved Elbow 2	3.60				0.08
	Curved Elbow 3	2.20				0.05
	Curved Elbow 4	3.20				0.07
	Square Elbow a/b=1.3	1.10				0.03
	Square Elbow a/b=0.8	1.15				0.03
	Single Turning Vanes	0.33				0.01
	Double Turning Vanes	0.25				0.01
5 Ton Unit	Curved Elbow 1	5.50	1950	282	996	0.34
	Curved Elbow 2	4.80				0.30
	Curved Elbow 3	3.20				0.20
	Curved Elbow 4	4.70				0.29
	Square Elbow a/b=2	1.03				0.06
	Square Elbow a/b=0.5	1.20				0.07
	Single Turning Vanes	0.33				0.02
	Double Turning Vanes	0.25				0.02

Parameter Considerations for Pressure Drop of Elbows

The loss coefficients for the curved elbow consider a blower with a blowout and outlet area connected directly to a curved elbow hence why the curved elbow is dependent on the blowout to outlet area ratio and the orientation of the curved elbow with respect to the blower. As seen in Figure 6, orientation 1 represents the elbow orientation that opposes the blower rotation whereas in orientation 3 (180 degree

rotation), the curved elbow rotates with the blower. The square elbow and square elbow with turning vanes assumes fully developed turbulent flow. The square elbow loss coefficients are dependent on the aspect ratio defined previously. The square elbow with turning vanes is found to be a constant and hence independent from geometry.

Considering the data from Table 2, several expectations can be stated. The double turning vanes have the lowest pressure loss coefficient hence they will be expected to perform well with a low pressure loss and with no dependence on geometry. The square elbow changes very little due to aspect ratio suggesting that aspect ratios between 0.5 and 2 do not affect the loss coefficient greatly. The curved elbow was the only elbow that was paired with a blower. As seen in Table 2, the loss coefficients increased as the aspect ratio became more severe from the 2 to the 5 ton unit and orientation 1 was always the highest while orientation 3 was always the lowest. More importantly since the curved elbow shows such a high sensitivity to orientation, the square elbow and square elbow with turning vanes could indeed show this dependence on elbow orientation as well even though The ASHRAE *Handbook Fundamentals* (ASHRAE 2009b) has no data for this.

In summary, the results could vary greatly from Table 2 because the tests will have many more influences affecting the loss coefficient, yet Moujaes and Aekula (2009) additionally showed with Computation Fluid Dynamics (CFD) and experimental data that the turning vane has much lower pressure drop compared with a square elbow with no turning vane due to the creation of a recirculating zone in square elbows, which increases the pressure drop significantly and may affect downstream measurements as well.

Combination of Loss Coefficient and Friction Factor

It is also important to note that the loss coefficients found in Table 2 (ASHRAE 2009b) do not relate to the friction factor, hence it is not calculating the pressure drop due to steady flow along a length of duct. The pressure drop from the loss coefficient is the dynamic pressure loss seen due to a change in the velocity profile and/or a change in

direction of the flow. Friction losses are also apparent in elbows, however, they are often ignored as the flow travels a short distance through most elbows. The average distance the fluid travels through the elbow can be estimated and the friction factor can be calculated if needed.

Airflow Measurement

ASHRAE Standard 37 also specifies the various accepted methods for measuring airflow. The most common method, and the one used in this project is employing ASME long-radius low-ratio proportion nozzles. These nozzles have been studied extensively in turbulent flow. As air moves through a nozzle it compresses increasing the density slightly after the nozzle. Due to mass conservation it is apparent that the airflow after the nozzle must be reduced for an increase in density. To compensate for this effect a discharge coefficient was developed relating the airflow after the nozzle to the airflow before the nozzle. This is known as the discharge coefficient. ASME has tabulated the values of the discharge coefficient for fully developed flow and Bohanon (1975) extended this discharge coefficient to airflow chambers. The below configuration illustrates the dimensions followed for the nozzle bank in an airflow chamber (Figure 7).

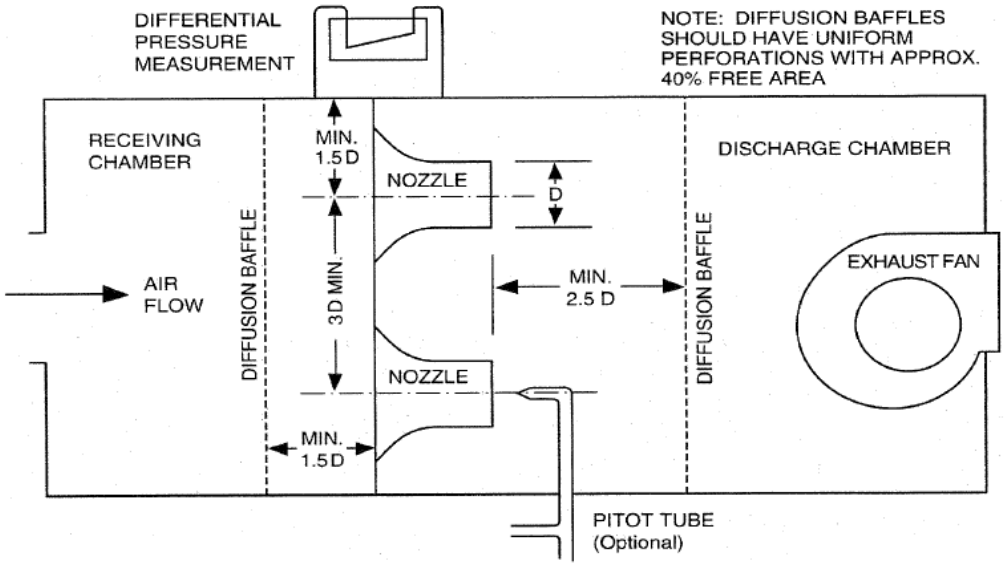

Figure 7: ASHRAE Standard 37 specifications for a nozzle chamber.

The diffusion baffles and area ratio between inlet and nozzle are of great importance to ensure that the inlet velocity profile is uniform and that the static pressure measurements are reading correctly (Bohanon 1975). Pressure tap rings are placed above and below the nozzle bank to obtain the differential pressure. Using differential pressure and nozzle area, the airflow is calculated as seen in the next section.

Steady Flow through Screens

Scenario 2 involves placing passive resistive pieces in the flow in order to create accurate static pressure measurements immediately afterwards. Laws and Livesey (1978) provide an extensive review of steady flow through screens. The parameters of interest governing the flow reactions are porosity, β, and the loss coefficient, K_o. Figure 8 illustrates an interwoven mesh with the geometrical parameters that affect porosity and the loss coefficient.

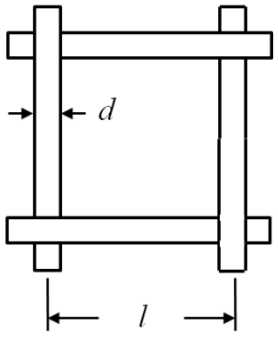

Figure 8: Dimensions for interwoven mesh.

For a screen with diameter *d*, and spacing *l* the porosity can be found by using Equation 8 (Laws and Livesey 1978).

$$\beta = \left(1 - \frac{d}{l}\right)^2 \tag{8}$$

Where the porosity is simply the ratio of open area to total area. Pinker and Herbert (1967) show that this is actually an underestimate of the porosity as the interweaving creates more open area than originally proposed. They developed the sinusoidal porosity, β', which is defined below in Equation 9.

$$\beta' = 1 - \frac{\pi d}{4l}\left[\left(\frac{d}{2l} + \frac{l}{2d}\right)\sin^{-1}\left(\frac{1}{\left(\frac{d}{2l} + \frac{l}{2d}\right)}\right)\right] \tag{9}$$

The derivation of this equation can be found by Zhao et al. (2013). It is important to define a different Reynolds number, Re_d, based off the upstream average flow and the mesh spacing. For a local Reynolds number of less than 250, the loss coefficient can be estimated by the Equation 10 (Pinker and Herbert 1967).

$$K_o = A_1\left(\frac{V}{v}\right)\frac{(1-\beta^2)}{\beta^2} \tag{10}$$

Where A_1 is a function of the Reynolds number. As the Reynolds number increases A_1 is shown to approach 0.52, for this project the parameter A1 is shown to vary from 0.52-0.60. As shown before, with the loss coefficient the pressure drop can be found and the effect of the passive resistive piece analyzed.

With knowledge of the important parameters, β and K_o, several key points highlighted by Laws and Livesey (1978) can be rendered useful.

Instability is shown to develop after the screen for porosity values lower than 0.50 (Baines and Peterson 1951). Bradshaw (1965) suggested that porosity below 0.57 could even show instability. He also mentioned that a non-uniform velocity profile could also create downstream instabilities after the mesh that could affect pressure measurements.

A general guideline also noted by Laws and Livesey (1978) is that the loss coefficient of around 2.8 is shown to create uniform velocity profiles downstream regardless of the upstream conditions. Larger loss coefficients are shown to reverse the inlet velocity profile. Table 3 shows the pressure drop associated with this loss coefficient of 2.8 for areas associated with the unit, the duct dimensions and the frame, and the blowout area of the fan.

Table 3: Pressure drop for different areas for a loss coefficient of 2.8.

	Area Type	Q	A	V	ΔP
Units		(cfm)	(in^2)	(fpm)	(in w.c)
2 Ton	Normal Duct	727	208	503	0.02
	Frame	727	187	560	0.03
	Blowout Area	727	166	629	0.03
3 Ton	Normal Duct	1123	264	612	0.03
	Frame	1123	240	674	0.04
	Blowout Area	1123	123	1317	0.15
5 Ton	Normal Duct	1950	282	996	0.09
	Frame	1950	256	1097	0.11
	Blowout Area	1950	113	2489	0.54

Since the passive resistive piece will be affected by all of the geometries previously mentioned, the pressure drop values are estimates of the actual pressure drop during experimentation. For a loss coefficient of 2.8, pressure drop could reasonably range from 0.02 to .54 in. of water. This may well not be acceptable for Scenario 2 as this is a large pressure drop compared with the AHRI rating points.

Another issue arises when back calculating from the loss coefficient of 2.8 to the porosity level. For such a large loss coefficient, it is difficult to find mesh with porosities over the instability levels (0.50). To get around this issue Bradshaw (1965) suggests the use of multiple screens. Multiple mesh screens were shown actually not to create uniform velocity profiles due to the interference they cause on each other unless they are placed very close together. Multiple meshes also show a high sensitivity to orientation, and Reynolds number. The loss coefficient is not easy to calculate either as both meshes affect each other creating an individual loss coefficient for each mesh that changes based on what the other mesh is doing. Due to all of the issues mentioned above, it is nearly impossible to attain a loss coefficient of 2.8 for Scenario 2.

The loss coefficient might need to be lower due to other concerns as well. Lau and Baines (1968) demonstrated that loss coefficients greater than 1 would cause bulges (high velocities) in the velocity profile near the walls after the screen. This too could affect static pressure measurements.

Regardless of the mesh, Baines and Peterson (1951) demonstrated that at least 5-10 mesh lengths is needed to establish the velocity profile although more often than not measurements are taken at least a full duct diameter downstream. Finally a word of caution was mentioned. Small differences in data taking could cause extreme and unexpected results. Brundrett (1993) showed that even small irregularities in the weaving of interwoven mesh could cause significant downstream effects. There are many factors to consider in Scenario 2. First, the velocity profile exiting from the unit is most certainly not uniform. Depending on the type of unit the flow has just left a blower or a heat exchanger. Every unit also has a different exit geometry causing large variations in velocity profile. In addition, there is the frame holding the passive resistive piece together. It is unrealistic to expect the mesh to be placed in the flow with no frame to hold it rigid. The frames used for Scenario 2 have thicknesses of 0.75 in., which would definitely increase velocity through the mesh and cause unexpected variations downstream. These variations would change drastically from unit to unit and could potentially affect the static pressure measurements.

The local loss coefficient calculated by Equation 7 is also questioned for compressible flow. Bommisetty et al. (2011) showed that density change across the screen is a major factor in determining the loss coefficient. Although some findings mentioned above accounted for compressibility, it is almost impossible to apply those findings to this project.

In summary, great care will be taken in designing the passive resistive pieces. Due to all the concerns mentioned above it might be best to start with a very low loss coefficient (high porosity) that has negligible pressure loss. In this way, changes in weave, velocity profile, etc., will not affect the overall performance of the air handling unit.

Velocity Profile Design and Measurement

Another aspect of this project is the velocity profile after the unit. There are several ways to measure local velocity in a flow. One of which being the use of pitot tubes, which are used for this project. The velocity profile is meant to be a visualization tool rather a measurement. To accommodate this, the velocity profile is placed in a section that is neither fully developed nor uniform. This is in order to visualize the effect of apparatus modifications on the velocity profiles. In this regard, an equal area method will be employed as shown in Figure 9.

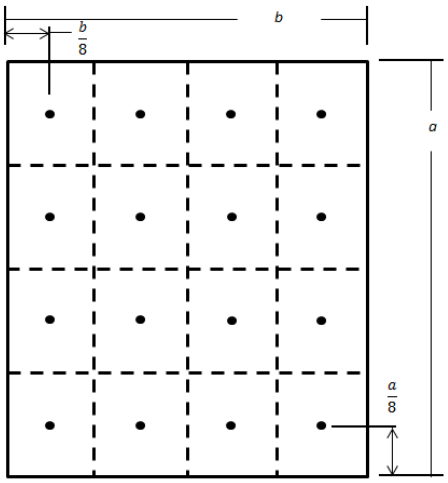

Figure 9: Pitot tube array dimensions.

The equal area method evenly divides the duct cross sectional area and measures the velocity in the middle of each divided section. The area is divided into 16 equal regions with a pitot tube in the middle of each one. Pitot tubes have two outputs; total pressure, and static pressure. The velocity pressure is measure using the following Equation 11.

$$P_v = P_{Total} - P_{Static} \tag{11}$$

The velocity pressure can then be related to a local velocity by applying the following Equation 12.

$$P_v = \frac{1}{2}\rho \, \mathrm{V}^2 \tag{12}$$

Various different papers have been published with velocity profiles downstream of a rectangular elbow and a rectangular with turning vanes. Moujaes and Aekula (2009) in particular investigated the differences in a rectangular elbow with and without turning vanes for several Reynolds numbers. The CFD analysis with long straight ducts before and after the elbow showed a very uniform velocity profile at roughly five hydraulic diameters from the elbow at a Reynolds number of an order of magnitude higher than seen for this project. Mandal et al. (2010) investigated the recirculation zone and velocity profile of a forward facing step for similar Reynolds numbers (same order of

magnitude) as this project. The findings showed highly non-uniform velocity profiles after 2.7 hydraulic diameters downstream of the second elbow. Furthermore, the friction factor after the second elbow varied greatly suggesting a very non-uniform velocity profile could possibly continue. This suggests that due to the addition of another rectangular elbow, higher disorder occurs than with simply one rectangular elbow. As in this project there is not only an inlet elbow (the damper-box) and an outlet elbow, but a blower, converging and diverging sections and a heat exchanger as well, it is expected that the velocity profiles could be highly non-uniform at the exit and after the elbow.

Propagation of Uncertainties

The Root of the Sum of the Squares (RSS) is commonly used for uncertainty analysis of instrumentation (Kline et al. 1953). An equation relating measurements is in the form with independent variables x_i and associated error, w_i for i = 1→ n:

$$R = F(x_1, x_2, x_3, \dots, x_n)$$

Then the uncertainty of R denoted as W_R can be found using the below Equation 13 if the uncertainty for each independent variable, w_i, is known:

$$w_R = \left[\left(\frac{\partial \mathrm{R}}{\partial x_1} \cdot w_1\right)^2 + \left(\frac{\partial \mathrm{R}}{\partial x_2} \cdot w_2\right)^2 + \cdots + \left(\frac{\partial \mathrm{R}}{\partial x_n} \cdot w_n\right)^2\right]^{.5} \quad (13)$$

This effectively measures the uncertainty due to the instrumentation. Uncertainty of important measurements were calculated for each scenario with a sample calculation in Appendix B.1.

EXPERIMENTAL TEST DESIGN AND SETUP

Unit Specifications

Three units were picked for testing that represented a range of residential air handlers (Table 4). As mentioned previously, the three units varied from 2 to 5 tons and featured two different motors. A PSC motor was used in the 2 ton unit, whereas ECM motors were found in the 3 and 5 ton units. All three featured a blower and a heat exchanger. The largest was a draw-through unit whereas the other two were blow-through units.

Table 4: Dimensions for 3 air handling units.

	Height	Outlet Dimensions	Outlet Duct	Inlet Dimensions	Inlet Duct	Motor
Tonnage	(in)	(in)	(in)	(in)	(in)	
2	49.9	14.5 x 14.35	36	14.5 x 17.15	22	PSC
3	55.7	18.4 x 14.4	41	18.4 x17.5	27	ECM
5	62.7	23.7 x 12	42	24 x 18	32	ECM

Static Pressure Measurement

Both Scenarios involved static pressure measurements. Scenario 1 had three pressure ring locations labeled as follows:

- *P0*- Inlet pressure ring.
- *P1*/P_A- ASHRAE Standard 37 pressure ring.
- *P2*- Pressure ring after elbow following ASHRAE Standard 37 pressure location calculation with reference to the end of the elbow.

The static pressure of the unit was found by subtracting P_A from *P0* for the baseline and Scenario 2 tests. The static pressure for Scenario 1 was measured by comparing P0 and *P2*. Five additional pressure rings, *P3-P7*, were used for Scenario 2 where *P3* was the lowest on the duct (closest to the unit) and P7 was the highest (farthest from the

unit). Locations of these additional pressure taps will be addressed in Scenario 2 Test Setup.

The actual dimensions of the static pressure taps (Figure 4) used in the pressure rings were 0.0625 in., 0.2 in., and .035 in. for *d*, *D*, and *l* respectively due to the materials at hand. The static pressure taps were manufactured by brazing copper tubing on to a copper sheet and drilling a hole through the copper sheet with a $\frac{1}{16}$ inch drill bit. The burrs were sanded off for a smooth pressure tap surface. The pressure rings were made using ¼ inch vinyl tubing in the conventional pressure ring approach as seen in Figure 5.

Baseline Test Setup Description

Each of the three units were tested with the same test configuration seen below in Figure 10 for the Scenario 1 baseline test and the Scenario 2 baseline test with the exception that the Scenario 2 baseline test had five additional pressure taps in between the unit outlet and the pressure ring, *P1*. A minimum of three baseline tests were completed at the AHRI Standard 210 static pressure settings for each unit.

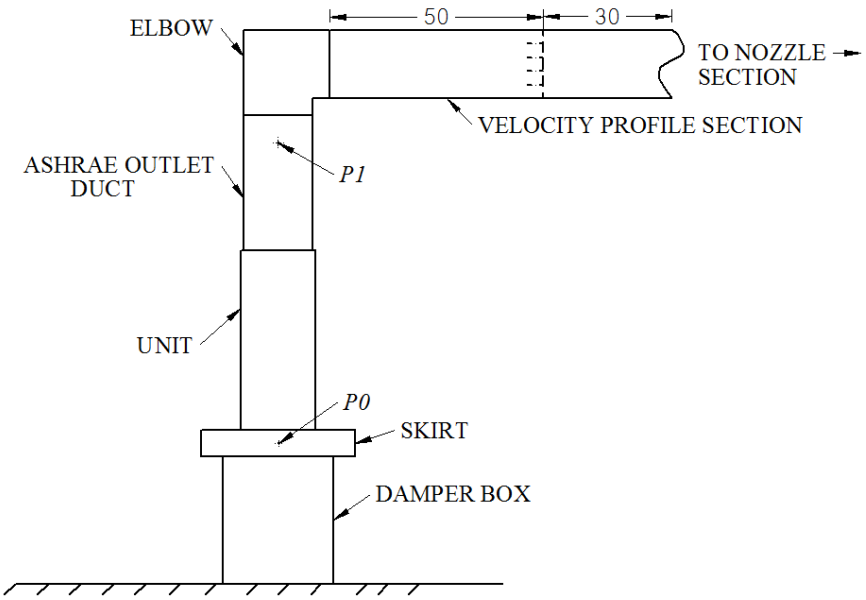

Figure 10: Scenario 1 baseline test setup.

The baseline tests followed ASHRAE Standard 37. Instead of the inlet duct, the damper-box and skirt configuration were used as mentioned previously to follow industry practice. As shown in Figure 10 the unit was resting on the skirt and damper-box. Above the unit was the ASHRAE Standard 37 specified outlet duct whose height was dependent on the outlet dimensions of the unit. According to ASHRAE Standard 37, any means can be used to attach to the flow measuring apparatus after the outlet duct. An elbow was placed after the unit of equal dimensions as the outlet duct. Pressure ring *P1* and pressure ring *P0* were used to measure the static pressure of the unit.

Velocity Profile Section

The next section shown in Figure 10 was for the 16 point velocity profile. The dimensions shown in Figure 10 were applied to all three units, with 50 inches of horizontal straight duct between the elbow and velocity profile measurement and 30 inches of straight duct after the velocity profile to reduce downstream effects. The velocity profile section was then connected to the nozzle section with flexible duct.

Nozzle Section

Both Scenario 1 and Scenario 2 also utilized the nozzle section. It featured 8 nozzles varying from 1 to 5 inches in diameter. The diameters were found by taking four measurements and averaging for a single value. Following the ASHRAE Standard 37 (refer to Figure 7), the nozzles were placed at least 1.5 times the diameter away from the wall and 2 times the largest diameter away from each other. Diffusion baffles were also placed before and after the nozzle bank. A variable assist fan was placed after the nozzle bank in order to control the static pressure point (Figure 11) as is recommended in the ASHRAE Standard 37.

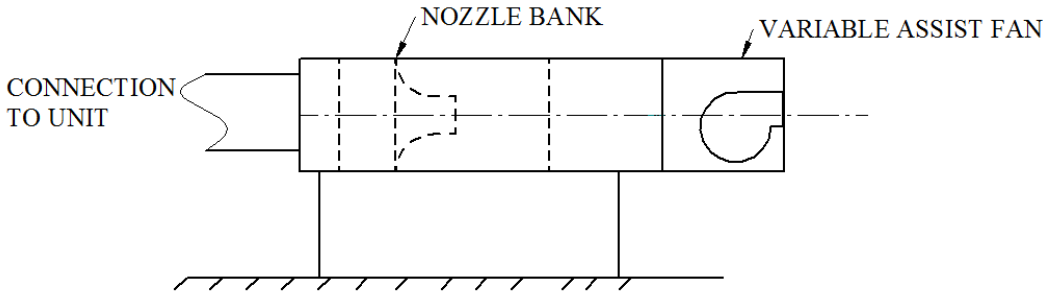

Figure 11: Nozzle chamber test setup.

Scenario 1 Test Setup Description

Several components of the Scenario 1 testing were important to mention including the general setup, the elbow type, and the elbow orientation. Each was described in detail in the following sections.

Scenario 1 Elbow Test Setup

The elbow tests were set up by removing the ASHRAE Standard 37 outlet duct from the test apparatus as shown in Figure 12. The skirt pressure ring, *P0*, remained while pressure ring, *P2*, was placed downstream of the elbow. The location of the pressure tap, *P2*, was dictated by the same equation used for the ASHRAE Standard 37 outlet duct with reference to the end of the elbow junction.

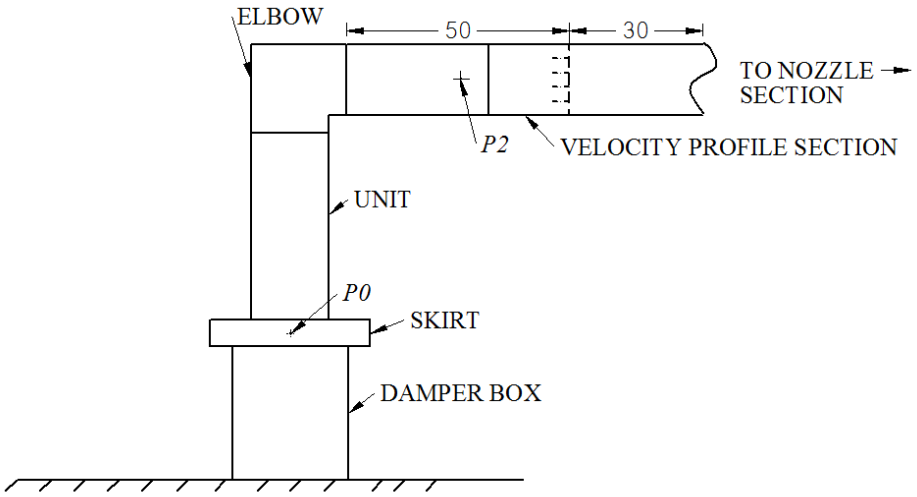

Figure 12: Scenario 1 elbow test setup.

Scenario 1 Elbow Type

The Project Monitoring Subcommittee picked the three elbow types. Figure 13 describes all three elbow types. Due to the aspect ratios of the 3 and 5 ton units, six elbows were needed as seen in Figure 13. The 2 ton unit had an aspect ratio of 1 and therefore only needed three elbows. Each elbow had a 1.5 inch throat distance to allow for flange connections. The double thickness turning vanes had a radius of two inches and were placed two inches apart.

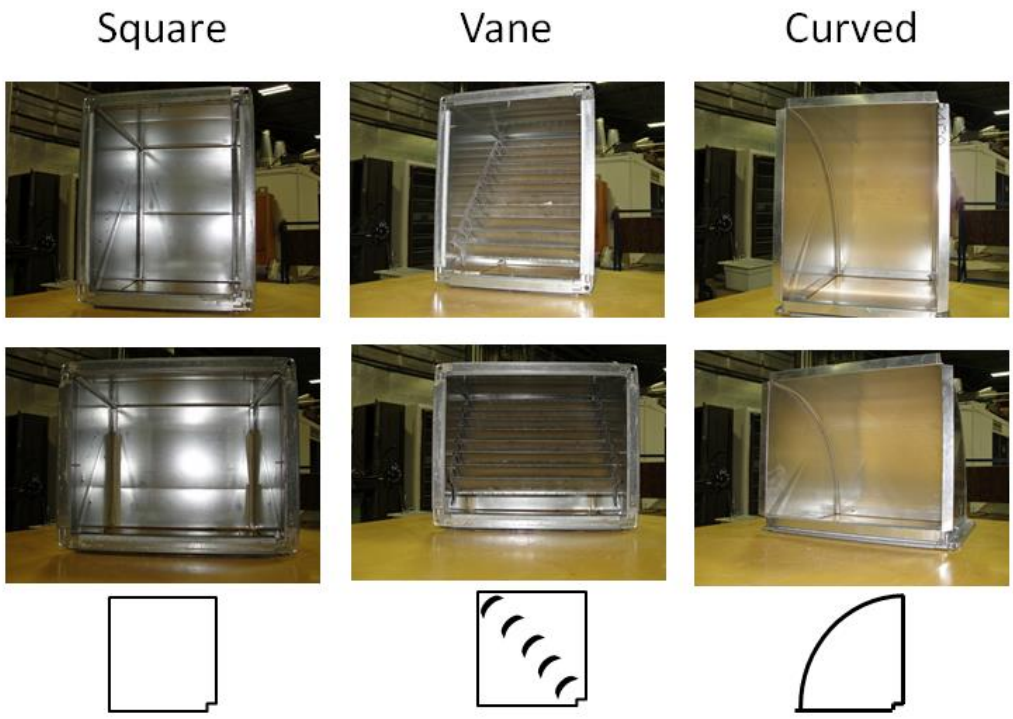

Figure 13: (Left) Square elbow, (center) square elbow with turning vanes, and (right) curved elbow.

Scenario 1 Elbow Orientations

The unit was rotated by 90 degrees for each test with the three different elbows resulting in twelve elbow tests. Figure 14 illustrates a blow through unit completing an entire rotation from test orientation 1 to test orientation 4 during an elbow test with the square elbow. In orientation 1, the flow completed a 180 degree turn. In orientations 2 and 4, the flow completed a corkscrew turn, and in orientation 3, the flow moved through a forward facing step.

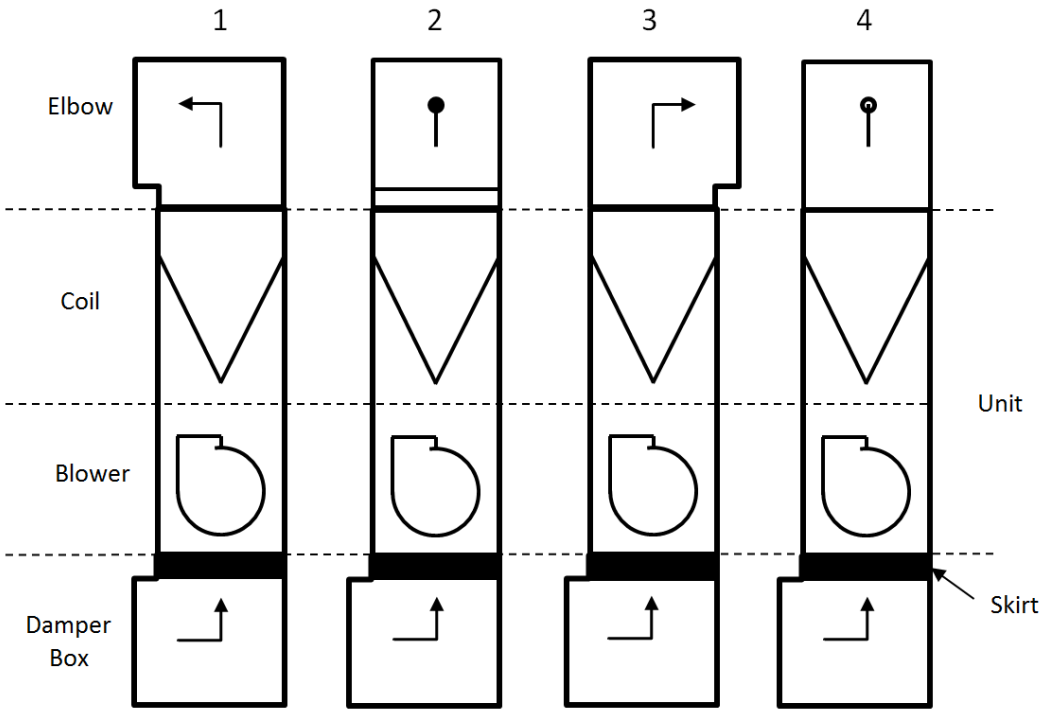

Figure 14: Elbow orientations 1-4.

Scenario 2 Test Setup Description

Scenario 2 similarly utilized elbows with different possibilities for elbow type and orientation, yet the elbow was placed downstream of the static pressure measurement and hence were not supposed to affect testing (this claim was investigated in CS-9). The most important parameters for Scenario 2 were the type of passive resistive pieces and the overall setup of the test rig.

Scenario 2 Passive Resistive Pieces

Various different passive resistive pieces were used depending on the unit. They are listed in Table 5. Pictures of each passive resistive piece can be found in Appendix C.

Table 5: Passive resistive pieces for the 2, 3, and 5 ton unit.

2 Ton	3 Ton	5 Ton
Metal Mesh	Metal Mesh	Metal Mesh
Plastic Mesh	Plastic Mesh	Parallel Rods
Half Plastic Mesh	Half Plastic Mesh	Frame Only
Single Bar	Double Strip	Large Mesh
Parallel Rods		Metal Mesh w Metal Frame

The passive resistive pieces are also described shortly below. Dimensions such as the diameter, mesh spacing, and thickness are also mentioned.

- Metal Mesh- An interwoven metal mesh with a diameter of 0.09 in. and spaced 0.055 in. apart. The thickness of the mesh was 0.015 in.
- Plastic Mesh- An interwoven plastic mesh with a diameter of 0.010 in. and spaced 0.050 in. apart. The thickness of the plastic mesh was 0.02 in.
- Half Plastic Mesh-The same material as the plastic mesh with only half of the area covered. The mesh was placed in the flow so as to lie directly over the blast area of the blower.
- Single Bar- A single 0.75 in. thick bar two inches from the frame and 1 inch tall. The bar was placed directly over the blast area of the blower and parallel to the axis of rotation of the blower.
- Parallel Rods- Metal rods with 0.1 in. diameter spaced one inch apart. They were placed in the flow parallel to the axis of rotation of the blower.
- Double Strip- The metal mesh material was cut into two inch wide strips and doubled over making sure the mesh aligned. Two of these metal mesh strips were placed in the frame with the first an inch away from the frame and the second three inches from the frame. They were placed over the blowout area of the fan and parallel to the axis of rotation of the blower.
- Frame Only- Just the frame made of wood that was 0.75 in. thick and one inch tall.

- Large Mesh- A flow straightener with spacing of 0.0485 in. and vane thickness of 0.015 in. The vanes were 0.045 in. tall.
- Metal Mesh w Metal Frame- Same material as the metal mesh with a thinner frame of only 0.125 in. thick and one inch tall.

Most of the passive resistive pieces with the exception of the "Metal Mesh w Metal Frame" used the same frame, which was 0.75 in. wide and one inch tall. The material was always placed in the flow so that it was directly on top of the unit. Therefore, some materials were only at the upstream end of the frame while others were thick enough to be as tall as the frame.

Scenario 2 Test Setup

Each unit was configured as seen below in Figure 15, which was the same as the baseline tests with the addition of the passive resistive piece.

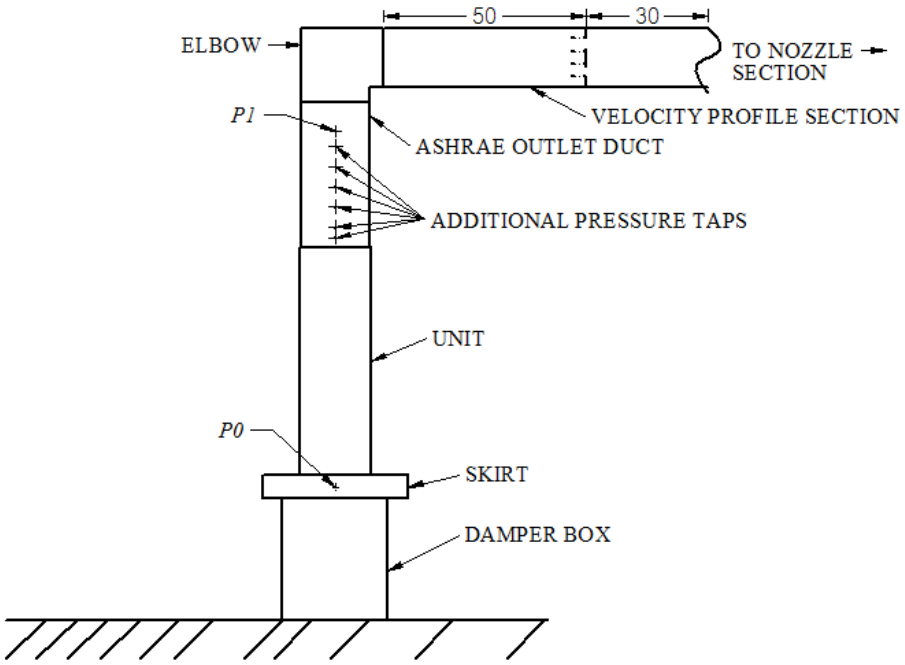

Figure 15: Scenario 2 test setup.

The dimensions of the outlet duct for the smallest unit are shown in Figure 16 in units of inches. On the left side of Figure 16 the dimensions required for ASHRAE Standard 37 are shown; that the duct be at least 36 inches long and the pressure tap be located 28.8 inches above the unit. To the right one can see the additional pressure tap locations with the first at 2.5 in. above the unit. The rest were spread five inches apart until the ASHRAE Standard 37 pressure tap location was reached. The shaded region in the figure represents the passive resistive piece.

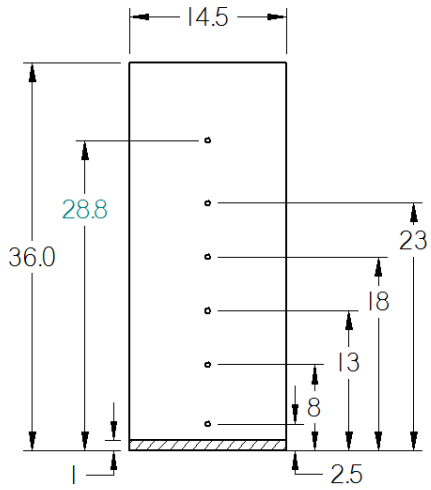

Figure 16: Dimensions [in] for Scenario 2 duct after the 2 ton unit.

In order to compare units, the additional pressure tap locations were scaled based on the ASHRAE Standard 37 pressure tap location. These values are shown in Table 6.

Table 6: Locations of pressure taps *P3-P*$_A$.

Pressure Tap	2 Ton	L/L$_A$	3 Ton	L/L$_A$	5 Ton	L/L$_A$
P3	2.5	0.08	2.5	0.08	2.5	0.07
P4	8	0.27	8.8	0.27	8*	0.24*
P5	13	0.43	13*	0.39*	11.9	0.35
P6	18*	0.60*	19.8	0.60	14.7	0.43
P7	23	0.77	25.3	0.77	20.4	0.60
P_A	30	1.00	33	1.00	34	1.00
* Denotes the physical limit due to the 85” requirement.						

The asterisked values represented the physical limit of each unit due to the 85 inch height constraint of the test apparatus including the height of the unit, the outlet duct, and an elbow.

The 3 ton unit had slightly different pressure tap locations due to the increase in height of the ASHRAE duct (Figure 17). As mentioned before, the dimensions required for ASHRAE Standard 37 are featured on the left of Figure 17 and the additional pressure taps on the right. The shaded region is for the passive resistive pieces.

Figure 18 illustrates the outlet duct for the 5 ton unit with the dimensions required for ASHRAE Standard 37 on the left and the additional pressure tap locations on the right.

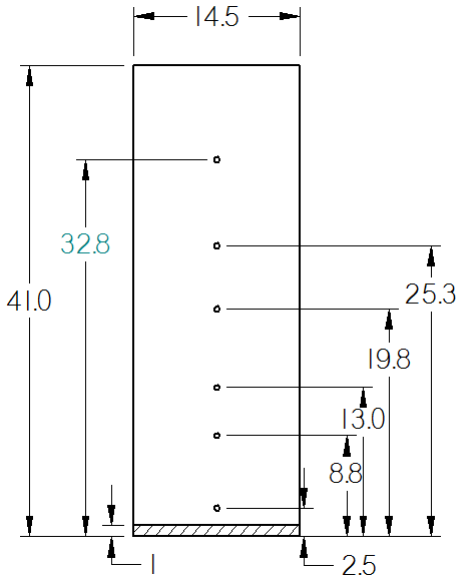

Figure 17: Scenario 2 dimensions [in] for the 3 ton unit.

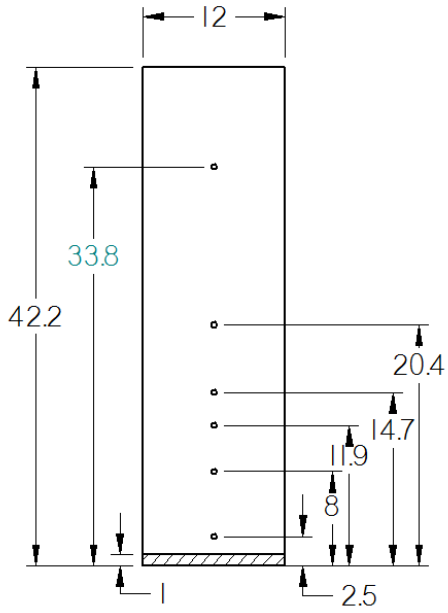

Figure 18: Scenario 2 dimensions [in] for the 5 ton unit.

Data Acquisition and Instrumentation

The collection of data was handled through two different National Instrument modules. One module collected the data from the four different pressure transmitters, the barometric pressure, and the dry bulb temperature of the nozzle. The other module (for the velocity profile) controlled the four pole double throw relay switches, R1-R4. Figure 19 illustrates the circuit powering the relay switches and the solenoids.

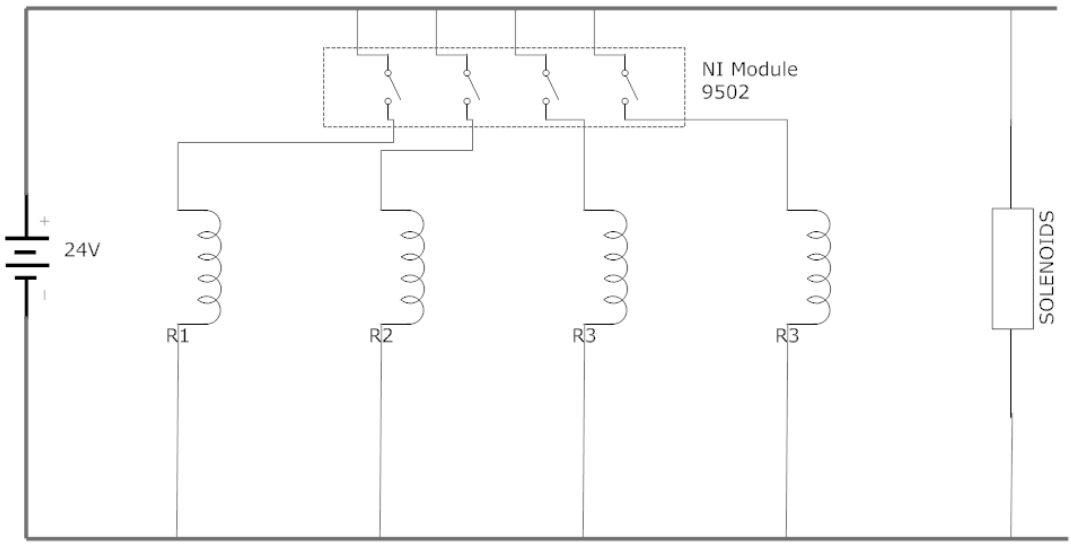

Figure 19: Electronic diagram of DAQ.

The 9502 module was connected with Labview, which controlled the four relays. The configuration as seen in Figure 19, led to eight banks of solenoids valves individually activated by a certain combination of relays. Looking further at the relays, R1-R4, Figure 20 details their setup.

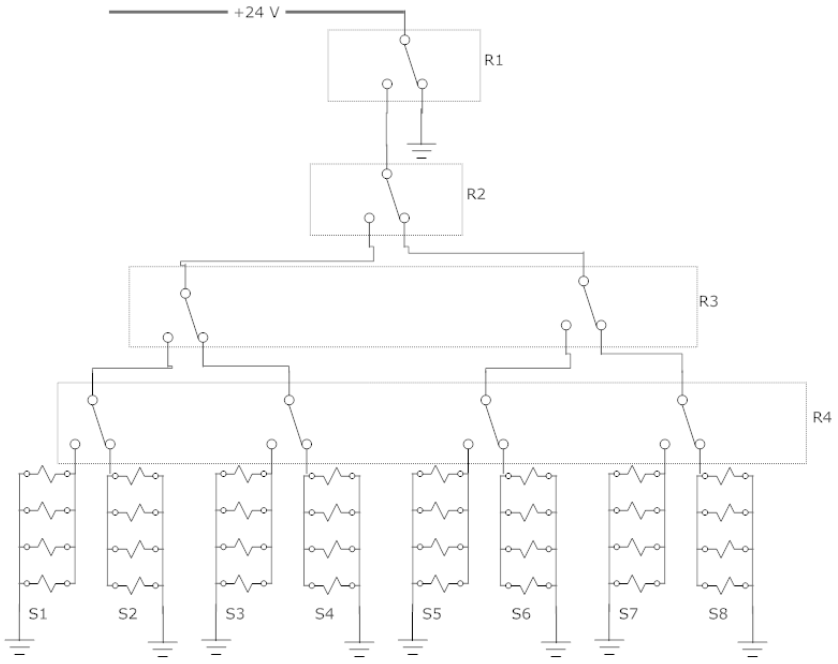

Figure 20: Ladder diagram for solenoid activation.

As shown in Figure 20, relay R1 was a master switch for the relay system. The other relays controlled the solenoid banks. The combinations to activate each solenoid bank are shown in Table 7 where 1 represents on (left) and 0 represents off (right).

Table 7: Solenoid activation table.

R1	R2	R3	R4	Solenoid Bank
0	0	0	0	-
1	0	0	0	S8
1	0	0	1	S7
1	0	1	0	S6
1	0	1	1	S5
1	1	0	0	S4
1	1	0	1	S3
1	1	1	0	S2
1	1	1	1	S1

These solenoids were used to operate the valves that in turn measured the 16 point velocity profile with sixteen 10 inch pitot tubes. Each pitot tube had two measurements, total and static pressure. This led to 32 measurements in total with each connected to an individual valve shown in Figure 21. Each solenoid was connected to a three port normally closed valve. When the solenoid was off, the valve closed the pressurized side (pitot tube).

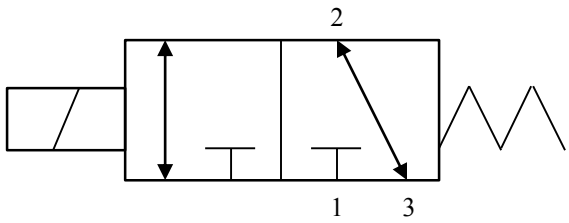

Figure 21: Solenoid valve configuration.

As seen from Figure 21, each solenoid valve had three ports. Port 1, the pressurized port connected with one of the pressure transmitters. Port 3 connected to atmosphere (relief valve), and port 2 connected to one of the pitot tube outputs. As seen in Figure 22, four manifolds contained 8 solenoid valves, with each port 2 connected with a pitot tube.

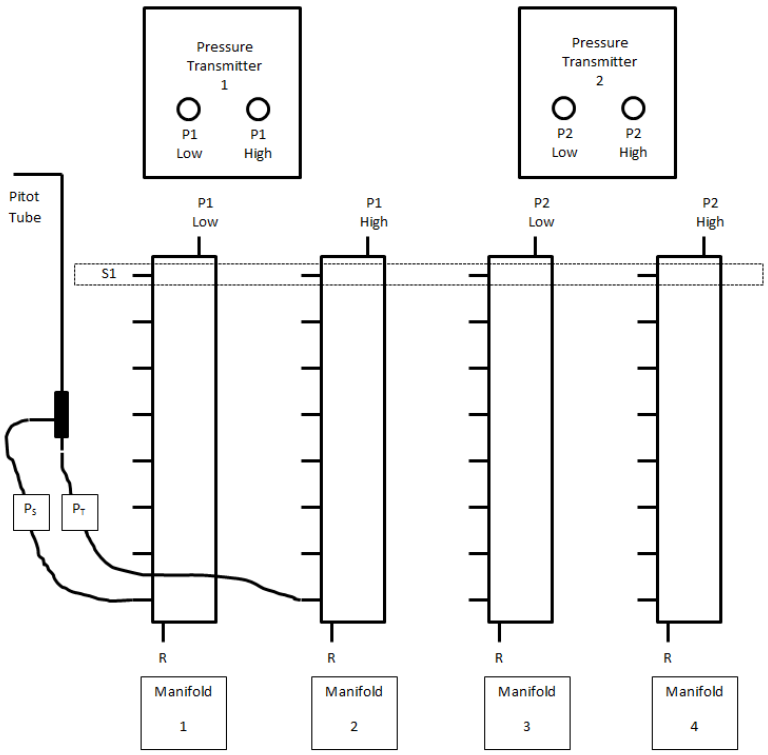

Figure 22: Instrument connections for the velocity profile.

The above Figure 22 illustrates how each bank was activated. One solenoid valve from each manifold was activated as the relays rotated through their cycle (S1-S8). The two pressure transmitters were connected to the pressurized side of the manifold. Each switch from Table 7, measured two locations for the 16 point velocity profile.

The pressure transmitters were also connected to a module in conjunction with several others measurements including, dry bulb temperature, barometric pressure, static pressure 1, static pressure 2, and differential nozzle pressure. Wet bulb temperature was manually collected from a psychometric station at the same height and 5 feet away from the test station, yet it was configured the same as the other instruments as seen in Figure 23.

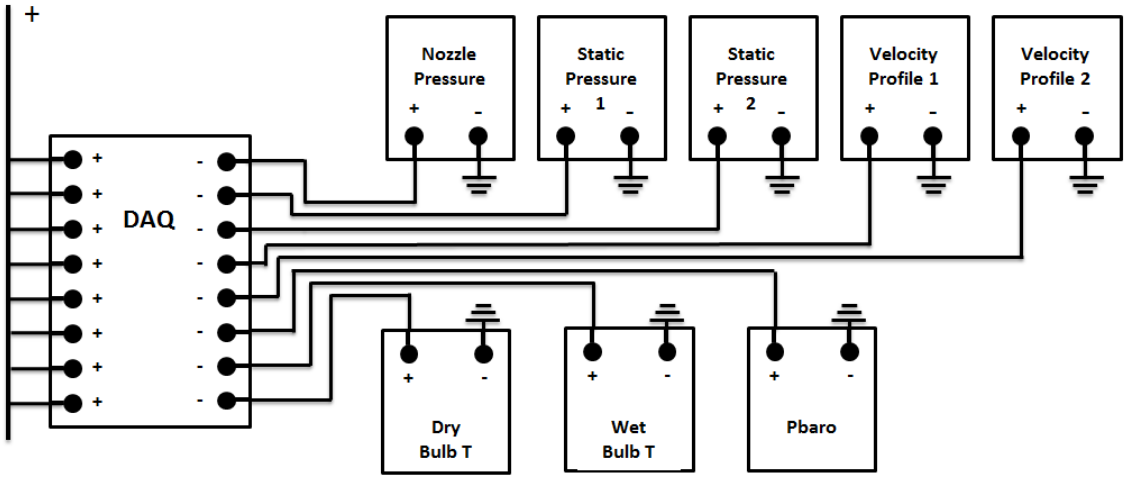

Figure 23: Electronic wiring of electronic instruments.

From Figure 23 it can see that all the instruments were connected to a data acquisition system (DAQ) and were constantly monitored throughout testing. A summary table of all the instruments used is presented below. Included in Table 8 are the instrument description, location, signal output, range, and accuracy. The nozzles were included with their diameter measurements, which were found by averaging four measurements. Two different nozzle pressure transmitters were used because the 2 and 5 ton unit required a higher range pressure transmitter. Nozzle Pressure 1, was only used for the 3 ton unit.

Table 8: List of instruments and accuracy.

Instrument Description	Location	Signal Output	Range	Accuracy
Nozzle Pressure 1	Nozzle Chamber	4-20mA	0-1in	± 1% F.S
Nozzle Pressure 2	Nozzle Chamber	4-20mA	0-3in	± 1% F.S
Static Pressure 1	P_A or *P2*	4-20mA	0-0.25in	± 0.25% F.S
Static Pressure 2	*P2* or *P3-P7*	4-20mA	0-0.25in	± 0.25% F.S
Velocity Pressure 1	Velocity Profile	4-20mA	0-0.1in	± 0.25% F.S
Velocity Pressure 2	Velocity Profile	4-20mA	0-0.1in	± 0.25% F.S
Nozzle Temperature	Nozzle Chamber	4-20mA	20-120^{o}F	± 0.36% F.S
Barometric Pressure	Damper-box Inlet	0-5V	600-1100 mb	± 1% F.S
Dry Bulb Temperature	Damper-box Inlet	4-20mA	20-120 F	± 0.36% F.S
Wet Bulb Temperature	Damper-box Inlet	4-20mA	20-120 F	± 0.36% F.S
1 in. Nozzle	Nozzle Chamber	Ø =0.9998 in.	-	Ø ± 0.001 in.
3 in. Nozzle	Nozzle Chamber	Ø =2.9944 in.	-	Ø ± 0.001 in.
5 in. Nozzle 1	Nozzle Chamber	Ø =4.9615 in.	-	Ø ± 0.001 in.
5 in. Nozzle 2	Nozzle Chamber	Ø =4.9675 in.	-	Ø ± 0.001 in.
5 in. Nozzle 3	Nozzle Chamber	Ø =4.9690 in.	-	Ø ± 0.001 in.
5 in. Nozzle 4	Nozzle Chamber	Ø =4.9695 in.	-	Ø ± 0.001 in.

TEST PROCEDURES AND METHODOLOGIES

Scenario 1 Test Procedure

Each unit was setup in the baseline test configuration (Figure 10) and the static pressure (P_A-$P0$) was set to the AHRI rating point by adjusting the variable assist fan. The voltage was adjusted as well to 230 volts, and the baseline test data were recorded. Data collected included, voltage, amperage, power, dry bulb temperature, wet bulb temperature, static pressure, differential nozzle pressure, and 16 local velocities averaged over thirty seconds for each test.

A minimum of three baseline tests were done for repeatability. The average airflow and power was found from the baseline test. The ASHRAE outlet duct was removed for the elbow test's setup. The variable assist fan was adjusted so the airflow was within 1% of the baseline average airflow. This same process was done for all three elbows and four orientations, resulting in twelve tests. Upon completion of the baseline and elbow tests the test matrix shown in Table 9, was filled.

Table 9: Test matrix for Scenario 1.

	Power	Nozzle Airflow	Unit Pressure	Density
Units	(W)	(CFM)	(in w.c)	(lbm ft-3)
Baseline 1	x	x	x	x
Baseline 2	x	x	x	x
Baseline 3	x	x	x	x
C1	x	x	x	x
C2	x	x	x	x
C3	x	x	x	x
C4	x	x	x	x
S1	x	x	x	x
S2	x	x	x	x
S3	x	x	x	x
S4	x	x	x	x
V1	x	x	x	x
V2	x	x	x	x
V3	x	x	x	x
V4	x	x	x	x

It should be noted that all the values placed in the test matrix were corrected for temperature variations (standardized). The elbow paired with elbow orientation that performed closest to the AHRI rating point was tested by setting the elbow test pressure ring, *P2*, at the AHRI rating point and observing the airflow. Thus in summary, the parameters for comparison were the power, airflow, and pressure for elbow tests and baseline tests. Since the power and airflow were required to be within 5% and 2.5% of the baseline test, the determining factor for a suitable elbow test was the static pressure.

Scenario 2 Test Procedure

The baseline tests were first performed for each unit for Scenario 2. The pressure ring, $P_{A,}$ was set to the AHRI rating point while each additional pressure ring was recorded. Similar to Scenario 1, the voltage, amperage, power, velocity profile and psychometric conditions were recorded for each test. The average airflow and power were found for the baseline tests and a passive resistive piece was set in the duct so that

the material was placed closest to the unit. The standard airflow was set to within 1% of the average baseline standard airflow while each additional pressure ring was recorded thus completing the text matrix shown in Table 10. The locations L_1-L_5, are normalized lengths that represent the distance of the pressure rings from the point of reference and are divided by the ASHRAE Standard 37 pressure ring location, L_A. It is important to note that all the pressure, airflow, and power measurements were adjusted for standard density, hence the subscript *s*.

Table 10: Test matrix for Scenario 2.

	Location	P_{AS}	P_s	Q_s	P_s	ρ
Units	(in)	(in w.c)	(in w.c)	(cfm)	(W)	(lbm.ft-3)
	L_1	x	x	x	x	x
	L_2	x	x	x	x	x
	L_3	x	x	x	x	x
	L_4	x	x	x	x	x
	L_5	x	x	x	x	x
	L_A	x	x	x	x	x

Each unit was tested with at least four passive resistive pieces. The list of passive resistive pieces was previously mentioned in Test Setup. The best performing passive resistive piece was tested at the AHRI required static pressure.

Similar to Scenario 1, the static pressure was analyzed to determine if a suitable passive resistive piece had been found. In addition to looking at the error of the static pressure as a test parameter the pressure curve was also analyzed for convergence with theoretical pressure drop.

Standard Airflow and Pressure Calculation

The below equations were provided by the ASHRAE *Handbook Fundamentals* (2009) to calculate the density of the moist air, and to correct the important parameters,

such as airflow, pressure and power, for temperature variation. Equation 14 and Equation 15 used the following constants to determine the vapor pressure at saturation temperature.

C8 = -1.0440397E +04

C9 = -1.1294650E +01

C10 = -2.7022355E -02

C11 = 1.2890360E -05

C12 = -2.4780681E -09

C13 = 6.5459673E +00

$$Pln = \frac{C8}{T_{WBr}} + C9 + C10(T_{WBr}) + C11(T_{WBr})^2 + C12(T_{WBr})^3 + C13 \ln(T_{WBr}) \quad (14)$$

$$Pws = e^{Pln} \quad (15)$$

Humidity ratio at saturation, Wxs, was then calculated using ideal gas relations in Equation 16.

$$Wxs = \frac{.621945\ Pws}{.491098\ P_{Baro} - Pws} \quad (16)$$

Assuming that the process of adding water to the air is adiabatic, enthalpy is conserved resulting in Equation 17, which finds the humidity ratio of the air.

$$W = \frac{(1093 - .556\ Tw)Wxs - .240\ (T_{DB} - T_{WB})}{1093 + .444T_{DB} - T_{WB}} \quad (17)$$

The specific volume of moist air relative to dry air (ft^3 $lbmda^{-1}$) was found with Equation 18.

$$v = \frac{.370486\ T_{DBr}\ (1 + 1.607858\ W)}{.491098\ P_{Baro}} \quad (18)$$

Since viscosity also varies with temperature, the dynamic viscosity (lbm ft^{-1} s^{-1}) was calculated (Equation 19).

$$\mu = (11.00 + .018\ T_{DB}) * 10^{-6} \quad (19)$$

To find the specific volume of wet air, the below relation from ASHRAE Standard 37 was used (Equation 20).

$$v_{np} = \frac{v}{1+W} \tag{20}$$

The Reynolds number was calculated by converting the differential pressure across the nozzles into an airflow measurement (Equation 21).

$$Re = 1.523 \frac{D_n C1}{\mu} \sqrt{\Delta P * v_{np}} \tag{21}$$

The discharge coefficient, C, which accounts for the effective area of a nozzle, is dependent on the Reynolds number as shown in Equation 22 (Bohanon 1975).

$$C = .9986 - \frac{7.006}{\sqrt{Re}} - \frac{134.6}{Re} \tag{22}$$

ASHRAE Standard 37 states that in order to use Equation 22, the Reynolds number at the nozzle must be over 12,000. This was checked for all tests taken in this project to ensure the validity of the discharge coefficient. An iterative process was used until the difference between C1 and C was less than 0.001 (ASHRAE 2007). Airflow was calculated from Equation 23.

$$Q = 1097C\ A_n \sqrt{\Delta P * vnp} \tag{23}$$

Noting that airflow is in cfm if A_n is in ft^2, ΔP is in inches of water and vnp is in ft^3/lbm moist air. Velocity was also calculated using Equation 24 for each point in the velocity profile where ΔP_v is in inches of water.

$$V = 1097 \sqrt{\frac{\Delta P_v}{\rho}} \tag{24}$$

Notice that the discharge coefficient is not part of Equation 24. This is due to the fact that the fluid is not compressed in the straight duct section as there is no geometry change in this location.

The airflow was corrected to standard airflow to make tests independent of temperature. The correction following mass conservation is seen in Equation 25.

$$Q_s = Q \frac{\rho}{\rho_s} \tag{25}$$

The standard density is set to $\rho_s = .075$ lbm ft^{-3}. Applying the same principles for pressure one gets Equation 26.

$$P_s = P \frac{\rho_s}{\rho} \tag{26}$$

A sample calculation for finding the standardized airflow and pressure can be found in Appendix B.2.

Power Calculation

The power factor was found for each test. This value relates the actual power to the calculated power due to a phase angle difference. The power factor is defined in terms of the phase angle, φ, as shown in Equation 27 (Fuchs and Mohammad 2008).

$$PF = \cos(\varphi) \tag{27}$$

The actual power was found from Equation 28.

$$\mathrm{P} = \mathrm{I\ V\ PF} \tag{28}$$

Given the power factor, the voltage and the current, it is possible to find the actual power. Power similarly needs to be corrected for temperature effects. Home Ventilating Institute states that the corrected power is found from Equation 29 (HVI 2009).

$$\mathrm{P}_s = \mathrm{P} \frac{\rho_s}{\rho} \tag{29}$$

Instrumentation Uncertainty

Before observing the results of the project it is important to understand the inherent error due to instrumentation. The RSS method was used to estimate the instrument error. Table 11 shows an estimation of error due to the instrumentation for all three units

Table 11: Uncertainty analysis of instrumentation.

Unit	Static Pressure	P_v	P_n	Q_s	V	ρ	Power	Reynolds
	(in w.c)	(in w.c)	(in w.c)	cfm	fpm	lbm.ft^{-3}	(W)	
2 Ton	0.003	0.001	0.012	8.3	13.3	5.83E-05	6.1	35
3 Ton	0.003	0.001	0.004	7.7	15.2	5.98E-05	8.7	29
5 Ton	0.003	.001	.012	26.0	15.2	5.98E-05	19.4	36

The static pressure error was found assuming a calibration error of 0.01 volts. It was shown to vary by 0.003 inches of water for all units due to the use of the same pressure transmitter. The pitot tube instrumentation error was slightly less as the pressure transmitter had a smaller range but the same error. The nozzle differential pressure was shown to change for the 3 ton unit. This was because the 3 ton unit nozzle differential pressure was small enough to allow for a more accurate pressure transmitter (smaller range). Airflow was in turn affected by the differential pressure measurement. The local velocity, V, was shown to be similar for the 3 and 5 ton unit while slightly lower for the 2 ton unit. This is due to the area increase causing a relatively similar mean velocity between 3 and 5 ton unit. Density error was due to temperature and barometric measurements and hence constant across all units. Power error increased as the unit number increased. The main error for the power measurement was due to the power factor reading. Reynolds number was simply a function of the nozzle airflow and represented the same pattern. Sample calculations of the instrumentation uncertainty for the 2 ton unit can be found in Appendix B.1.

Statistical Analysis for Pressure and Airflow Measurements

In turbulent systems it is inherent to have statistical variations in measurements. It is important to consider the amount of data needed for accurate measurements. The most important measurements are airflow and pressure.

First it is important to consider the difference between a population and a sample. Often in statistics a slice of data are used with the intent that these values will represent an average of the data. The mean and standard deviation of this data are known as the

sample mean and sample standard deviation. The entire set of data is known as the population mean, and population standard deviation.

A test with 2,439 points was taken over a period of 5 minutes to determine what is seen as the population test. Figure 24 shows airflow versus static pressure. The dependence of the two variables with each other can be seen due to the distribution around the population mean of both pressure and airflow.

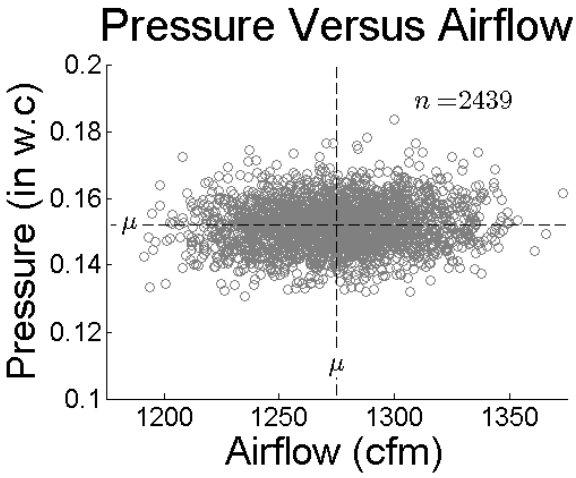

Figure 24: Pressure versus airflow distribution.

Since the data do not follow any relationship it appears that the variations of the pressure and airflow at one point are uncorrelated hence, airflow and static pressure can be looked at separately (Montgomery et al. 2007). A Gaussian curve is fit for both airflow and pressure populations in Figure 25.

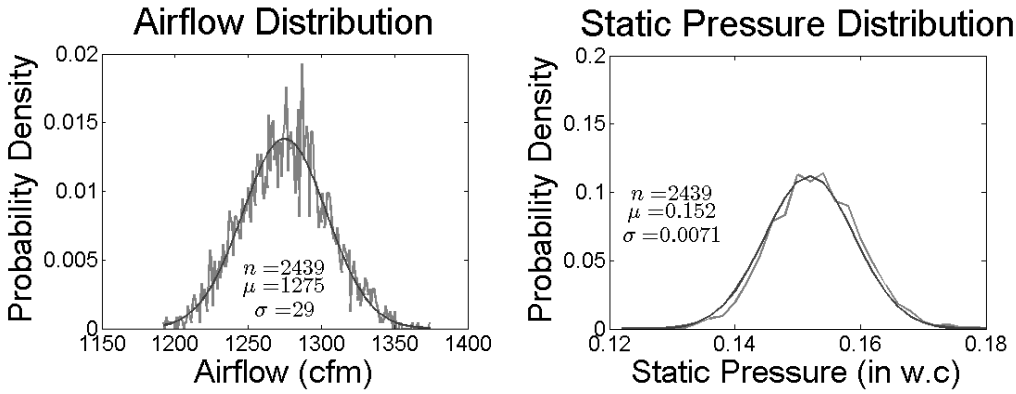

Figure 25: Gaussian distributions for airflow and static pressure.

Due to the Gaussian fit, the sample size can be found with the following Equation 29 (Montgomery et al. 2007)

$$n = \left(\frac{z\,\sigma}{\mu - \bar{x}} \right)^2 \tag{30}$$

Z is the area under the curve for a certain probability. Table 12 below calculates the number of samples needed for different confidence intervals (z).

Table 12: Estimated sample size for various confidence intervals.

	$(\mu - \bar{x})$	σ	90.2	95	99	99.5	99.9
Airflow	6	30	68	96	163	190	242
Pressure	0.002	0.011	82	116	197	230	293

With an assumed error of six cfm for airflow and 0.002 in. of water and the standard deviation calculated from the population data, the sample size can be calculated for various different confidence intervals. As can be seen in Table 12 for a confidence interval of 99.9%, around 300 samples would be needed to be within the specified error of the population mean. This can be explained further in Figure 26 and Figure 27. Various different sample sizes were taken from this population of data to see the sample

size needed for data that would accurately represent the population mean for airflow and pressure. Below Gaussian curves for various different sample sizes are shown.

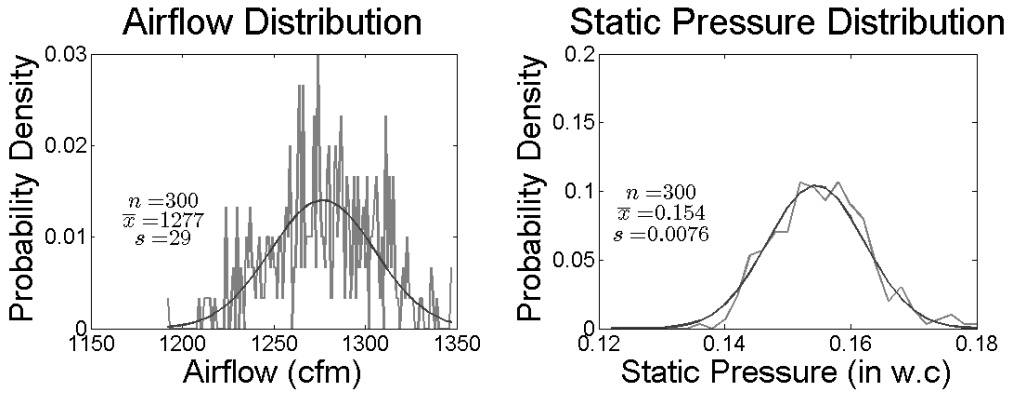

Figure 26: Gaussian distribution for a sample size of 300.

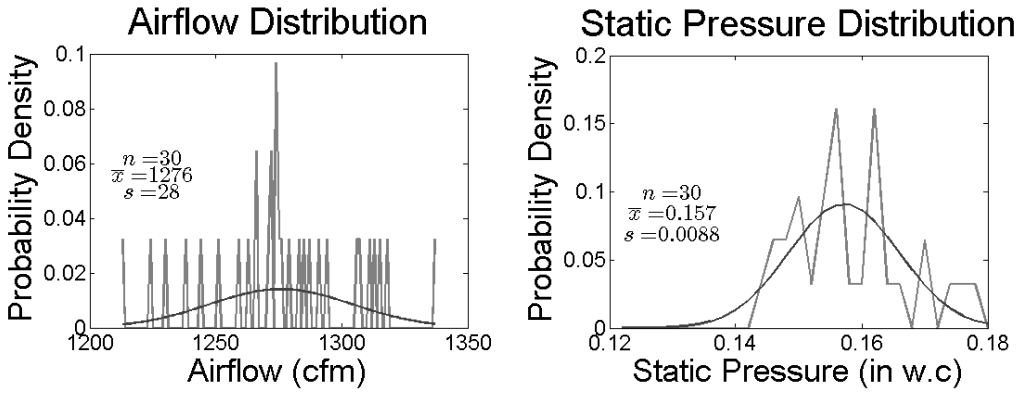

Figure 27: Gaussian distribution for a sample size of 30.

From looking at the distribution curves of the smaller samples and from the table it was decided to take a minimum of 300 samples to ensure validity of the results.

RESULTS

Scenario 1 Results

The data for Scenario 1 were organized in tests of the 2 ton unit, the 3 ton unit, the 5 ton unit, the 2 ton unit with the largest duct, and finally the 3 ton unit with the largest duct. Density was calculated following the ASHRAE *Handbook Fundamentals* (2009) and all values including power, airflow and static pressure were corrected for local temperature conditions and the compressibility of air. The test name fully describes the test taken. The letters C, S, and V correspond to curved, square, and square elbows with turning vanes. The numbers 1-4 describe the elbow orientation of the test. The baseline tests are denoted with a B. Since the power and airflow were matched, the static pressure was the variable of interest for most of the tests with exception of the Scenario 1 constant pressure tests where the static pressure was set and airflow was the variable of interest.

Scenario 1 Data for the 2 Ton Unit

The 2 ton unit displayed a complete test set with additional baseline tests as shown below in Table 13. Twelve baseline tests were completed to ensure that the elbow type and orientation did not cause downstream effects on the static pressure measurement. Airflow and power were measured and recorded after being corrected for temperature differences as mentioned above. The averages for the baseline tests were 725 cfm and 234 watts for the airflow and power respectively. Density for each test was found in order to find the correction factor and standardize power, airflow and pressure.

Table 13: Scenario 1 data for the 2 ton unit.

2 TON Units	Power (W)	Nozzle Airflow (CFM)	Unit Pressure (in w.c)	Density (lbm ft-3)
BC1	233	723	0.10	0.0737
BC2	234	724	0.10	0.0736
BC3	234	721	0.10	0.0733
BC4	232	721	0.10	0.0733
BS1	236	724	0.10	0.0739
BS2	235	734	0.10	0.0742
BS3	238	724	0.10	0.0735
BS4	231	733	0.10	0.0744
BV1	237	722	0.10	0.0746
BV2	230	723	0.10	0.0739
BV3	235	719	0.10	0.0738
BV4	235	726	0.10	0.0738
C1	236	724	0.07	0.0727
C2	236	724	0.05	0.0728
C3	233	720	0.09	0.0731
C4	239	720	0.08	0.0731
S1	237	724	0.05	0.0726
S2	234	723	0.05	0.0728
S3	238	725	0.02	0.0724
S4	232	723	0.06	0.0728
V1	238	722	0.09	0.0733
V2	235	723	0.06	0.0731
V3	237	719	0.09	0.0732
V4	237	726	0.09	0.0731

Scenario 1 Data for the 3 Ton Unit

The three ton unit was tested with three baseline tests to ensure repeatability and only the square elbow with turning vanes for the elbow tests (Table 14). The average for power and airflow were 257 watts and 1154 cfm. The static pressure for the elbow tests remained very close to the AHRI rating point with the exception of test V1. Density was shown to vary slightly due to temperature variations.

Table 14: Scenario 1 data for the 3 ton unit.

Test	Power	Nozzle Airflow	Unit Pressure	Density
Units	(W)	(CFM)	(in w.c)	(lbm ft-3)
BV3A	257	1152	0.149	0.0743
BV3B	260	1155	0.150	0.0737
BV3C	256	1157	0.149	0.0743
V1	264	1153	0.164	0.0732
V2	268	1153	0.148	0.0729
V3	262	1153	0.149	0.0735
V4	259	1154	0.148	0.0730

Scenario 1 Data for the 5 Ton Unit

The five ton unit was tested with three baseline tests and only the square elbow with turning vanes similar to the 3 ton unit as shown in Table 15. The average power was 725 watts and the average airflow was 1948 cfm for the baseline tests.

Table 15: Scenario 1 raw data for the 5 ton unit.

Test	Power	Nozzle Airflow	Unit Pressure	Density
Units	(W)	(CFM)	(in w.c)	(lbm ft-3)
BC1A	720	1946	0.200	0.0731
BC1B	724	1942	0.201	0.0727
BC1C	730	1956	0.200	0.0732
V1	706	1957	0.000	0.0732
V2	722	1949	0.249	0.0737
V3	728	1950	0.213	0.0737
V4	726	1949	0.237	0.0737

The five ton unit behaved very differently than the other units as can be seen from Table 15. Only one elbow test, V3, remained appreciably close to the AHRI rating point. As the static pressure varied so too did the power. This was seen especially with test V1 where both static pressure and power were much different than the baseline averages.

Scenario 1 Data for the 2 Ton Unit with the Larger Duct

The 2 ton unit was tested with the largest duct. Three baseline tests were performed as well as twelve elbow tests with the tests shown in Table 16. The baseline tests were performed with the square elbow with turning vanes after the static pressure measurement. The average airflow of the baseline tests was 714 cfm and average power was 226 watts. This was different from the airflow found for the 2 ton unit with the duct sized for its dimensions.

Table 16: Scenario 1 data for the 2 ton unit with the largest duct.

Test	Power	Nozzle Airflow	Unit Pressure	Density
Units	(W)	(CFM)	(in w.c)	(lbm ft-3)
BV3A	224	715	0.099	0.076
BV3B	225	715	0.100	0.076
BV3C	227	713	0.100	0.076
C1	231	714	0.106	0.074
C2	232	715	0.060	0.074
C3	233	715	0.081	0.074
C4	232	714	0.054	0.073
S1	227	715	0.075	0.074
S2	231	713	0.053	0.074
S3	231	717	0.064	0.074
S4	235	716	0.049	0.073
V1	226	714	0.100	0.075
V2	234	715	0.069	0.074
V3	225	715	0.111	0.075
V4	234	715	0.088	0.073

Scenario 1 Data for the 3 Ton Unit with the Oversized Duct

The 3 ton unit was also tested with an oversized duct (Table 17). The average airflow of the baseline tests was 1141 cfm, whereas the baseline airflow for the 3 ton previously was 1153 cfm.

Table 17: Scenario 1 data for the 3 ton unit with the largest duct.

Test	Power	Nozzle Airflow	Unit Pressure	Density
Units	(W)	(CFM)	(in w.c)	(lbm ft-3)
BC4A	266	1141	0.15	0.0733
BC4B	261	1138	0.15	0.0732
BC4C	260	1143	0.15	0.0732
C2	270	1145	0.09	0.0735
C4	272	1144	0.17	0.0735
S1	268	1145	0.14	0.0742
S2	269	1143	0.10	0.0737
S3	271	1143	0.15	0.0735
S4	271	1144	0.15	0.0738
V1	267	1144	0.18	0.0735
V2	269	1142	0.16	0.0738
V3	270	1144	0.17	0.0734
V4	272	1145	0.16	0.0736

Scenario 1 Results Set Pressure

From the unprocessed data, it is relatively obvious that the best elbow test was V3. The best elbow was further tested by setting the static pressure and measuring the airflow. Table 18 summarizes the results.

Table 18: Data for the best elbow test with airflow as the variable.

	Test	Power	Nozzle Airflow	Unit Pressure	Density
Units		(W)	(cfm)	(in w.c)	(lbm ft-3)
2 Ton	V3	230	718	0.100	0.0738
3 Ton	V3	262	1153	0.149	0.0735
5 Ton	V3	727	1954	0.201	0.0738

Scenario 2 Results

Compared with Scenario 1, the Scenario 2 data were too large to display in table format. The data results can be found in the Appendix D.1, graphical results are displayed below after the baseline tests.

Scenario 2 Baseline Tests

For reference, the baseline tests for the three air handling units were displayed in Table 19. The average baseline airflow was 728, 1153, and 1956 cfm for the 2, 3, and 5 ton unit respectively. The average power was 240, 257, and 720 watts for the 2,3, and 5 ton unit respectively.

Scenario 2 Data for the 2 Ton Unit

The 2 ton unit results for Scenario 2 were shown in Figure 28. In the figure, the AHRI rating point was plotted as a dashed line for reference. The normalized length indicates the top of the unit on the left as zero and the AHRI rating point location as unity (direction of flow to the right). The baseline test can clearly be seen. It is immediately apparent that the baseline pressure curve or pressure profile increased for the entire length of the duct.

Table 19: Scenario 2 baseline tests.

2 Ton Baseline	Location	P_{AS}	P_s	Q_s	P_s	ρ
Units	(in)	(in w.c)	(in w.c)	(cfm)	(W)	(lbm.ft-3)
	2.5	0.101	0.078	725	243	0.07512
	8	0.100	0.082	729	243	0.07510
	13	0.101	0.086	727	238	0.07509
	18	0.100	0.095	728	238	0.07509
	23	0.100	0.099	728	238	0.07503
	30	0.100	0.100	728	240	0.07509
3 Ton Baseline	Location	P_{AS}	P_s	Q_s	P_s	ρ
Units	(in)	(in w.c)	(in w.c)	(cfm)	(W)	(lbm.ft-3)
	2.5	0.151	0.132	1156	256	0.07450
	8.8	0.149	0.137	1151	257	0.07432
	13	0.151	0.138	1154	257	0.07426
	19.8	0.149	0.139	1150	257	0.07424
	25.3	0.149	0.146	1154	257	0.07427
	33	0.150	0.150	1153	257	0.07432
5 Ton Baseline	Location	P_{AS}	P_s	Q_s	P_s	ρ
Units	(in)	(in w.c)	(in w.c)	(cfm)	(W)	(lbm.ft-3)
	2.5	0.200	0.080	1961	717	0.0736
	8	0.200	0.052	1957	717	0.0737
	11.9	0.201	0.076	1955	727	0.0736
	14.7	0.199	0.096	1953	717	0.0734
	20.4	0.198	0.125	1956	724	0.0735
	33.8	0.200	0.200	1956	720	0.0736

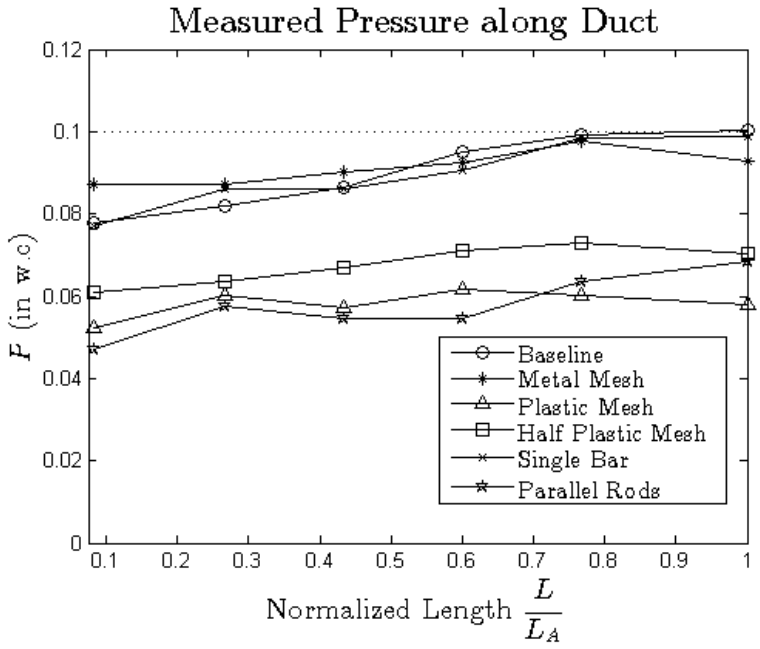

Figure 28: Pressure curves for the 2 ton unit passive resistive pieces.

Several passive resistive pieces displayed static pressure that increased similar to the baseline test initially and then began dropping. This was an indication that the pressure measurements were reading correctly as theory shows that pressure should drop for fluid moving through a duct (Churchill 1977 and Moody 1944). The metal mesh and single bar profiles appeared to follow the baseline profile closely while the plastic mesh, half plastic mesh, and parallel rod pressure curves were much more level and showed lower average static pressure.

Scenario 2 Data for the 3 Ton Unit

The Scenario 2 data for the 3 ton unit involved four passive resistive pieces in addition to the baseline test as shown in Figure 29. Most passive resistive piece pressure profiles appeared relatively level with the exception of the double strip pressure profile, which rose until a normalized length of 0.8. The half plastic mesh profile appeared to begin dropping at around 0.3 normalized length which looked promising.

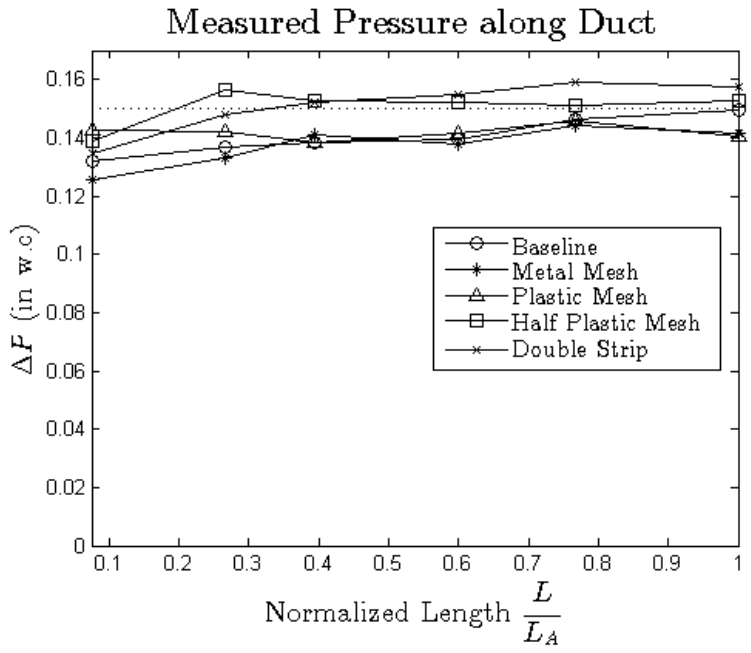

Figure 29: Pressure drop of 4 passive resistive pieces and the baseline test for the 3 ton unit.

Scenario 2 Data for the 5 Ton Unit

Figure 30 displays the passive resistive pieces that were tested for the 5 ton unit. The pressure drop due to the passive resistive pieces was especially prevalent with the 5 ton unit as almost all the static pressure points of the materials were below the baseline test pressure profile. The maximum pressure drop was for the metal mesh with a metal frame, which showed a drop of 0.16 inches of water.

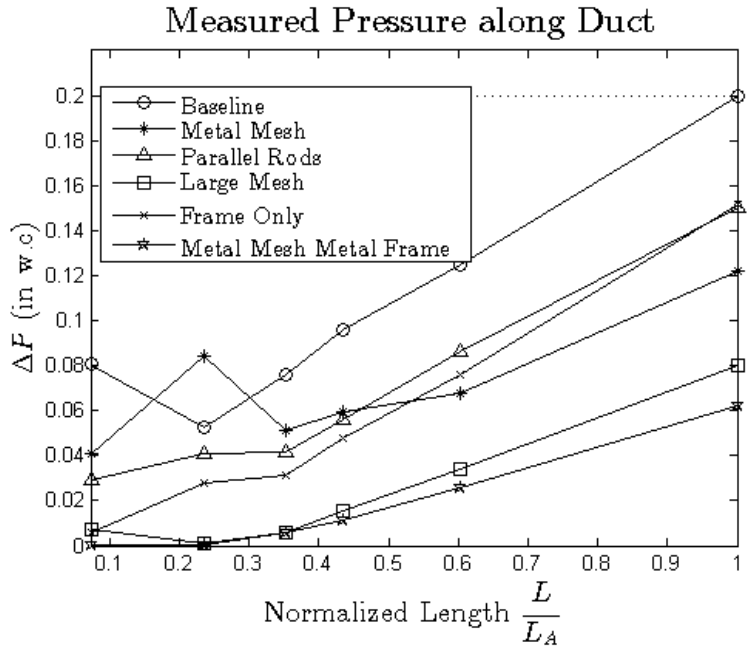

Figure 30: Pressure drop of 5 passive resistive pieces and the baseline test for the 5 ton unit.

Scenario 2 Results Set Pressure

The best passive resistive pieces for the 2 and 3 ton unit were further tested by setting the static pressure at the AHRI rating point and looking at the airflow and pressure curve. The 5 ton unit was not tested with set pressure due to the large pressure drops seen in the results.

2 Ton Unit Set Pressure

Below, results of both metal mesh tests are shown in Figure 31. As said before, the two tests plotted the same material with different set points, baseline airflow, Q_B, and AHRI rating point, P_A. The metal mesh pressure curves appeared to be very similar. Both began to drop at the same normalized length of 0.8 and had the same slope for the beginning of the curve.

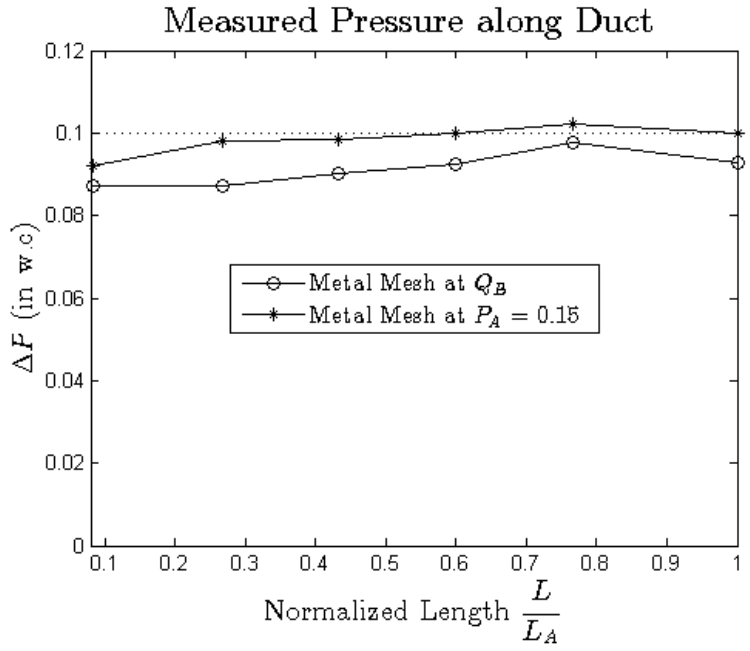

Figure 31: 2 ton unit metal mesh performance for set pressure and airflow.

3 Ton Unit Set Pressure

Due to the good performance of the plastic mesh for the 3 ton unit and the good performance of the metal mesh for the 2 ton unit, both were further analyzed for the 3 ton unit by setting the pressure at 0.15 in. of water and comparing airflow and pressure measurements as shown in Figure 32. Both the metal mesh and plastic mesh profiles appeared level, although there was a noticeable average increase of the static pressure in the set pressure tests.

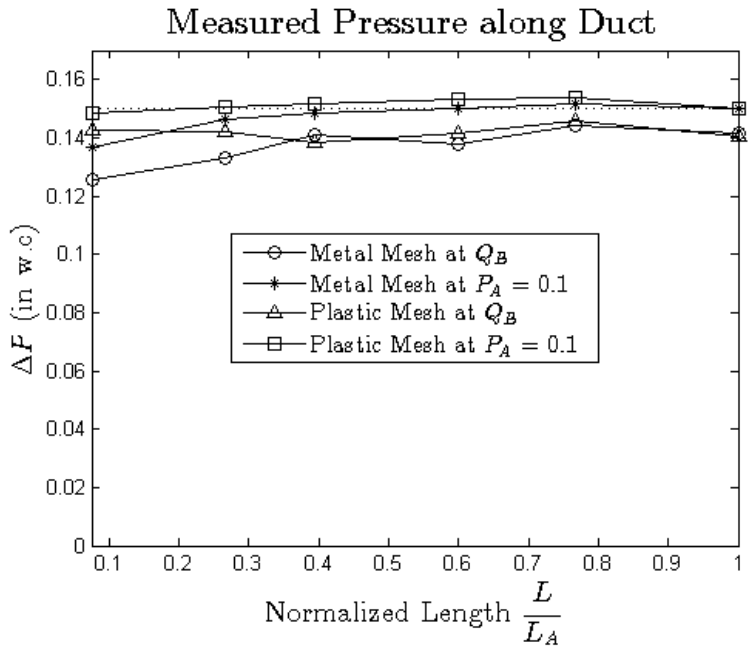

Figure 32: Comparison of metal and plastic mesh performances for the 3 ton unit.

ANALYSIS

Comparison of Baseline Tests

Different baseline tests were completed for each unit and each scenario. It is worth comparing the average values of airflow and power amongst baseline tests to ensure repeatability. Table 20 displays the average results for all the baseline tests in this project. Table 21 normalizes these values compared with Scenario 1 for ease of understanding.

Table 20: Average airflow and power for baseline tests for all units and scenarios.

	Scenario 1		Scenario 1 Largest Duct		Scenario 2	
	Power	Airflow	Power	Airflow	Power	Airflow
Units	(W)	(cfm)	(W)	(cfm)	(W)	(cfm)
2 Ton	234	725	226	714	240	728
3 Ton	257	1154	262	1141	257	1153
5 Ton	725	1948	-	-	720	1956

In general, the values appear to agree readily although if the largest duct were compared with Scenario 2, differences above 5% for power would be seen. The only issue comes from Scenario 1 with the largest duct in fact.

Table 21: Normalized baseline test airflow and power for Scenario 1 with the largest duct and Scenario 2 with respect to Scenario 1 baseline.

	Scenario 1L		Scenario 2	
	Power	Airflow	Power	Airflow
2 Ton	-3.7	-1.4	2.5	0.4
3 Ton	1.8	-1.2	-0.3	-0.1
5 Ton	-	-	-0.6	0.4

It differs enough from the three units with their original size duct and from Scenario 2 that it deserves mentioning. The largest duct dropped the baseline power and airflow by 3.7% and -1.4% for the 2 ton unit (Table 21). The 3 ton unit similarly changed in airflow by -1.2%. This suggests that the increase in area from the unit to duct may have created error in the measurements. Since the static pressure was set, this error possibly translated to the airflow measurement explaining the decrease in airflow for both units with the largest duct. There may even be a relationship between the ratio of unit exit area to the duct area and the airflow error but the data are too close to the instrumentation error to be sure.

Comparison of Scenario 1 Tests

As mentioned in the Introduction and the TRP-1581, the different Scenarios were to be compared with a baseline test. In the following sections the 2, 3, and 5 ton units were compared with the baseline tests for analysis of results.

Comparison of Baseline and Elbow Tests: 2 Ton Unit

Table 22 compares the baseline tests and the elbow tests for the 2 ton unit and calculates the percent difference. The largest difference between baseline and elbow test in power was 2.7% and the largest difference in airflow was 1.5%. This was well below the maximum difference of power and airflow of 5% and 2.5% as stated in the RFP, yet the differences in unit pressure varied significantly and were dependent on elbow type and orientation.

Table 22: Comparison of baseline and elbow tests for the 2 ton unit.

2 TON Units		P_B (W)	P (W)	% Diff	Q_B (cfm)	Q (cfm)	% Diff	ΔP_B (in w.c)	ΔP (in w.c)	% Diff
	C1	233	236	1.5	723	724	0.1		0.066	-35
	C2	234	236	1.1	724	724	0.1		0.050	-50
	C3	234	233	-0.4	721	720	-0.2		0.090	-9
	C4	232	239	2.7	721	720	-0.1		0.075	-25
	S1	236	237	0.2	724	724	0.0		0.052	-48
	S2	235	234	-0.6	734	723	-1.5	0.10	0.046	-54
	S3	238	238	-0.1	724	725	0.2		0.023	-76
	S4	231	232	0.5	733	723	-1.3		0.055	-44
	V1	237	238	0.7	722	722	0.0		0.089	-12
	V2	230	235	2.1	723	723	0.1		0.065	-35
	V3	235	237	0.8	719	719	0.0		0.093	-7
	V4	235	237	1.1	726	726	0.0		0.089	-11

As expected, all of the static pressure values for the elbow tests were less than the AHRI rating point of 0.1 in. of water due to the additional pressure loss that occurred at the elbow. The elbow that performed the best was the square elbow with turning vanes. This elbow had three different tests that were within 12% of the unit pressure of the baseline tests. The curved and square elbows consistently performed worse than the square elbow with turning vanes as was predicted (Table 2). The square elbow performed the worst. The elbow unit pressure was much lower than the baseline tests. This suggested that the dynamic pressure loss for the square elbow was too great and would not be an appropriate alternative for ASHRAE Standard 37 outlet geometry as mentioned previously. Although the curved elbow was within 9% of the AHRI static pressure for C3, all the other elbow orientations with the same elbow had a much higher percent error suggesting that this type of elbow would also be a poor fit.

Comparison of Baseline and Elbow Tests: 3 Ton Unit

Table 23 shows a summary of the baseline results for the 3 ton unit. Three elbows recorded static pressures within 1% of the AHRI static pressure while keeping within the

requirements for power and airflow. Orientation 1 showed a 10% increase in the static pressure with the addition of the elbow for the elbow test. This again pointed to the importance of orientation in reducing pressure drop across the elbow.

Table 23: Comparison of baseline and elbow tests of the 3 ton unit.

3 Ton		PB	P	% Diff	QB	Q	% Diff	ΔPB	ΔP	% Diff
Units		(W)	(W)		(cfm)	(cfm)		(in w.c)	(in w.c)	
	V1		264	2.6		1153	-0.1		0.164	10
	V2	257	268	4.1	1154	1153	-0.1	0.149	0.148	-1
	V3		262	1.8		1153	-0.1		0.149	0
	V4		259	0.8		1154	0.0		0.148	-1

Comparison of Baseline and Elbow Tests: 5 Ton Unit

The 5 ton unit summarized results are shown in Table 24. In this particular test matrix the relationship between power and airflow was more clearly seen. Power was shown to change with static pressure, although the power difference was within the TRP-1581 requirements. The static pressure varied greatly with the best performance for the test V3.

Table 24: Comparison of baseline and elbow tests for the 5 ton unit.

5 Ton		P_B	P	% Diff	Q_B	Q	% Diff	ΔP_B	ΔP	% Diff
Units		(W)	(W)		(CFM)	(CFM)		(in w.c)	(in w.c)	
	V1		706	-2.5		1957	0.5		0.000	-100
	V2	725	722	-0.3	1948	1949	0.0	0.200	0.249	24
	V3		728	0.4		1950	0.1		0.213	6
	V4		726	0.2		1949	0.0		0.237	18

Oversized Duct Comparison of Baseline and Elbow Tests: 2 Ton Unit

The 2 ton unit was also tested with the largest duct. Table 25 summarizes the results. Even when changing the outlet duct dimensions, the square elbow with turning vanes performed the best, although there was a marked improvement in curved and square elbow performance. The elbow pressure drop measured during the baseline tests can explain this. As shown in Table 16, the values were negative, showing that the increase in area dropped the mean velocity enough to reduce the elbow dynamic pressure drop for the baseline test with a square elbow with turning vanes. With no settling means and a shorter distance to reach the elbow, a significant pressure drop was seen in the elbow tests in some orientations, but if one were to increase the area more significantly the pressure drop from the elbows could be decreased to become negligible.

Table 25: Comparison of baseline and elbow tests for the 2 ton with the largest duct.

2 TL		P_B	P	% Diff	Q_B	Q	% Diff	ΔP_B	ΔP	% Diff
Units		(W)	(W)		(CFM)	(CFM)		(in w.c)	(in w.c)	
	C1		231	2.3		714	0.1		0.106	6
	C2		232	2.5		715	0.2		0.060	-40
	C3		233	3.2		715	0.1		0.081	-19
	C4		232	2.6		714	0.0		0.054	-46
	S1		227	0.3		715	0.1		0.075	-25
	S2	226	231	2.2	714	713	-0.1	0.100	0.053	-47
	S3		231	2.2		717	0.4		0.064	-36
	S4		235	3.8		716	0.2		0.049	-51
	V1		226	-0.1		714	-0.1		0.100	0
	V2		234	3.4		715	0.1		0.069	-31
	V3		225	-0.5		715	0.1		0.111	11
	V4		234	3.7		715	0.2		0.088	-12

Oversized Duct Comparison of Baseline and Elbow Tests: 3 Ton Unit

The 3 ton unit was tested with the oversized duct. The data can be found below in Table 26. Several elbows performed better due to the increase in duct dimension. The square elbow with turning vanes had three orientations under 10%.

Table 26: Comparison of baseline and elbow tests for the 3 ton unit with the largest duct.

3 TL		P_B	P	% Diff	Q_B	Q	% Diff	ΔP_B	ΔP	% Diff
Units		(W)	(W)		(CFM)	(CFM)		(in w.c)	(in w.c)	
	C2		270	3.1		1145	0.3		0.085	-43
	C4		272	3.7		1144	0.3		0.17	10
	S1		268	2.1		1145	0.4		0.14	-6
	S2	262	269	2.8	1141	1143	0.2	0.15	0.10	-34
	S3		271	3.4		1143	0.1		0.15	-2
	S4		271	3.6		1144	0.3		0.15	1
	V1		267	2.1		1144	0.2		0.18	19
	V2		269	2.6		1142	0.1		0.16	7
	V3		270	2.9		1144	0.3		0.17	10
	V4		272	3.9		1145	0.4		0.16	5

Comparison of 2, 3, and 5 Ton Units with Set Pressure

The best elbows were picked and retested with the static pressure set to the AHRI rating point as seen in Table 27. The largest difference between baseline and elbow tests was for the power measurement, yet it was within the 5% requirement. Airflow and static pressure were negligibly different.

Table 27: Comparison of baseline and elbow test with set static pressure.

	P_B	P	% Diff	Q_B	Q	% Diff	ΔP_B	ΔP	% Diff
Units	(W)	(W)		(CFM)	(CFM)		(in w.c)	(in w.c)	
2 Ton	235	230	-1.9	719	718	-0.1	0.1	0.100	0.4
3 Ton	257	262	1.8	1154	1153	-0.1	0.149	0.149	-0.4
5 Ton	725	727	0.3	1948	1954	0.3	0.200	0.201	0.3

Scenario 1 Analysis Summary

The previous sections have taken time to compare the elbow tests for section of testing within Scenario 1 (units, oversized duct, and set pressure). This section focuses on the comprehensive view. As it was shown that power and airflow remained within 5% and 2.5% for power and airflow, respectfully, it was helpful to compare the elbow test's performance in terms of only pressure percent error compared with the AHRI rating point for all the units. First the pressure percent error of the 2 ton unit, 2 ton unit with the oversized duct, and the 3 ton unit with the oversized duct (denoted L in the table) were compared in Table 28 as they were the only complete test matrices.

Table 28: Percent error of the static pressure measurement for the complete elbow tests.

	2 Ton	2 Ton L	3 Ton L
C1	-34.8	5.8	-
C2	-50.3	-39.8	-43.3
C3	-8.9	-19.1	-
C4	-24.8	-46.3	10.2
S1	-47.8	-25.2	-5.8
S2	-53.5	-47.5	-34.2
S3	-76.3	-35.9	-2.3
S4	-44.4	-50.8	0.8
V1	-11.8	0.0	19.1
V2	-34.8	-30.8	7.1
V3	-7.4	11.1	10.1
V4	-11.3	-12.1	5.5

Every square and curved elbow had at least one test with over 34% error with the exception of C3. In general the larger duct dropped the static pressure error although this was not always the case. For example, the square elbow with turning vanes did not change drastically in Table 28, suggesting that it was the least sensitive to upstream disturbances. The square elbow with turning vanes clearly had the lowest pressure error when comparing to the other two elbow types. Comparing only the square elbow with

turning vanes further analysis which orientation from the best elbow type performed the best (Table 29).

Table 29: Pressure percent error of the square elbow with turning vanes for Scenario 1.

	2 ton	3 ton	5 ton	2 ton L	3 ton L
V1	-11.8*	9.8*	-99.9	0.0*	19.1
V2	-34.8	-0.7*	24.5	-30.8	7.1*
V3	-7.4*	-0.4*	6.2*	11.1*	10.1*
V4	-11.3*	-0.7*	18.5	-12.1	5.5*
* Denotes percentages below 12%.					

The values under 12% error were asterisked to clearly show the best elbow test. There were certain tests that performed better than V3 with certain units but overall, V3 had the least percent error with pressure.

Comparison of Scenario 2 Tests

Scenario 2 results similarly found large amounts of data for the 2, 3, and 5 ton units. For analysis, the passive resistive tests were compared with the baseline tests. In this way, the passive resistive pieces that performed the closest to the baseline could be found.

2 Ton Unit Passive Resistive Pieces

At first appearance, the metal mesh and 1 bar passive resistive pieces appeared to perform well in comparison with the baseline test. As seen in Figure 28, the other materials lowered the static pressure average from the AHRI rating point. This may be due to the pressure drop of the passive resistive piece or the instrumentation error in airflow. In order to further look at the results, percent error was calculated compared with each test's ASHRAE Pressure and shown in Figure 33 below.

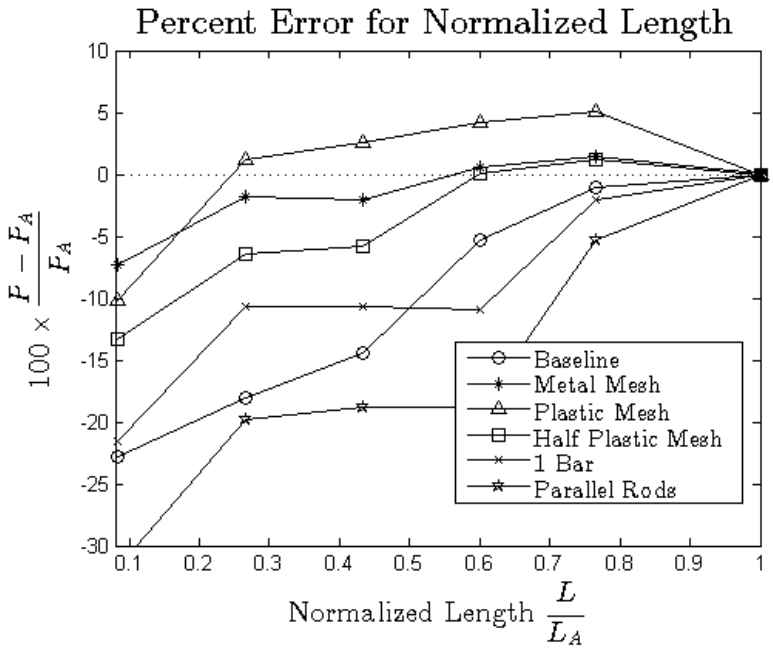

Figure 33: Percent error of the pressure drop along the outlet duct.

Figure 33 illustrates the pressure curves of the passive resistive pieces along the straight duct with no comparison to the AHRI rating point. This effectively ruled out instrumentation error due to airflow. From Figure 33, it can be deduced that the parallel rods performed worse than the baseline, suggesting an increase in non-uniformity. In addition, the 1 bar passive resistive piece was separated from the metal mesh. The metal mesh had the least percent error and was the top performer in Figure 28. In Figure 33, the metal mesh was able to record zero error at the 85 in. cutoff limit of .6 normalized length or 18 inches. The largest error for the metal mesh was less than 10% of the static pressure obtained at P_A at the pressure ring closest to the top of the unit. Another test with the metal mesh was performed with the static pressure at 0.1 in. of water and the airflow as the variable due to the good performance in the previous test.

Airflow and power changed to by -2.12% and 1.33% respectively. This was less than the maximum allowed variation stated by TRP-1581.

3 Ton Unit Passive Resistive Pieces

To better separate the four materials, the percent error was found compared with the ASHRAE pressure tap location in Figure 34. All of the materials were within 15% error compared to the ASHRAE pressure tap. The plastic mesh and half plastic mesh resulted in the least amount of error, however, due to the performance of the metal mesh in the 2 ton unit, both the plastic mesh and the metal mesh were chosen for additional testing.

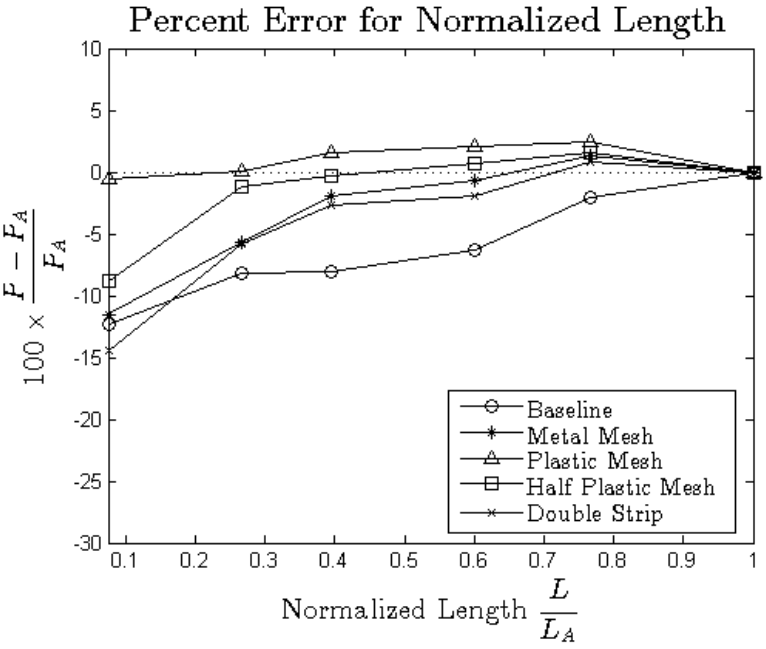

Figure 34: Percent error of the 3 ton unit for Scenario 2.

Comparison of airflow and power resulted in less than 0.34% and 1.3% error between the four tests, which led to the conclusion that the plastic and metal mesh did not appear to affect airflow and power outside the instrumentation error.

5 Ton Unit Passive Resistive Pieces

Of note were two tests from the 5 ton unit. The "Frame only", was the test of just the frame that was .75 in. wide. This test was performed after the other passive resistive

pieces that had been tested previously did not perform as expected. The frame only test may have explained all the other curve shapes, as they were all very similar in shape. The "Metal Mesh Metal Frame" was a test with the metal mesh with a different frame to ascertain the effect of the thickness of the frame. This test had a similar shape as the others although the increase in pressure was slightly less suggesting that the pressure change had leveled slightly. The poor performance was therefore left to two possibilities, either the air handler type or the air handler capacity. Either the fact that the blower was above the heat exchanger created an irreversible non-uniform velocity profile, or the airflow was too quick to allow for settling. Either way due to the height limit the 5 ton unit needed a passive resistive piece to measure static pressure accurately within 0.24 normalized length (8 in.) of the top of the unit. None of the passive resistive pieces were within 30% error of their pressure at the ASHRAE Standard 37 location at 0.24 normalized length as shown in Figure 35, hence it was considered that the 5 ton unit was not suitable for a passive resistive piece solution.

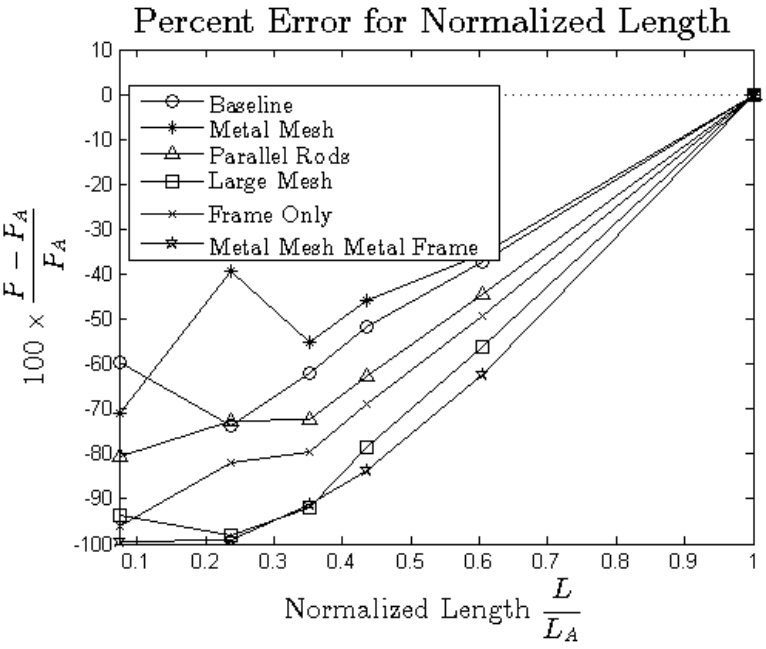

Figure 35: Percent error of the 5 ton unit compared to the AHRI rating point.

VELOCITY DATA AND ANALYSIS

Velocity Profile Data

The visual results for the 16 point velocity profile are displayed in Appendix D. At least 90 velocity profiles were taken. Since it was important to see the effects of the upstream configuration, the normal lengths before and after velocity profile measurements were not adhered to (per ASHRAE Standard 37 recommendations), otherwise it would be likely to only see uniform velocity profiles which would not be as helpful for analysis.

Velocity Profile Observations

The observations of the velocity profiles were summarized below in bullet format due to the large amount of velocity profiles and observations.

Velocity Profile Observations for the 2 Ton Unit

- The curved and square elbow velocity profiles were very similar.
- The turning vane baselines had a lower crosswise velocity gradient than the square and curved elbows and at times almost approached symmetry.
- Elbow tests S1, C1, S3, C3 displayed the most uniform velocity profiles possibly due to a recirculation zone that increased velocity mixing.
- The orientations 2 and 4 were often mirror images of each other (refer to the 2 Ton unit S2 and S4, Appendix D.2).

Velocity Profile Observations for the 3 Ton Unit

- The baseline velocity profiles displayed a concentration of high velocity at the top of the duct.
- Elbow tests V2 and V4 displayed the largest crosswise velocity gradients.
- The maximum velocity was found in elbow test V4.

Velocity Profile Observations for the 5 Ton Unit

- The 5 ton unit marked a noticeable increase in average velocity as high as 25 FPS.
- The baseline tests displayed the horseshoe shape defined earlier.
- V1 and V3 had concentrated high velocity sections on the left side.
- V2 and V4 were mirror images of each other. They both featured high velocity sections at the top that extended down past the middle of the duct.

Velocity Profile Observations for the 2 Ton Unit with the Oversized Duct

- Average velocity dropped significantly due to the increase in area with the larger duct.
- High velocity gradients were still seen in orientations 2 and 4.
- Square and curve elbow velocity profiles were very similar.

Velocity Profile Observations for the 3 Ton Unit with the Oversized Duct

- Baseline velocity profiles showed large velocity gradients.
- The square elbow with turning vanes had less extreme velocity gradients.
- The square elbow with turning vanes also displayed two horseshoe shaped velocity profiles.

Scenario 1 Velocity Profile Observations Summary

From the velocity profiles a couple points can be made directly for Scenario 1.

- Table 30 summarizes the aspect ratios related to orientation number. Aspect ratio was shown to affect the velocity profile greatly.

Table 30: Aspect ratios of all three units related to elbow orientation.

Orientation	2 Ton Unit	3 Ton Unit	5 Ton Unit
1	1.0	0.8	0.5
2	1.0	1.3	2.0
3	1.0	0.8	0.5
4	1.0	1.3	2.0

The largest extremes in velocity were found in orientations 2 and 4 for all units in Scenario 1. This corresponded with aspect ratios greater than 1 even for the 2 ton unit, which was not perfectly square (14.35 by 14.5) but nearly so.

- Mean velocity (due to blower size) and aspect ratio affected the velocity profile greatly.
- Baseline tests in general portrayed a high velocity section in the upper to middle section. They also had lower maximum local velocities than other tests.
- Aspect ratios larger than 1 showed a dramatic increase in velocity gradients.
- For the aspect ratios less than 1, a progression seemed common from large velocity gradients, to horseshoe, and finally uniform profile. The type of elbow appeared to affect the rate at which this progression occurred.
- Recirculation zone may be the reason for uniform velocity profiles for S1 and S3 due to increased mixing, yet can cause large pressure drop as shown in background. Orientations 2 and 4 show no such formation.
- Orientations for 2 and 4 for all units always switch high velocity profile bias from left to right or vise versa.
- As mean velocity increased the high velocity section appeared to increase in size with over half of the duct area recording high velocities for the 5 ton unit.

Scenario 2 Velocity Profile Observations

From the velocity profiles a couple points can be made directly for Scenario 2.

- Every passive resistive piece increased the settling (even the frame only) compared with Scenario 1 even though all three elbow types were used.
- Velocity profiles for the 3 ton unit approached perfect uniformity. It is possible this is due to the motor type.
- The velocity profiles were very similar amongst the units with high velocity sections in the upper region, possibly because the same elbow types and orientations were used for each passive resistive piece and due to the small pressure drop across them. This was with one exception where the large mesh, which was predicted to have the largest pressure drop, flipped the velocity profile.

Velocity Profile Analysis

- The baseline tests displayed a "horseshoe" shaped velocity profile often. This is defined by the low velocity section, which has at least a three point section of low velocity. This is an important distinction for velocity profiles as the baseline tests are meant to show accurate and reliable results hence why an exemplary velocity profile is redisplayed in Figure 36.

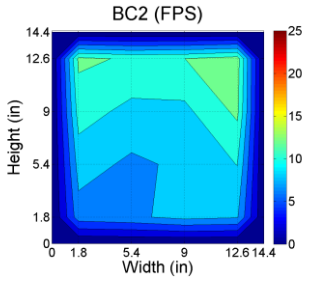

Figure 36: Example of horseshoe shaped velocity profile for the 2 ton unit.

The elbow tests that were the closest to the AHRI rating point displayed this horseshoe shape as well.

- Orientations 1 and 3 for the squared and curved elbow were the most uniform velocity profiles. The square elbow associated orientations 1 and 3 with a large difference from the AHRI rating point suggesting that the uniform velocity profile was due to a recirculation zone that mixed velocities but also increased the pressure drop across the elbow. The curved elbow in orientations 1 and 3 at times was close to the AHRI rating point in addition to being uniform.
- Uniform velocity profiles were not always associated with low pressure drop across the elbow.
- The horseshoe shape was most often seen to correlate with low pressure drop.

CASE STUDIES

As the project neared completion, a number of questions arose that were determined to be important for the TRP-1581 project objectives and scope either directly, because the questions pertained to the Scenario 1 and Scenario 2 recommendations for modifying ASHRAE Standard 37, or indirectly because the questions revealed potential issues in ASHRAE Standard 37 testing. Many of the questions were partly answered with a minimum amount of data being collected for the purpose of supporting Scenario 1 and Scenario 2 recommendations. Some of the questions were not answered through data collection; instead, they were addressed through analysis based on extensive testing and experiments previously done as part of this project. In this case, additional work would be required to fully answer the question in focus. Analysis and experimental data associated with these "questions" were not in the TRP-1581 project scope, even though it was performed in support of the project. Even so, it is important to document the data and analysis that resulted from addressing these questions as the analysis, which is partially given in this report or suggested as the subject of a future study, is important for accurately evaluating unit performance through experimentation. ASHRAE Standard 37 similar to most standards is continuously being critically evaluated and improved by industry engineers on standard committees, and the "question" data and analysis presented herein may contribute to improving ASHRAE Standard 37. These important questions and their partial answers are documented herein in the form of ten case studies.

CS-1: ASHRAE Standard 37 Static Pressure Measurement Position Validation

Is the ASHRAE Standard 37 static pressure ring location, based on the calculated distance between the unit outlet and the static pressure measurement point, correctly specified for an accurate pressure measurement?

According to ASHRAE Standard 37 the duct section length, L_E, attached to the unit outlet must be calculated from Equation 29.

$$L_E = 2.5\sqrt{a\ b} \tag{31}$$

With “a” and “b” being duct cross-sectional dimensions. The pressure ring location referenced to the outlet, is defined by Equation 30.

$$L_A = 2\sqrt{a\ b} \tag{32}$$

It can be assumed that those calculations are based on ensuring that the pressure ring reads accurately relying on an appropriate distance for straightening the flow and minimizing maldistributions (Appendix B.3). An important question is whether Equation 30 provides enough distance to accurately measure the static pressure? This question was investigated in this project by identifying the parameters important for the static pressure measurement.

Figure 37 illustrates the blast area versus the outlet area of a common air-handler unit.

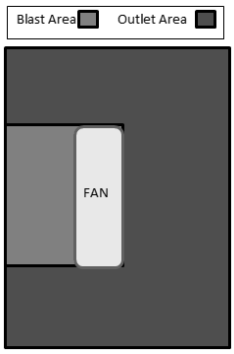

Figure 37: Blower outlet dimensions at the unit outlet.

The measured velocity profile directly downstream of the unit is non-uniform as seen in Figure 38. Of special importance, this profile shows a high velocity section right above the blast outlet from the fan signifying that this flow is highly non-uniform; however, it is expected to change along the duct.

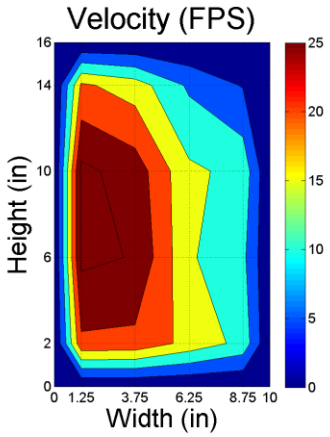

Figure 38: Velocity profile directly after the unit.

To evaluate the accuracy of the static pressure measurement location, as calculated per Equation 30, further measurements were taken and plotted both upstream and downstream of the aforementioned pressure measurement location. For baseline data from Scenario 2, static pressure along the outlet duct can be seen in Figure 39 for all three units.

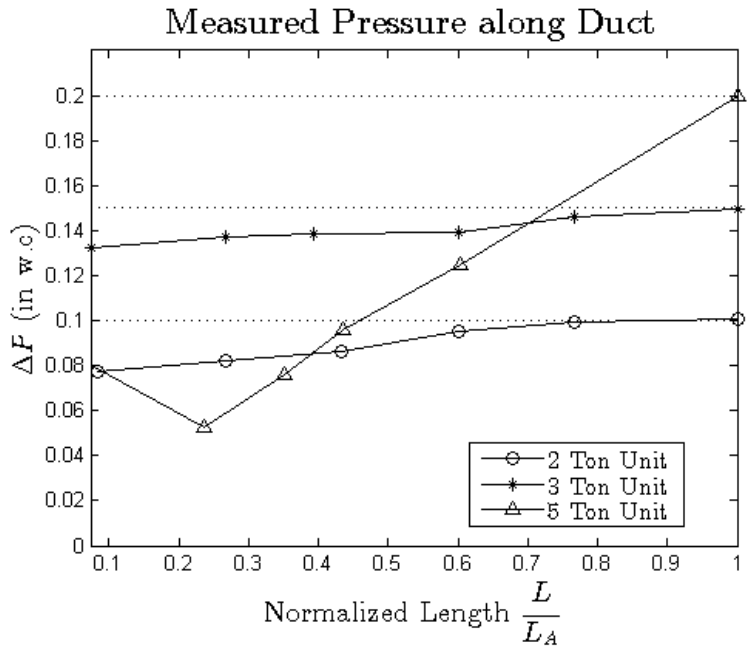

Figure 39: Pressure along the outlet duct after the unit.

Figure 39 shows static pressure measurements at a number of locations between the unit outlet and ASHRAE Standard 37 measuring points, which again were taken during Scenario 2 baseline testing. The normalized length shown in the figure referenced the actual measurement point to the ASHRAE Standard 37 pressure tap location governed by Equation 42. All three units show an increase in pressure as the flow exits the unit and moves through the straight duct. This increase is contrary to theory and expectations suggesting a misreading of the static pressure for pressure rings located too close to the unit, and prior to the flow achieving a uniform flow condition. It is important to note that both the 2 and 3 ton units appear to be asymptotically approaching the AHRI rating point (the dashed lines), while the 5 ton unit appears to cross the AHRI rating point. This suggests that the 2 and 3 ton unit measurement points are conforming to theory meaning the ASHRAE Standard 37 pressure measurement location is correct, while the 5 ton unit is obviously not.

To further investigate the correctness of the pressure locations governed by Equation 42 for the 2 and 3 ton unit, the test apparatus was reconfigured with a straight outlet duct

with a length of 4.5 hydraulic diameters (73 in.) that extended the region for pressure measurements beyond the ASHRAE Standard 37 calculated location. Pieces of tape were attached to the end of the duct to restrict the flow so that the AHRI rating pressure of 0.15 in. w.c. could be achieved. The test setup is shown in Figure 40.

Figure 40: ASHRAE Standard 37 static pressure measurement verification.

As can be seen in Figure 40, the 3 ton unit was configured and tested with eight pressure rings above the unit, which allowed for six additional pressure rings being placed downstream of the ASHRAE Standard 37 pressure measurement point. The pressure locations in inches and normalized values from the unit exit are shown in Table 31.

Table 31: Locations of pressure rings for baseline verification case study.

Units	*P3*	P_A	*P4*	*P5*	*P6*	*P7*	*P8*	*P9*
(in)	8	33	43	49	54	60.5	65.8	73.25
$\frac{L}{L_A}$	0.2	1	1.3	1.5	1.6	1.8	2.0	2.2

It should be noted that the ASHRAE 37 Standard pressure tap location, L_A, was calculated to be around 33 inches from the top of the 3 ton unit . While testing, P_A was set at 0.15 in. w.c. The pressure results for two separate tests are plotted in Figure 41 with the measured pressure along the straight duct being plotted as a function of position normalized to the Equation 30 position of 33 inches. Also shown in Figure 41 are the Scenario 2 baseline data for the 3 ton unit, as presented earlier in Figure 39.

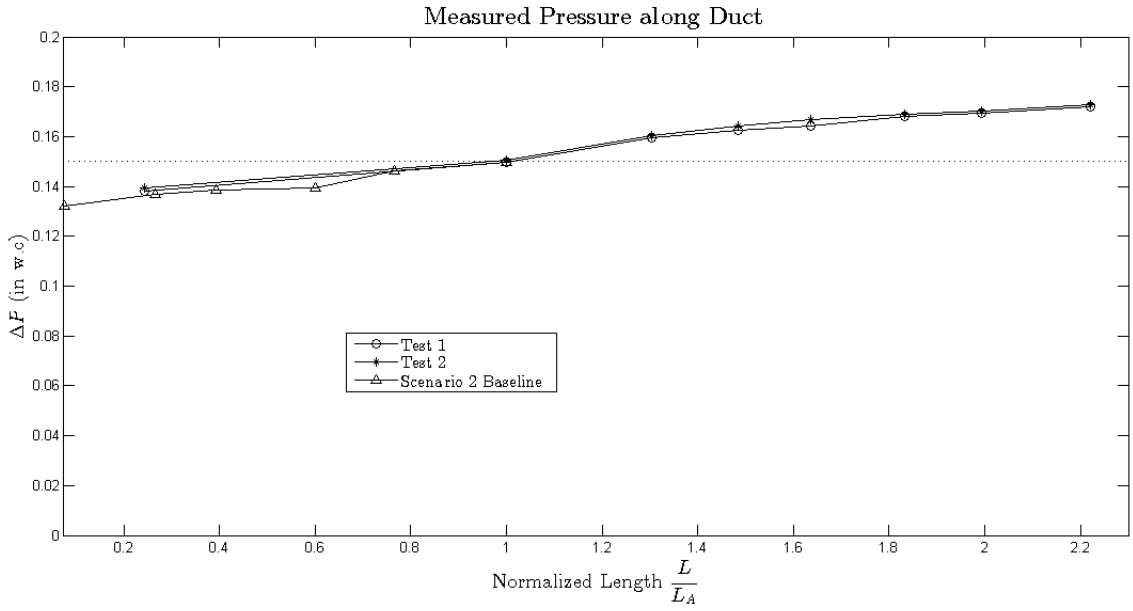

Figure 41: Measured pressure of the 3 ton unit with a long straight outlet.

Observations of Figure 41 reveal that Test 1 and Test 2 results are very similar and aligned well with the Scenario 2 baseline data, meaning there is continuity between the

data plots upstream and downstream of the ASHRAE Standard 37 measurement point. This particular result is analyzed further in CS-11. The most important conclusion that one can draw from figure is that for the 3 ton unit (and thus probably the 2 ton unit) the Standard ASHRAE 37 pressure measurement is not correct because similar to the 5 ton unit the flow has not straightened to a more uniform condition, which would be indicated by a pressure decrease along the duct. Combining observations of Figure 39 and Figure 41 one might also conclude that even though none of the units have reached uniform flow at the measurement flow point, the flow is even less uniform for the 5 ton unit, probably because the lack of a heat exchanger near the unit exit increases flow maldistribution.

CS-2: Elbow Static Pressure Location Validation

Does the ASHRAE Standard 37 calculated pressure measurement location downstream of the elbow provide an appropriate measurement location for Scenario 1?

This CS-2 question is a variation of the CS-1 question with CS-1 referring directly to ASHRAE Standard 37 baseline tests and CS-2 referring to the Scenario 1 investigation of utilizing an elbow to reduce height. The main consideration of the CS-2 question is whether or not Equation 43 applies to the Scenario 1 static pressure measurement after the elbow. The answer to this question as in CS-1 for ASHRAE Standard 37 is important for establishing the elbow test static pressure measurement location, *P2*. All three units were tested with additional pressure ring locations downstream of the elbow in the horizontal section. One measurement is taken after pressure ring *P2* allowing for a more detailed analysis. Table 32 shows the locations of the pressure rings referenced to the end of the elbow.

Table 32: CS-2 pressure ring locations.

	2 Ton		3 Ton		5 Ton	
Pressure Ring	L	$\frac{L}{L_A}$	L	$\frac{L}{L_A}$	L	$\frac{L}{L_A}$
P3	6	0.2	7.5	0.2	8.2	0.2
P4	13	0.4	15.2	0.5	21.6	0.6
P5	18	0.6	20.7	0.6	27.3	0.8
P6	23	0.8	27.5	0.8	30.1	0.9
P2	28	0.9	31.7	1.0	34	1.0
P7	33.5	1.1	38	1.2	39.5	1.2

The normalized length was also found and is shown in Table 32. The *P2* values vary slightly from the pressure ring length used during Scenario 1 testing; however, this was done primarily to reduce the time spent on this CS-2 investigation as it is outside the project scope. As can be seen in the figures this decision does not have affect results when considering the instrumentation error. Again for ease of time and in order to validate the best elbow test, only tests of the V3 elbow test (which is the only orientation and elbow being recommended in this project) were performed. In Figure 42, the static pressure along the duct for the 2 ton unit is shown to be relatively constant within the pressure measurement uncertainty (± 0.003 in. w.c.), which is an indication that the static pressure measurement follows pressure drop theory supporting the use of the ASHRAE Standard 37 calculation for use in a horizontal duct after an elbow (Scenario 1).

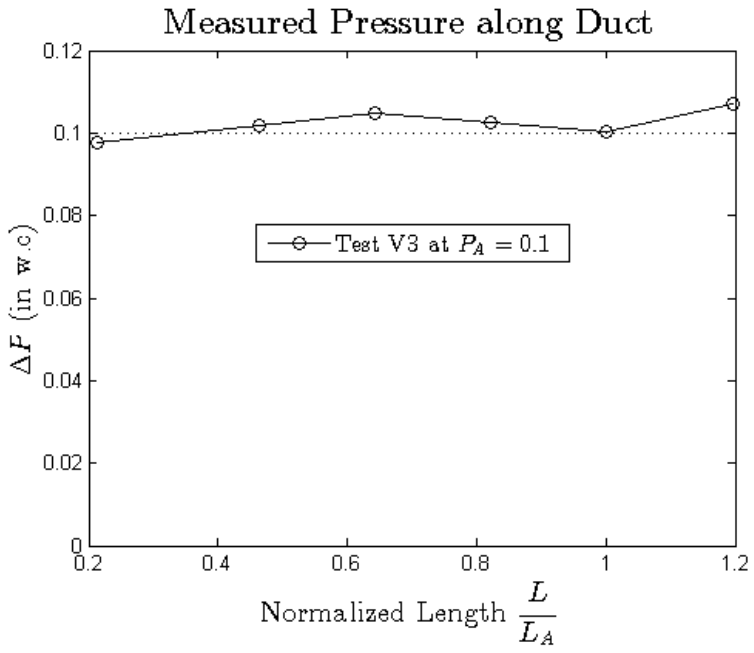

Figure 42: Pressure change after the elbow for the 2 ton unit.

The 3 ton results are shown in Figure 43 are similar to the 2 ton results in that the ASHRAE Standard 37 calculation approach is appropriate.

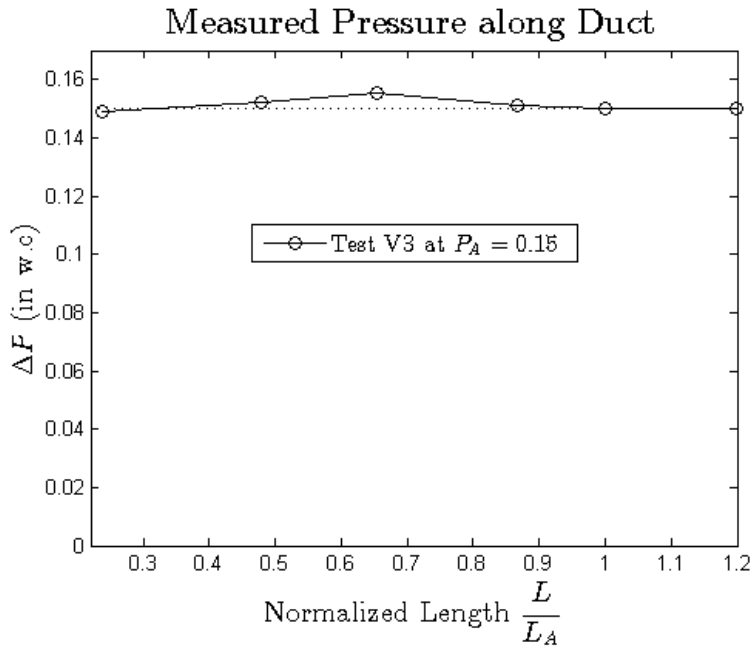

Figure 43: Pressure change after the elbow for the 3 ton unit.

It is interesting to note that the previous Case Study (CS-1) showed that for ASHRAE Standard 37 the baseline test with a vertical duct installed after the unit for the 3 ton unit resulted in pressure measurements that did not appear to level out after 70 in. of straight ducting with the possible conclusion that the calculation method, namely Equation 43, in ASHRAE Standard 37 may not be appropriate or accurate for conventional testing. In contrast it would appear that the ASHRAE Standard 37 equation may in fact be appropriate for the Scenario 1 testing approach with elbow test V3 and the horizontal test section. This difference suggests that the V3 elbow test reduces the length needed to straighten the flow so that pressure decreases along the duct and conforms with theory.

The 5 ton results are shown in Figure 44, in which it can be observed that the pressure curve increases throughout the duct length.

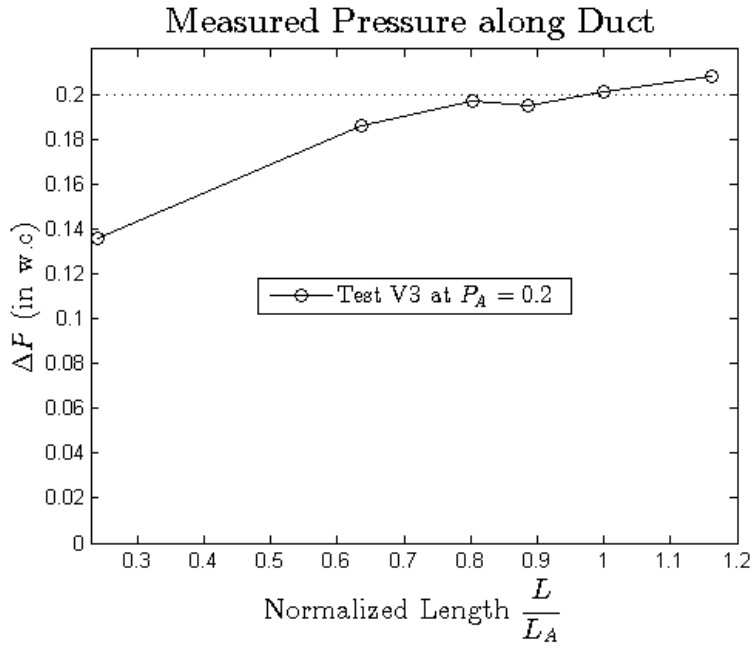

Figure 44: Pressure change after the elbow for the 5 ton unit.

This suggests that uneven flow maldistributions persist into the horizontal section downstream of the elbow, questioning the applicability of the ASHRAE Standard 37 equation for the 5 ton unit in Scenario 1. The heat exchanger location either upstream or downstream of the blower is the most likely reason for the difference between the 5 ton unit and the smaller units. In summary, the ASHRAE Standard 37 location equations appears to be applicable for Scenario 1 when a heat exchanger is located upstream of the blower outlet.

CS-3: Calculation of Loss Coefficients for the Baseline Tests

Why do the experimental loss coefficients in this study not agree with ASHRAE loss coefficient values?

During the baseline tests for Scenario 1, an additional pressure ring was placed at a distance of 0.5 times the square root of the exit area away from the elbow. The net result

of adding this measurement point is that the static pressure can be measured on either side of the elbow allowing for an elbow pressure value. These pressure drop measurements were used to calculate the experimental loss coefficient following previously presented Equation 7, which is repeated below.

$$K_o = \frac{\Delta P}{\rho \left(\frac{V}{1097}\right)^2} \tag{7}$$

Several loss coefficients can be found in the ASHRAE Handbook based on the work done by Idelchik et al. (1986). A comparison of these ASHRAE loss coefficients and the measured loss coefficients are shown in Table 33 for similar conditions to the baseline tests. Various different geometrical parameters were required for the curved and square elbow. The curved elbow ASHRAE loss coefficients are dependent on the blowout area to outlet area ratio, the orientation of the curved elbow with respect to the blower, and the length of the straight duct between the unit outlet and the elbow. The loss coefficients for the square elbow and square elbow with turning vanes assume fully developed turbulent flow. The square elbow loss coefficients are dependent on the aspect ratio defined previously. The loss coefficients for the square elbow with turning vanes are constant according to the ASHRAE Handbook and hence independent from geometry.

Table 33: Experimental and ASHRAE loss coefficients for baseline tests.

Unit	Test	Experimental	ASHRAE
2 Ton	BC1	2.2	0
	BC2	2.6	0
	BC3	1.5	0
	BC4	2.7	0
	BS1	2.6	1.15
	BS2	2.8	1.15
	BS3	2.0	1.15
	BS4	2.8	1.15
	BV1	0.9	0.25
	BV2	0.7	0.25
	BV3	0.6	0.25
	BV4	0.7	0.25
3 Ton	BV3	0.5	0.25
5 Ton	BC1	1.3	0
2 Ton*	BV3	-0.6	.25
3 Ton*	BC4	0.51	0
* Denotes tests with the over-sized duct.			

It should be noted that the square elbow ASHRAE loss coefficients are constant because the 2 ton unit outlet dimensions result in an aspect ratio of 1 and the square elbow loss coefficients found in the ASHRAE Handbook were dependent on aspect ratio. Furthermore, the curved elbow loss coefficients are zero because ASHRAE Handbook shows that for a long enough straight duct in between the blower and curved elbow, no dynamic pressure drop is found across the elbow.

Several observations can be made based on comparing the loss coefficients in Table 33.

- All of the experimental loss coefficients were larger than the ASHRAE loss coefficients, with this larger difference being independent of elbow type. This disparity in loss coefficient values is possibly due to the existence of non-uniform velocity profiles exiting from the air handling unit, and then passing through the elbow so that elbow pressure drop increases.

- Loss coefficients for the square elbow with turning vanes appeared nearly independent of aspect ratio as the BV3 2 and 3 ton tests were similar. This closeness supports the ASHRAE Handbook claim that the square elbow with turning vanes is independent of geometries.
- As aspect ratio decreased, so did the loss coefficient, which is apparent when comparing the BC1 2 and 5 ton tests and the BV3 2 and 3 ton tests.
- Elbow orientations (i.e. elbow orientation exiting the unit and referenced to the blower mounting position) for numbers 2 and 4 were always within a few points of each other possibly because the change in orientation of the blower position from 2 to 4 simply changed the blast area and hence the high velocity section from left to right or vice versa with respect to the horizontal section of the elbow.
- Orientation number 3 consistently resulted in the lowest loss coefficient for all three elbows. This suggested that even after travelling through the heat exchanger (the 2 ton unit is a blow through unit with the heat exchanger mounted at the blower outlet) there was a large effect on the pressure drop across the elbow due to the blower.
- The loss coefficients calculated for the 2 and 3 ton units with the oversized ducts were suspect due to the lower average velocity as a direct result of the increased area of the oversized duct. For example, the 2 ton unit oversized duct loss coefficient was negative which is impossible as pressure change should never increase across an elbow.

Several of the above observations were based on the blower relative to the elbow orientation (four options exist). Table 33 showed no pattern of ASHRAE loss coefficients and elbow orientation. Although the experimental results were done with a straight duct in between the unit outlet and elbow, elbow orientation effects were still seen, hence why Table 34 displays the ASHRAE curved elbow loss coefficients (ASHRAE 2009b) for the curved elbow immediately downstream of the unit outlet. In this manner the ASHRAE loss coefficients in Table 34 and the experimental results in Table 33, are not directly comparable but the patterns related to orientation of the elbow

with respect to the blower can be analyzed. As a reminder, elbow orientation 1 represents the placement of the elbow that opposes the blower rotation whereas in orientation 3 (180 degree rotation), the curved elbow rotates with the blower.

Table 34: Orientation dependence of the elbow loss coefficients (ASHRAE 2009b).

Test	ASHRAE K_0
C1	1.40
C2	1.25
C3	0.80
C4	1.20

The ASHRAE *Handbook Fundamentals* (2009b) values in Table 34 show elbow orientations 2 and 4 with relatively similar loss coefficients while orientation 3 has the lowest value and orientation 1 has the highest. The only ASHRAE loss coefficient pattern not repeated in the experimental data is that of orientation 1. Specifically, orientation 1 was often not the largest loss coefficient in the experimental data unlike the ASHRAE values; however, other effects and parameter differences could be causing these disparities. It is possible that due to an aspect ratio less than 1, the experimental orientation loss coefficient is less than orientations 2 and 4, as the ASHRAE values do not account for aspect ratio.

In summary, the experimental loss coefficient values measured in this study differed from the ASHRAE Handbook loss coefficients for fully developed flow. Directional affects were found in the measured loss coefficients which were not expected according to the ASHRAE data and did not follow all the same patterns as ASHRAE findings of an elbow placed directly upstream of a blower. The parameters affecting the measured loss coefficients are numerous and complicated and would undoubtedly require a detailed experimental investigation. At a minimum, parameters affecting the loss coefficient can be identified as the inlet velocity profile, aspect ratio, and orientation, with the inlet

velocity profile affecting the average values of the loss coefficients regardless of orientation and the aspect ratio having the greatest effect on the orientational variation of the loss coefficients.

CS-4: Draw-Through versus Blow-Through Air Handler Units

Does the position of the heat exchanger downstream or upstream of the blower have an effect on ASHRAE Standard 37 testing results?

Air handling units of similar tonnage can vary in any number of ways, including motor type, cross-sectional dimensions, and unit height to name just a few. Each of these parameters affect the test results differently in their own way, but these effects were beyond the project scope However, it would appear that none of these differences are as influential as the heat exchanger placement in relation to the blower, either in a draw-through (heat exchanger upstream of the blower) or blow-through (heat exchanger downstream of the blower) position. The reason for this testing influence is two-fold. One, the relative position of the heat exchanger and blower can affect the unit performance (the functional relationship between discharge pressure power and flow rate) and two, the dynamics of the airflow exiting the unit (meaning the velocity distribution or profile) is different for each case, which could affect the accuracy and reliability of pressure measurements. Of those two influences, only the second is within the scope of this project because static pressure measurements were a main part of the Scenario 1 and 2 investigation.

In this study, there were several occasions where the airflow exiting the 5 ton unit was singled out because of flow maldistribution. This raised the question of what did the heat exchanger do downstream of the unit? In almost every situation it appeared to straighten the flow out before leaving the unit. The situations where the heat exchanger position played a vital role are mentioned below.

- Baseline tests: Pressure profiles along the outlet duct were found for the 2, 3, and 5 ton units and plotted on the same figure for comparison. All three pressure

profiles increased from the unit outlet to the ASHRAE Standard 37 pressure measurement location. What separated the 5 ton unit from the 2 and 3 ton units was the rate at which the 5 ton unit pressure profile increased, namely, it increased 10 times faster for the 5 ton unit compared to the 2 and 3 ton units. This difference indicates a high level of flow maldistribution leaving the 5 ton unit, which could be caused by the lack of a heat exchanger downstream of the blower. CS-1 focuses on an analysis of these same results.

- Scenario 1 validation: CS-2 investigated whether the static pressure measurement location was accurate and reliable for elbow test V3 (square elbow with turning vanes in orientation 3). Pressure profiles were measured along the straight horizontal duct downstream of the Scenario 1 elbow. Both the 2 and 3 ton unit pressure profiles remained constant from the end of the elbow to the static pressure measurement location while the 5 ton unit pressure profile steadily increased throughout the horizontal section after the elbow. This increase is an indication of an inability to measure static pressure because of flow maldistribution caused by the lack of the heat exchanger downstream of the blower.
- Scenario 2 passive resistive pieces: Scenario 2 investigated the use of a passive resistive piece to reduce the distance required to straighten the flow exiting the unit outlet and, as a result to hopefully reduce the distance from the unit outlet to the static pressure measurement location (thus reducing test apparatus height). The indication of flow straightening because of the passive resistive piece was whether or not the pressure profile was leveling out along the straight duct downstream of the piece. For the 2 and 3 ton units, several passive resistive pieces leveled the pressure profile, but in contrast no passive resistive piece showed an ability to level the profile for the 5 ton unit, possibly because the exit flow was so maldistributed that there was no hope of straightening the flow and obtaining a viable pressure measurement.

- Pressure differences between baseline and Scenario 1 tests: CS-10 analyzed in depth the differences between baseline and Scenario 1 pressure measurements. It was shown that the addition of the elbow for Scenario 1 should actually decrease the static pressure reading at the Scenario 1 pressure measurement location because of the additional loss of pressure across the elbow, compared to the baseline setup. Therefore, the baseline static pressure should always be higher than the Scenario 1 static pressure. It may be that it is physically impossible for the Scenario 1 static pressure to be greater than the baseline static pressure because the same straight duct is used for both test setups and the only difference is the elbow. However, there were several tests that resulted in the Scenario 1 static pressure being higher than the baseline static pressure. Specifically, this situation happened with the 5 ton unit (i.e. the heat exchanger upstream of the blower) for the Scenario 1 tests of the V2, V3, and V4 elbow configuration and orientation. The elbow test, V1, was negative yet it had the largest error of all the Scenario 1 tests when comparing static pressure to the baseline static pressure. Previously, CS-10, did not answer the question of why the positive difference is occurring, but rather it only explained the test patterns that resulted in positive pressure difference.

It would appear that having a blower with the heat exchanger at the unit inlet rather than at the exit causes an increase in flow maldistribution exiting the unit. It is difficult to say whether maldistribution has an effect on the unit's performance, as this determination was not part of the project scope. However, what can be concluded from this study, as discussed above, is that the accuracy and viability of static pressure measurements, even when following ASHRAE Standard 37 guidelines and requirements, may be questionable for draw-through units, most likely because of exit flow maldistributions. These uneven exit flows for the 5 ton draw-through unit were also the source of difficulties in finding a satisfactory passive resistive piece. In summary, the heat exchanger position upstream of the blower had negative implications for static pressure measurements in the baseline, Scenario 1, Scenario 2, and even case study

testing, which brings into question the validity of using the alternate geometries for draw-through units in this project or even using ASHRAE Standard 37 specifications for measuring static pressure of draw-through units. As a minimum, this is an issue that needs to be investigated especially because this standard does not make a distinction between testing draw-through and blow-through units.

CS-5: Effects of Using an Inlet Damper-Box and Skirt Configuration

How does testing with a damper-box and skirt inlet configuration affect fan performance in comparison to testing with other inlet configurations?

The test setup as described in ASHRAE Standard 37 was previously mentioned, but is reviewed in this case study as well. Testing air-conditioners and heat pumps requires accurate and reliable measurements of static pressure. As seen in Figure 1, ASHRAE Standard 37 details the lengths of ductwork on either side of the unit. In Figure 1, specifications are given of the straight duct for the unit inlet and outlet static pressure measurement. The inlet section is recommended but it is often not used. Instead a damper-box with a small skirt is used to measure the inlet pressure. This inlet configuration is not used to reduce test apparatus height, rather to have a damper system at the inlet for cyclic testing following AHRI Standard 210 (AHRI 2008). It was mentioned previously that the unit inlet condition has a potential to affect fan performance. Possible configurations at the inlet (upstream of the heat exchanger and blower) are:

1) ASHRAE Standard 37 recommended duct.
2) Damper-box and skirt configuration.
3) Straight inlet duct with a skirt for inlet pressure measurement.

It would appear that a need exists for a detailed experimental investigation to determine what, if any, is the effect of the inlet configuration on testing according to ASHRAE Standard 37. Specifically, if the ASHRAE Standard 37 static pressure is set at the specified value at the calculated distance required for the baseline tests, are the

measured power and flow rates different for the possible inlet configurations because ASHRAE Standard 37 does not mandate a specific inlet configuration for all tests (it only makes a suggestion) thus implying that the inlet configuration has a negligible affect on ASHRAE Standard 37.

In this project, only one test was prepared for only a limited set of parameters; therefore, the results do not provide a conclusive and far-reaching answer to the question proposed in this study. This single test was performed on the 5 ton unit for elbow test V3 when a straight inlet section of three hydraulic diameters in length replaced the damper-box used throughout this study. The skirt remained so that the inlet pressure measurement was in the same location for this case study as Scenario 1 (for later comparison). At least 20 inches of space was provided between the floor and the beginning of the straight inlet duct. The test setup is shown in Figure 45.

Figure 45: Test setup of the 5 ton unit with a long inlet duct.

The static pressure was set to 0.20 in. of water at the Scenario 1 static pressure measurement. The testing results for this new inlet configuration were power and airflow of 726 watts and 1971 cfm, respectively compared to the original elbow test (Scenario 1 test V3) results of 726 watts and 1954 cfm. This airflow difference of 17 cfm was only slightly within the instrumentation error (± 26 cfm or ±1.3%). It should be noted that the 5 ton unit may in fact be the least sensitive to inlet conditions because the heat exchanger straightened out the flow before reaching the blower. The 2 and 3 ton units do not have heat exchangers before the blower and upon further investigation, might yield larger differences in airflow depending on the inlet configuration.

CS-6: Test Parameter: Airflow versus Static Pressure

What parameter (either airflow or static pressure) was best suited as the set point test parameter (independent) and as the comparison parameter (dependent) during Scenario 1 and 2 investigations?

In this project, the baseline tests were performed by following ASHRAE Standard 37, and by setting the static pressure to the AHRI rating point of 0.1, 0.15, and 0.20 inches of water for the 2, 3, and 5 ton units respectively, while measuring the power and airflow. Following the directions of the project monitoring subcommittee, Scenario 1 and Scenario 2 used the airflow as the set parameter with the airflow set to the baseline measured airflow value and then the power and pressure were measured and compared; hence, static pressure became the comparison parameter. Then the test parameter was changed to the AHRI rating point and the power and airflow were measured. Therefore, the static pressure became the set point parameter (independent) and the airflow became the comparison parameter (dependent). There were apparent differences in the three values of interest, namely power, airflow and pressure when changing the set parameter. This investigation of changing the set parameter during Scenario 1 and 2 testing from airflow (which was what was used in this study) to static pressure was not called for by TRP-1581 or by the Project Monitoring Subcommittee so the comparisons are limited

(additional studies may be warranted). The results for the tests where the test set parameter was changed are shown in Table 35.

Table 35: Comparison of test parameters for the 2, 3 and 5 ton units

Unit	Test	Set Parameter	Power	Nozzle Airflow	Static Pressure
	Units		(W)	(cfm)	(in w.c.)
2 Ton	Baseline	Pressure	235	719	0.100
	Scenario 1	Airflow	237	719	0.093
	Scenario 1	Pressure	227	720	0.100
2 Ton	Baseline (b)	Pressure	240	728	0.100
	Scenario 2	Airflow	236	728	0.093
	Scenario 2	Pressure	229	713	0.100
3 Ton	Baseline	Pressure	257	1153	0.150
	Scenario 2	Airflow	266	1155	0.142
	Scenario 2	Pressure	263	1156	0.150
3 Ton	Baseline	Pressure	257	1153	0.150
	Scenario 2	Airflow	262	1151	0.141
	Scenario 2	Pressure	266	1155	0.150
5 Ton	Baseline	Pressure	725	1948	0.200
	Scenario 1	Airflow	728	1950	0.213
	Scenario 1	Pressure	727	1954	0.201
b denotes a different baseline test for the same unit.					

Various patterns based on comparison of the different set parameters (airflow or static pressure) can be observed in Table 35. However, the instrumentation error needs to be presented again as it is crucial in determining the patterns in Table 35. The static pressure error was ±0.003 in. w.c. for all units. The airflow error was ±8.3, ±7.7, and ±26 cfm and the power error was ±6.1, ±8.7, ±19.4 watts for the 2, 3, and 5 ton units, respectively.

The only values that are outside of the instrumentation error in Table 35 are the static pressure measurements for all the units, the power measurements for the 2 ton unit, and the airflow during Scenario 2 tests for the 2 ton unit. The 2 ton unit power noticeably

decreased as static pressure increased. The Scenario 2 tests also showed that for an increase in static pressure, the airflow decreased. These two results are expected trends for PSC motors, similar to the one installed in the 2 ton unit. The 3 and 5 ton units showed a relatively constant airflow and power (within the instrumentation error) for changes in static pressure (near the AHRI rating point) possibly due to the fact that they both utilized ECM motors. Motor type appears to be a factor in determining the effects that the test parameters have as evidenced by the fact that different trends were observed for the two motor types.

In conclusion, for a PSC motor the Scenario 1 and Scenario 2 alternate geometries are expected to change the power and airflow, but will remain within the required 5% and 2.5% respectively. For an ECM motor, Scenario 1 and Scenario 2 are expected to change the power and airflow very little compared to ASHRAE Standard 37 specifications as the ECM motors for both the 3 and 5 ton unit changed very little for different static pressure points.

CS-7: Theoretical versus Experimental Pressure Profile Curves Downstream of the Unit

What are the test parameters and flow conditions that affect static pressure measurement accuracy and reliability in the exit ducting?

Throughout the project, experimental static pressure data were measured along a straight duct, thus forming pressure profiles, for various sized ducts corresponding to the 2, 3, and 5 ton units. These measured static pressure profiles often do not appear to conform to theoretical pressure drop profiles that one would expect to find in ducts and pipes, namely fluid pressure decreasing in the direction of flow. One possible explanation for this disagreement between measured and theoretical pressure profiles is that the measured value is in error because of non-uniform flow. The agreement, or lack of agreement, between the theoretical and experimental pressure profiles can possibly be used as an indication that the fluid flow has straightened to a more uniform condition,

thus allowing for a pressure measurement that accurately represents static pressure. The validity of this analytical certainly has an effect on CS-1 and CS-2 presented earlier, along with the Scenario 2 investigation that focused on determining an accurate pressure measurement point close to the unit outlet so as to reduce the tests apparatus height. Therefore, this case study investigated the significant and difference between theoretical and experimental.

As discussed above, some type of pressure measurement verification was needed for several of the case studies and for the Scenario 2 testing in order to find the minimum distance for measuring pressure. This verification is not based on agreement of values but rather of trends. It can be surmised that at the point where the experimental pressure curve decreases, the measured values are conforming to theoretical pressure drops and a valid measurement is occurring. Figure 46, Figure 47, and Figure 48 display the theoretical and baseline pressure measurements along the vertical outlet duct starting at the unit exit for the 2, 3, and 5 ton units. The theoretical pressure drop was calculated based on a range of Reynolds numbers from 15,000 to 18,000 (for the 2, 3, and 5 ton units), which resulted in a friction factor of 0.016 from Equation 1 (Churchill 1977). Theoretical and baseline pressure drop for the 2 ton unit were also compared in Figure 46 along the normalized length where L_A was the location of the ASHRAE Standard 37 pressure tap.

Baseline versus theoretical pressure change along the duct is shown in Figure 47 for the 3 ton unit. The baseline measured pressure profile and the theoretical pressure profile for the 2 and 3 ton units appear to converge to a similar trend or profile shape near the normalized length of 1.

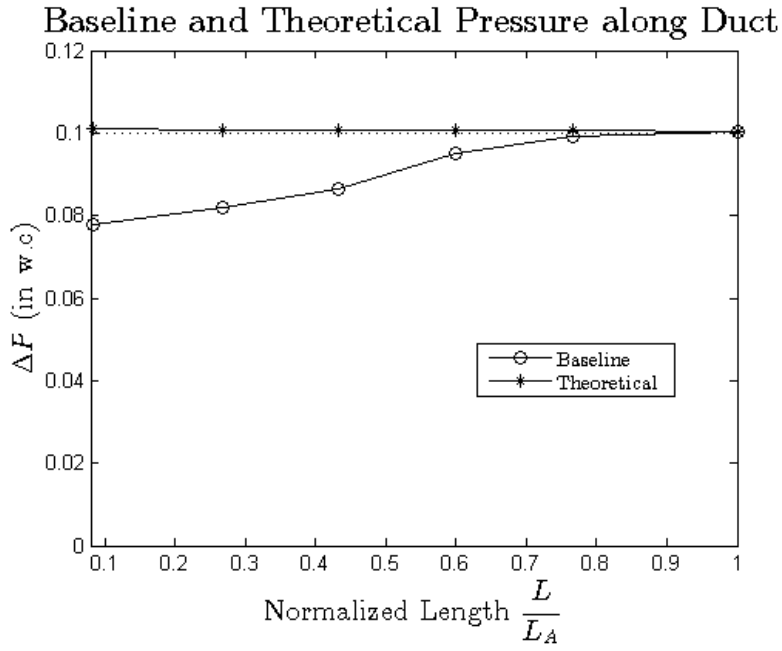

Figure 46: Baseline versus theoretical pressure drop along the outlet duct for the 2 ton unit.

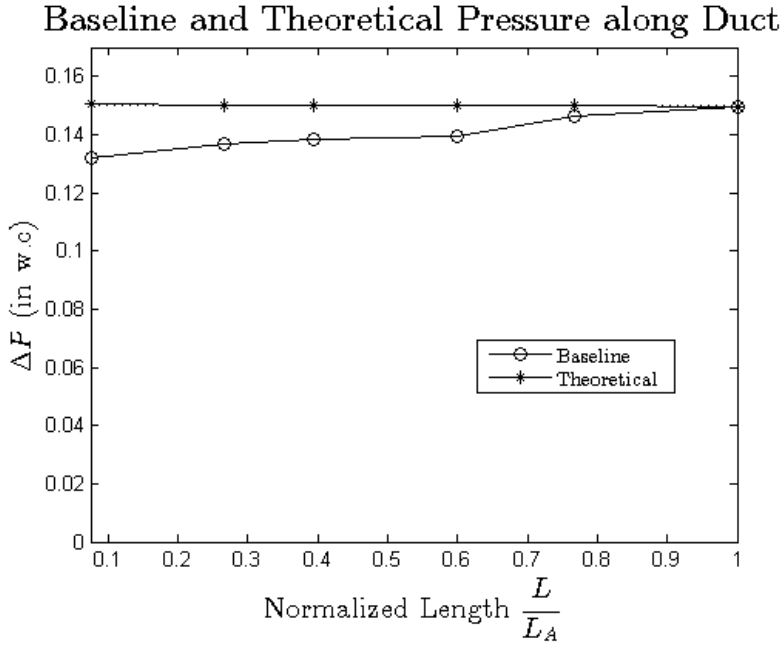

Figure 47: Baseline and theoretical pressure drop along the outlet duct for the 3 ton unit.

The fact that the measured and theoretical pressures agree at the normalized length of 1 is irrelevant because the theoretical pressure profile is based on assuming the experimental value at this point. Again, only the trend agreement is important for validating the measurement point.

Figure 48 shows the measured baseline values versus the theoretical values of the pressure drop along the duct for the 5 ton unit. The high pressure reading for the first baseline static pressure tap could be due to the higher mean velocity leaving the blower area only a few inches upstream of the pressure measurement. In contrast, to the 2 and 3 ton units, the 5 ton unit measured profile trend is significantly different from the theoretical curve. The experimental and theoretical profiles in Figure 46, Figure 47, and Figure 48 are explored in more detail in paragraphs to follow.

As shown in Figure 46, Figure 47, and Figure 48, the theoretical pressure drop is so small that it appears at first glance that the static pressure is constant from the exit of the unit to the ASHRAE Standard 37 pressure measurement location (in actuality the pressure changes around 1%). It should be noted that the theoretical pressure drop applies to uniform, fully-developed turbulent flow and as noted previously it is logical to assume that measured profile contrasted to the theoretical pressure drop curve is likely to represent pressure measurements in error or unreliable at the very least.

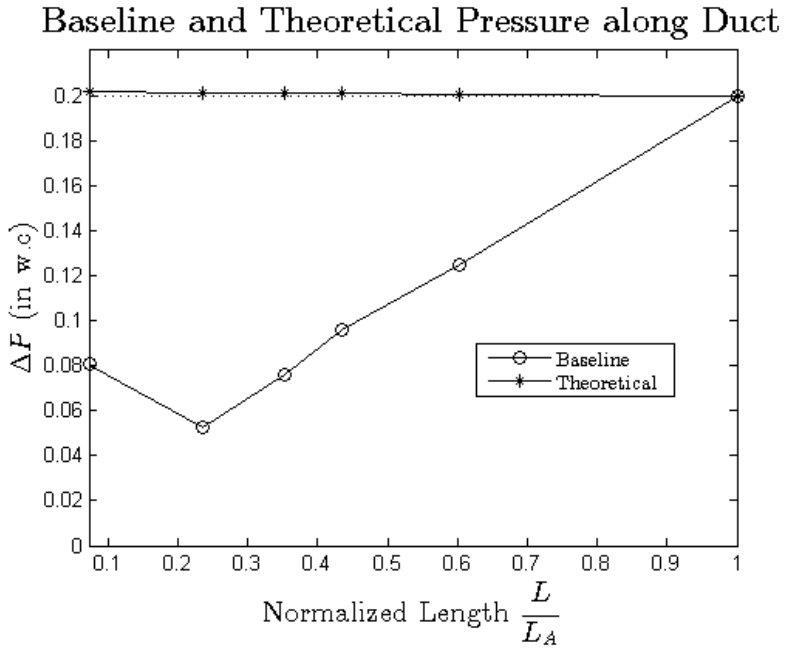

Figure 48: Baseline and theoretical pressure drop along the outlet duct for the 5 ton unit.

In the experiment, as the fluid moves down the duct farther away from the unit outlet one would expect a more uniform flow with the measured profiles trend approaching the theoretical. In other words, the pressure readings are validated as the curve shape approaches the theoretical curve shape.

Another important parameter is the slope of the pressure curve. For comparison Figure 49 displays the pressure normalized by the AHRI rating point for each unit (0.10, 0.15, and 0.20 inches of water).

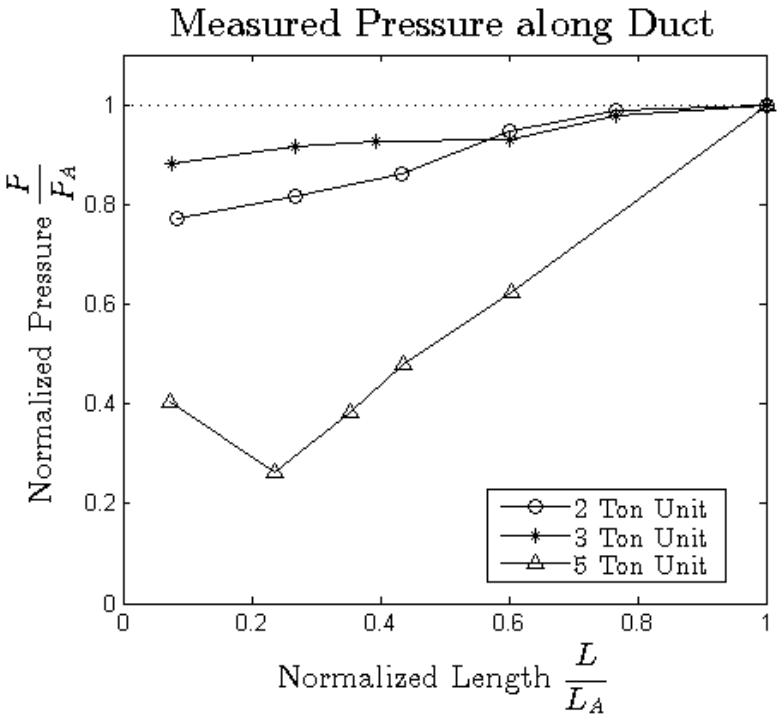

Figure 49: Normalized pressure versus normalized length of the 2, 3, and 5 ton units.

As can be seen from Figure 49, the 2 and 3 ton units appear to have a slope of around 0.13. In comparison, the 5 ton unit has a slope of around 1 normalized pressure per normalized length, which is a factor of ten higher than both of the smaller units. This highlights the importance of conforming with theory because only at that point can one be assured that velocity profiles are not affecting the results. As an example at the normalized length of 0.60, Figure 63 shows that the normalized pressure would be 0.95, 0.94, and 0.63 (0.095, 0.139, and 0.125 inches of water) for the 2, 3, and 5 ton units. Obviously the pressure ratio is comparable for the 2 and 3 ton units yet the 5 ton unit is much less. At that same arbitrary pressure measurement location, the 5 ton unit would be at a completely different stage of flow development and hence would not be measuring the same pressure the other units would be. The most likely reason for the differences in the pressure profile slopes as mentioned before, is the location of the heat exchanger, namely whether it is placed upstream or downstream of the blower. As discussed earlier

in this section, the 5 ton unit does not have a heat exchanger downstream of the blower which would otherwise straighten the flow. As a result, one would expect a maldistribution of flow exiting the 5 ton unit and greater pressure measurement error. By setting an arbitrary pressure measurement location, the type of unit becomes a factor in what pressure the unit is being tested at. The only way to ensure that all units are tested equally is to make sure that the pressure change along the duct has begun to drop as then the flow maldistribution is not affecting the static pressure measurement. This is why conformance with theory is important for the alternate ASHRAE Standard 37 geometries found in this project, as this is the only way to ensure that tests are equal amongst all unit types.

CS-8: Pressure Measurement Accuracy and Pressure Ring Approaches

What type of pressure ring configuration and approach provides the most reliable and accurate static pressure measurements?

With the goal of improving reliability of testing in ASHRAE Standard 37 and in this project, an investigation of methodologies for measuring static pressures in ducts was performed. This investigation focused primarily on reviewing literature, and it was found that inherent errors in static pressure measurements for fluids flowing in ducts or pipes can be reduced by simply changing the requirements for pressure tap and ring configurations. Pressure taps and rings were previously discussed in this report yet an extension of that material is provided in this case study with the emphasis on improving pressure measurements.

Static pressure for fluids flowing inside ducts, tubes, and pipes is most often measured by using pressure taps as shown in Figure 4. ASHRAE Standard 37 recommends that the diameter of the hole, d, be 0.04 in. and the larger diameter, D, be 0.25 in (D/d of 6.25). ASHRAE Standard 51 (2007) limits the parameters mentioned in Figure 4 as well, requiring that d be less than 0.125 inches, D/d be larger than 2, and that l/d be larger than 2.5. Shaw (1960) similarly showed that the same dimensionless

parameters used in ASHRAE Standard 51, and to some degree ASHRAE Standard 37, to define the pressure tap (figure 3) are important for pressure measurement accuracy. These pressure error experiments primarily looked at the relationship of the *l/d* ratio, concluding that in contrast to ASHRAE 51, the *l/d* ratio should be small to decrease pressure error. The other claim from ASHRAE Standard 51 is supported by Shaw (1960) who noted that as *d* decreases, the pressure error decreases until the true static pressure is reached at $d \rightarrow 0$. The error in pressure was also related to the mean velocity, with the pressure error being significant for an average velocity at 200 FPS to inconsequential at 50 FPS (the maximum velocity of the 5 ton unit was 25 FPS). For this project the mean velocities were so low as to create almost no difference in pressure reading for hole diameters (*d*) ranging from 0.025-0.2 in (Shaw 1960). Shaw also mentioned that the significance in the dimensionless parameter *D/d* was apparent for values less than 10, but trends in pressure error were not mentioned. Unfortunately it is unclear where ASHRAE Standard 51, or for that matter ASHRAE Standard 37, found the evidence to suggest the values that are mentioned in the standards, but Shaw (1960) corroborates with some and disagrees with others. In summary, the parameters, *l*, *d*, and *D*, and their relationships to each other are important in reducing static pressure error. It is certainly worth an investigation to determine the ranges and limitations of these parameters to ensure reliability and accuracy in the static pressure taps.

For rectangular ducts, four pressure taps are placed in the center of each face and can be connected in two different configurations as shown in Figure 5. These pressure rings, known as the conventional pressure ring or the “Triple T” pressure ring, are recommended by ASHRAE Standard 37 for measuring pressure. The standard does not prefer one approach to the other, and it does not explain either differences or advantages. In reality, research studies found in existing literature make a distinction between the two approaches and one method may be preferable in spite of the guidance in the standard. As mentioned previously, the conventional pressure ring approach, rather than the “Triple T” ring approach was used in this project; however, Blake (1976) suggests that this conventional pressure ring approach is less effective for antisymmetric flow in

round ducts due to the possibility that the pressure reading may be influenced by the closest pressure tap. The study first proved that the "Triple T" pressure ring approach mathematically had less error than the conventional approach, then proved the same through experimentation with four pressure taps placed in line with the flow direction so that each of the four pressure taps would be recording a different pressure values similar to a very antisymmetric velocity profile where each pressure tap sees a different velocity and static pressure. Blake (1976) found that when increasing the hole diameter, *d*, by a factor of ten from 0.016-0.157 in. that the average pressure readings could be in error by up to 10% for the largest hole diameter, again with the conventional pressure ring approach. In contrast, the "Triple T" pressure ring had errors consistently less than 1%, even for a hole diameter of 0.157 in. Blake (1976) proves mathematically and experimentally that the "Triple T" configuration is the most accurate approach for measuring static pressure in flowing fluids. The question arises whether or not this is a factor for rectangular duct as it is unclear what fluid was used and at what Reynolds numbers the data were collected.

As noted, two different pressure ring configurations are suggested in ASHRAE Standard 37, namely the conventional and "Triple T" pressure ring approaches, without guidance for preference. It would be beneficial to experiment on unit testing per ASHRAE Standard 37 if an investigation could determine if the "Triple T" pressure ring approach as defined by Blake (1976) is indeed better suited to measuring true static pressures while testing unitary air conditioners and heat pumps. This outstanding question for the best approach for measuring static pressure is particularly important for RP-1581 because of the need to accurately and reliably analyze the pressure profiles for validation of static pressure measurement locations for the baseline, Scenario 1, and Scenario 2 testing. When using the conventional pressure ring approach, this project showed that the static pressure measurement increased past the ASHRAE Standard 37 static measurement location, contrary to fluid flow theory. Also the velocity profiles suggests that the baseline, Scenario 1, and Scenario 2 testing all produce antisymmetric velocity profiles, which was what Blake (1976) warned against when using the

conventional pressure ring approach. Better results may occur during ASHRAE Standard 37 testing by requiring the use of the "Triple T" configuration approach because one could probably always expect antisymmetric flow at the blower outlet regardless of the test situation.

CS-9: Minimum Distance Limitation for Mounting an Elbow Downstream of the Static Pressure Measurement Point

Is the ASHRAE Standard 37 minimum-distance calculation for mounting an elbow downstream of the static pressure measurement point correctly specified?

One can view the CS-9 question in two ways and in this light the question variations are:

1) Is the baseline elbow too close to the static pressure measurement point based on the Standard 37 calculation.
2) Is the baseline elbow too far from the static pressure measurement point and can the downstream elbow distance be reduced (less than the ASHRAE Standard calculation) so as to lower the test apparatus height.

Every test in this project, from baseline to Scenario 2, either directly or indirectly involved the use of the ASHRAE Standard 37 straight duct specifications, L_e, calculated by Equation 29 (reprinted from CS-1).

$$L_e = 2.5\sqrt{a\ b} \tag{29}$$

With "a" and "b" being duct cross-sectional dimensions. In addition all the tests also used Equation 30, also known as the ASHRAE Standard 37 static pressure measurement location, L_A, which is related to the outlet cross-sectional dimensions similar to the straight duct specification. In fact, the calculated straight duct length is simply a larger scale of the distance from the unit outlet to the pressure measurement.

$$L_A = 2\sqrt{a\ b} \tag{30}$$

Simple algebra (divide L_e and L_A) can find the relationship between pressure measurement location, L_A, and the end of the outlet duct, L_e, as seen in Equation 31.

$$L_e = 1.25\ L_A \tag{33}$$

It should be noted that Equation 31 is only dependent on L_A, meaning it does not have to relate to the cross-sectional dimensions (unless L_A is related to them). This then decouples the straight duct height from the cross-sectional dimensions, which is important for Scenario 2 as described later. Similarly, the distance between pressure measurement, L_A, and straight duct can be found, which is denoted as L_e- L_A as shown in Equation 32.

$$L_e - \mathrm{L_A} = 0.25\ L_A \tag{34}$$

As mentioned in CS-1 and plotted in Figure 41, two tests (Test 1 and Test 2) were performed with a vertical duct, roughly 4.5 hydraulic diameters in length, at the exit of the 3 ton unit with pressure rings before and after the ASHRAE Standard 37 pressure measurement location (normalized length of 1). The baseline for Scenario 2 is also plotted in Figure 41 and it is shown to align well with Test 1 and Test 2. The baseline test static pressure location had an elbow placed after the vertical straight duct following Equation 31 (L_e = 1.25 L_A), while the ASHRAE Standard 37 pressure measurement location for Test 1 and Test 2 had more than 2 hydraulic diameters worth of straight duct downstream before exiting to atmosphere (which is a distance of 73 inches). Since Test 1, Test 2, and the baseline for Scenario 2 aligned so well, it is logical to conclude that the elbow had little effect on the ASHRAE Standard 37 pressure measurement at the calculated point for the 3 ton unit. In other words, the distance to the elbow did not affect the static pressure measurement, which raised the question as to whether the straight duct distance can be reduced to a value less than the ASHRAE Standard 37 of 1.25 L_A, thus reducing the test apparatus height. The answer to this question has implications not only for baseline tests, but also for Scenario 2 testing.

A complete array of tests including 3 elbow types and 4 orientations were completed on the 2 ton unit. There appeared to be little effect in the power and airflow between tests suggesting that orientation and elbow type were not affecting the static pressure

measurement. In conclusion, it appears that Equation 32 (L_e- L_A), which is the ASHRAE Standard 37 calculated distance from the pressure measurement location to the elbow, provides a sufficient distance to eliminate minor downstream effects due to the elbow regardless of elbow type or orientation.

The goal of Scenario 2 was to find the minimum distance between a passive resistive piece and an accurate and reliable static pressure measurement point. Results for the 2 and 3 ton unit indicated that at a distance of 18 in. and 13 in. (new distances for L_A independent of cross-sectional dimensions), respectively, from the top of the unit, only a 5% static pressure error was found. However, these results were found with a straight duct with a length governed by Equation 29. This meant that the static pressure measurement location was reduced but the straight duct was not. For example, the 2 ton unit results found a minimum static pressure distance of 18 in., yet the duct this was tested in was 35 in. long, which is much larger than specified by Equation 31. It is possible that the straight duct could be reduced to a total length of 22.5 in. (compared with 35 in.) and 16.25 in. for the 2 and 3 ton units, following Equation 31. Reduction of the straight duct by changing the relation of the governing equation from a function of cross-sectional direction to a function of pressure tap location (L_A) would truly reduce the test apparatus height for Scenario 2. Unfortunately as this was outside the scope of the project, data were not taken that would be able to prove that Scenario 2 could use Equation 31 for the straight duct height.

The above tests and discussions do not provide a definitive answer as to whether Equation 31 can be used with the new experimental pressure measurement locations from Scenario 2 or if the straight duct can even be reduced more, but with further study, this could be answered and the test apparatus could potentially be shortened further by reducing the distance between ASHRAE Standard 37 pressure measurement location and the end of the straight duct. Specifically, it is possible that the coefficient, 1.25, in Equation 31, could be reduced further (to a minimum of 1.0) effectively shortening the baseline and Scenario 2 test apparatus.

CS-10: Positive Static Pressure Error for Scenario 1 Elbow Tests

Should the elbow and duct pressure drops for Scenario 1 always be greater than pressure drops for the baseline tests for the same duct length?

The difference between baseline tests according to ASHRAE Standard 37 and Scenario 1 tests is the addition of an elbow immediately downstream of the unit outlet, which converts the ASHRAE Standard 37 outlet duct from a vertical to a horizontal position as can be seen in Figure 50.

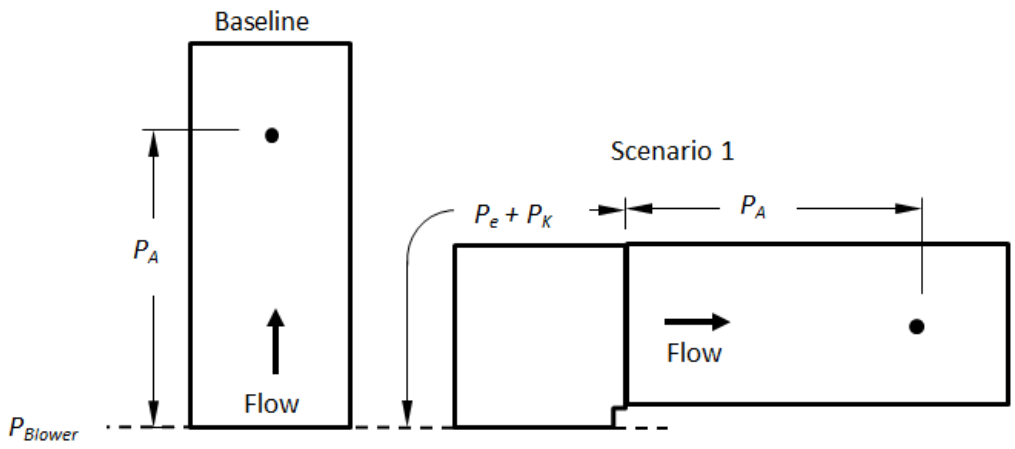

Figure 50: Pressure drop for baseline and elbow tests.

For the vertical duct, the pressure measurement point is measured from the unit outlet based on a calculation given in the ASHRAE Standard 37. This distance to pressure measurement point is the same for the horizontal duct as it is for the vertical duct except the distance is measured from the point where the horizontal duct attaches to the elbow. The only difference between baseline and Scenario 1 for the pressure measurement location can be related to the static pressure drop from the elbow, P_e, and the dynamic pressure drop of the elbow, P_K, which is related to the loss coefficient. It

should also be noted that the blower pressure, P_{Blower}, actually creates a pressure increase whereas pressure change due to flow through the duct, P_A, and elbow in Scenario 1, represent a pressure loss. Therefore, the measured pressure of baseline tests is related to Equation 33

$$P_B = P_{Blower} - P_A \tag{35}$$

The value, P_B, represents the baseline static pressure measurement. With the addition of the elbow, Scenario 1 follows Equation 34.

$$P_{Sc1} = P_{Blower} - P_e - P_K - P_A \tag{36}$$

A common form of comparison can be calculated with the percent difference formula as shown in Equation 35.

$$PE = 100 * \frac{P_{Sc1} - P_B}{P_B} \tag{37}$$

Substituting in Equation 33 and Equation 34 leads to Equation 36.

$$PE = 100 * \frac{-(P_e + P_K)}{P_B} \tag{38}$$

The static pressure percent difference between baseline and elbow test should always be negative as seen in Equation 36, which explains why it is nonsensible to obtain a positive percent error. From Table 29 however, it is apparent that there is positive error for the over-sized ducts used with the 2 and 3 ton units, for the 5 ton unit, and for one Scenario 1 test from the 3 ton unit. There are only two options for a positive reading: The Scenario 1 pressure reading is too high, or else the baseline reading is too low. No conclusive answer is available; however, this issue is probably related to flow abnormalities and flow maldistributions at the unit outlet possibly, which resulted in one or both static pressure measurements being incorrect. If in fact, these measurements are in error, it would be because the abnormal and maldistributed flow could not straighten to a more uniform condition by the time the fluid reaches the pressure measuring points on either side of the elbow. As has been discussed elsewhere, both the over-sized duct and the 5 ton unit have flow disturbances at the unit outlet created by the area expansion in the case of the over-sized duct, and the lack of heat exchanger downstream of the blower in the case of the 5 ton unit. The elbow orientation related to the positive pressure

error for the 3 ton unit was the one orientation that most opposed the blower high velocity section (orientation 1), which could have altered the elbow pressure drop due to flow maldistribution similar to the oversized duct and 5 ton unit. Additional experimental investigations are required to determine whether or not a problem exists and how to possibly alleviate any positive error from occurring.

CS-11: Baseline Test Results for Different Downstream Elbow Types and Orientations

Does the downstream elbow type and orientation affect the accuracy of ASHRAE Standard 37 in the baseline test measurements?

Twelve baseline tests (three elbow types and four orientations) were performed according to ASHRAE Standard 37 on the 2 ton unit to ensure that elbow type and orientation did not affect the power and airflow measurements. The baseline raw data are shown in Table 36.

Table 36: Baseline tests for the 2 ton unit.

2 TON Units	Power (W)	Nozzle Airflow (CFM)	Unit Pressure (in w.c)	Density (lbm ft-3)
BC1	233	723	0.10	0.0737
BC2	234	724	0.10	0.0736
BC3	234	721	0.10	0.0733
BC4	232	721	0.10	0.0733
BS1	236	724	0.10	0.0739
BS2	235	734	0.10	0.0742
BS3	238	724	0.10	0.0735
BS4	231	733	0.10	0.0744
BV1	237	722	0.10	0.0746
BV2	230	723	0.10	0.0739
BV3	235	719	0.10	0.0738
BV4	235	726	0.10	0.0738

The power was shown to range from 230-238 watts and the airflow ranged from 719-734 cfm. The maximum percent differences compared to the average for power and airflow were 1.6% and 1.4% respectively. The airflow variation of 1.4% was slightly outside the instrumentation error (which was ±1.1%) yet leakage could easily account for the slight variations. Therefore, for all practical purposes, the different elbow types and orientations probably has only a negligible effect on the power and airflow measurements. Because the elbow was located downstream of the pressure measurement point at a distance of 0.25 L_A (which was 8.25 inches for the 2 ton unit), it is not necessarily surprising that the elbow's effect is negligible. Also, for the 2 ton unit the duct is essentially square (cross-section has an aspect ratio of unity) so orientation effects should also be negligible. However, in the case of the 3 and 5 ton units, the aspect ratio of the duct cross-section is not unity so an investigation is necessary to ascertain the effects of aspect ratio and elbow orientation on the test values for baseline tests following ASHRAE Standard 37 specifications.

CONCLUSIONS AND RECOMMENDATIONS

Conclusion

Testing of unitary air conditioners and heat pumps following ASHRAE Standard 37 under standard conditions is essential for evaluating and predicting equipment performance. Unfortunately, many companies find it difficult to fit the test apparatus into their psychometric testing facilities because of the duct lengths required by this ASHRAE testing standard. It has been suggested by industry that this testing problem could be eliminated if alternative geometries were found that maintained the reliability of testing while reducing the overall height of the test apparatus below 85 in. In this light, ASHRAE Committee TC 8.11, Unitary Air Conditioners and Heat Pumps, initiated an ASHRAE funded project, TRP-1581, to solve this problem. This report documents experimental tests to evaluate two alternative approaches for height reductions below 85 in. for three different sized units (2, 3, and 5 tons). Specifically, the project investigated changing the outlet direction from vertical to horizontal (Scenario 1) and shortening the outlet duct with a passive resistive device (Scenario 2). A thorough experimental evaluation of these two approaches under standard conditions, along with a comparison to the conventional baseline was necessary to ensure that the reliability of ASHRAE Standard 37 was not compromised.

A test facility capable of testing units according to ASHRAE Standard 37 was designed and built. The facility was assembled with the flexibility to test the Scenario 1 and Scenario 2 setups under standard conditions. Calibrated instrumentation and a sophisticated data acquisition system were installed for measuring several static pressures, psychometric conditions, airflow rate, and a 16 point velocity profile.

Scenario 1 evaluated three different elbow geometries in four orientations for the three unit sizes. These elbow geometries shifted the exit duct from a vertical plane to a horizontal plane, thus reducing the test height. It was possible to evaluate each elbow and orientation for each unit by comparing the measured power, airflow, and static pressure to the results of an ASHRAE Standard 37 setup, which consisted of a vertical

air handler with a damper-box and skirt at the inlet. The elbows that were used included a square elbow, a curved elbow, and a square elbow with double turning vanes spaced 2 in. apart and with a radius of 2 in. The Scenario 1 tests required that 36 different elbow and horizontal duct assemblies, utilizing three duct sizes, three elbow geometries, and four elbow orientations, be designed, constructed, and tested. In the elbow tests, the power and airflow were controlled to be within 5% and 2.5% of the ASHRAE Standard 37 setup values, leaving static pressure as the variable of interest.

The Scenario 1 test results showed that the only elbow test with measured static pressure values within 12% of the AHRI rating point for all tests was V3, which represents a square elbow with turning vanes and elbow orientation 3. As a further check, the elbow test V3 was tested by setting the static pressure for each of the three air handling units at the AHRI rating points, which were 0.1, 0.15 and 0.2 in. of water for the 2, 3, and 5 ton units, respectively. The power, airflow, and static pressure measurements for V3 were within the instrumentation error for all three units, which provided conclusive evidence that V3 was a viable alternative geometry for testing the performance of air handling units.

Scenario 2 evaluated a series of passive resistive geometries that were placed at the unit outlet with the goal of reducing the height between the unit and the static pressure ring. Power and airflow were controlled to be within 5% and 2.5% of the baseline values, leaving measured static pressure as the variable of interest. Each of the six passive resistive pieces involved some type of material mounted in a frame placed directly above the unit. Scenario 2 tests required that 14 resistive pieces be designed, constructed and tested. Of special importance in Scenario 2 was determining through experimentation the position where the outlet static pressure could be accurately measured, with the hope that the resistive piece would enable the pressure to be measured closer to the unit outlet, at least compared to the baseline measurement point. To accomplish this task, static pressure measurements were taken at different distances from the unit outlet.

The Scenario 2 test results showed that the metal mesh geometry with a 0.75 in. frame was able to achieve a static pressure within 5% error of the AHRI rating points at the duct lengths of 18 in. and 13 in. for the 2 and 3 ton unit, respectively. These maximum duct lengths produced an overall test apparatus height of 85 in. when including the unit height, outlet duct, and an elbow. Furthermore, when tested at the AHRI rating point, the power and airflow remained within 3.6% and 2.2% respectively, of the baseline test. All the passive resistive pieces performed remarkably better with the 3 ton unit compared to the 2 ton unit, possibly suggesting that ECM motors are more conducive to Scenario 2. None of the passive resistive devices for the 5 ton unit were able to produce results comparable to the ASHRAE Standard 37 baseline. A logical explanation is that the heat exchanger for the 5 ton unit was upstream of the blower (i.e. a draw through unit), and as a result the passive resistive pieces were thus unable to level the maldistribution leaving the blower within the required 8 in. length.

Scenario 1 test also included a modified over-size duct test matrix with the 5 ton ducting being mounted on the two smaller units. Therefore, the 2 and 3 ton units each had two baseline tests, one for the oversized duct and one for the original duct. Both units showed a slight decrease in baseline airflow when using the over-sized duct, suggesting that the increase in area of the outlet duct may have changed the unit operating point even when set to the AHRI rating point. An added benefit of the over-sized duct was that several elbows performed better due to the increase in area and the subsequent decrease in average velocity. This reduced the pressure drop across the elbow tests so that some of the curved and square elbow tests were comparable to the square elbow with turning vanes. Yet, the square elbow with turning vanes still performed well, with less than 12% pressure error for the smaller units with the over-sized duct.

The 16-point velocity profiles for all of the tests performed in this project provided insight into flow changes at the unit outlet due to parameter changes. Contrary to expectation, the most uniform velocity profiles were not necessarily associated with low-percentage error tests. For Scenario 1, "horseshoe" shaped velocity profiles were

associated with low pressure drop in the elbow. In Scenario 2 all of the velocity profiles appeared more uniform compared to the velocity profiles in Scenario 1, possibly due to the flow straightening effects of the resistive pieces. It should also be noted that the velocity profiles for Scenario 2 were very similar amongst the units in that the higher velocities were in the upper region, possibly because the same elbow types and orientations were used for each passive resistive piece. All of the Scenario 2 profiles were similar to the baseline tests of the same elbow type and orientation with just a slightly more distributed velocity profile due to settling of the flow.

In addition to the above Scenario 1 and 2 studies, eleven case studies of varying degree of sophistication were performed. Each of these eleven case studies was the result of a specific issue or problem that was encountered in either the baseline, the Scenario 1 or the Scenario 2 testing. Because none of the case studies were investigated to full completion as they were beyond the scope of this project, they are recommended for future work.

In summary, the results for Scenario 1 have shown that ASHRAE Standard 37 can be modified to reduce testing height restrictions by using a horizontal pressure measurement location downstream of a square elbow with turning vanes, provided it is oriented in a specific manner relative to the blower. Furthermore, additional Scenario 1 testing with an over-sized outlet duct (sized to the 5 ton unit) shows that possibilities exist for using a single over-sized duct to successfully meet ASHRAE Standard 37 testing conditions when testing a variety of units. Finally, the results of Scenario 2 have shown that the height constraints of the outlet duct can be reduced by installing a passive resistive device consisting of a mesh at the outlet; however, this approach applies only to those units with the heat exchanger located downstream of the blower, such as the 2 and 3 ton units.

Recommendations for Future Work

Every aspect of the TRP-1581 project scope was completed and every test required was carried out. In addition, the project objective was met in that several approaches for

reducing test height while satisfying ASHRAE Standard 37 test conditions were found and documented. However, as with any lengthy complicated and detailed research study, a number of questions arose and were left unanswered because of time constraints. Several case studies related to these questions were started; however, none of these were carried to completion, again because of the project scope and time constraints. The results from these case-study research topics may be beneficial for future work. They are introduced below for consideration as future studies, with some summarizing results that were found during this project being presented. A more detailed analysis of each of these topics can be found in the Case Study Chapter. The nomenclature "CS" refers to case studies, while the number refers to each case study in the order presented in this report. Eleven of these "Recommendations for Future Work" are outlined below.

CS-1: Validation of the ASHRAE Standard 37 Static Pressure Measurement Position

Is the ASHRAE Standard 37 static pressure ring location, based on the calculated distance between the unit outlet and the static pressure measurement point, correctly specified for an accurate pressure measurement?

A series of tests that measured static pressure between the unit outlet and the ASHRAE Standard 37 measurement point showed that for the 2 and 3 ton unit, the measured pressure curves in the baseline appeared to approach the ASHRAE Standard 37 location; however, for the 5 ton unit the pressure did not asymptotically approach the ASHRAE Standard 37 value as evidenced by the results of the baseline test for Scenario 2. This baseline result brought up the question of was happening to the pressure profiles downstream of the ASHRAE Standard 37 pressure measurement location. In addition, the outlet duct length was doubled for the 3 ton unit and the static pressure was shown to increase past the pressure tap location. This increase is unrealistic because one would normally expect the static pressure to decrease in the direction of the flow, assuming a fully developed or settled flow, so that a true measure of the static pressure can be obtained. An additional investigation may be necessary to resolve this dilemma.

CS-2: Validation of the Static Pressure Measurement Position Downstream of the Elbow in Scenario 1 Testing

Does the ASHRAE Standard 37 calculated pressure measurement location downstream of the elbow provide an appropriate measurement location for Scenario 1?

The Scenario 1 pressure measurement location downstream of the elbow was determined by the same equation used to calculate the ASHRAE Standard 37 pressure measurement location. It is questionable that this same equation for calculating the pressure measurement location applies equally well to a flow exiting a blower and an elbow because the geometry and flow dynamics of a unit exit and an elbow exit are so different. To investigate further, Scenario 1 was set up with the square elbow with turning vanes in elbow orientation 3 (bend of elbow opposes the rotation of the blower) with pressure points before and after the Scenario 1 pressure location in order to create a pressure profile along the horizontal duct. The pressure profiles for the 2 and 3 ton units remained relatively constant, while the pressure profile for the 5 ton unit increased from the elbow to the Scenario 1 pressure measurement location. The lack of a heat exchanger downstream of the blower could be the reason for the difference in the pressure profile for the 5 ton unit. The applicability of this standard distance equation for Scenario 1 testing after an elbow needs further investigation.

CS-3: Experimental Loss Coefficients for Baseline Tests

Why do the experimental loss coefficients in this study not agree with ASHRAE loss coefficient values?

An additional pressure ring was placed in the horizontal duct downstream of the elbow for baseline tests that were performed according to ASHRAE Standard 37 (note: this is not Scenario 1). The elbow pressure drops were found for all three elbows and all four elbow orientations of the 2 ton unit with some additional elbow pressure drops for the other units. Loss coefficients were calculated and compared with the ASHRAE

Handbook Fundamentals (ASHRAE 2009b) values based on the work of Idelchik et al. (1986). Additional testing would be needed to determine why differences in loss coefficients exist.

CS-4: Draw-Through versus Blow-Through Air Handler Units

Does the position of the heat exchanger downstream or upstream of the blower have an effect on ASHRAE Standard 37 testing results?

The outcome of tests performed on the 5 ton unit consistently differed from the results of tests performed on the 2 and 3 ton units with the results of the latter two units being similar. These differences existed regardless of whether the tests were performed for Scenario 1, Scenario 2, baseline according to ASHRAE Standard 37 or even the case study for that matter. It was determined that the reason for these differences was most likely the lack of the heat exchanger downstream of the blower in the 5 ton unit, which allowed flow maldistributions to exit the unit. It caused such drastic effects as to question the use of Scenario 1, Scenario 2, and ASHRAE Standard 37 test specifications. The effect of the heat exchanger upstream of the blower on ASHRAE Standard 37 testing should be investigated.

CS-5: Effects of Testing with an Inlet Damper-Box and Skirt Configuration Compared to Other Configurations

How does testing with a damper-box and skirt inlet configuration affect fan performance in comparison to testing with other inlet configurations?

Published literature suggests that the blower performance could be affected by inlet conditions and the inlet configurations; however, any study related to the inlet was beyond the scope of this project. For all tests reported herein, with the exception of two tests with the 3 ton unit, the damper-box and skirt inlet configuration was chosen based on the guidance from the project monitoring committee, which they stated was

consistent with industry practice. It should be noted that ASHRAE Standard 37 makes a recommendation regarding inlet configurations, but it does not mandate a specific type. The two exceptions used the skirt (for inlet pressure measurements) and a straight inlet duct three hydraulic diameters in length while the outlet of the unit was configured for Scenario 1 test V3. The comparison indicated an increase in airflow for a straight inlet duct versus the Scenario 1 test V3 with the skirt and damper-box configuration. Definitive answers regarding inlet configurations would require an additional study.

CS-6: Test Parameter: Airflow versus Static Pressure

What parameter (either airflow or static pressure) was best suited as the set point test parameter (independent) and as the comparison parameter (dependent) during Scenario 1 and 2 investigations?

The Scenario 1 and Scenario 2 tests were performed by setting airflow to the same value obtained from the baseline tests and then measuring the power and static pressure. This approach was directed by the project monitoring committee. However, the tests from Scenario 1 and Scenario 2 with the best results were repeated as a check setting the static pressure as the AHRI rating points (0.1, 0.15, and 0.20 inches of water for the 2, 3, and 5 ton units) and then measuring power and airflow as was done in the original baseline tests. The results from the two types of Scenario 1 and Scenario 2 tests with different set test parameters (airflow or static pressure) were compared. The results showed a large effect due to motor type, which caused different trends, even though the largest static pressure difference was only 0.13 inches of water. Neither test parameter was found to be the best as they were dependent on each other, yet for ECM motors it was beneficial to set airflow first as it showed the largest change in static pressure, therefore highlighting the best test. Additional studies are recommended to determine definitively the relationship between motor type and the advantage of selecting one parameter over the other as the set test condition.

CS-7: Theoretical versus Experimental Static Pressure Profiles Downstream of the Unit

What are the test parameters and flow conditions that affect static pressure measurement accuracy and reliability in the exit ducting?

In Scenario 1 and 2, numerous tests were performed that provided opportunities for measuring the pressure before and after the designated static pressure measurement point. In these cases, pressure profiles were created by plotting the experimentally measured pressure versus the measurement location along the straight duct. Different shapes of pressure profiles were created, anywhere from a constant profile to ones that increased along the duct, which runs contrary to intuition. A method of validation was needed to find when accurate and reliable pressure measurements were being found in relation to the duct length. Therefore, a theoretical pressure drop profile was created as a form of comparison for the purpose of determining whether the pressure measurements along the duct and their profile trends were reasonable, and reliable. The difference in theoretical and experimental profile shapes and trends were in some cases substantial enough to warrant additional studies.

CS-8: Pressure Measurement Accuracy as a Function of the Pressure Ring Configuration

What type of pressure ring configuration and approach provides the most reliable and accurate static pressure measurements?

ASHRAE Standard 37 recommends several methods for measuring static pressure in the duct at the unit outlet. Specifically, the standard gives pressure tap dimensions for two pressure ring configurations used to obtain average pressure readings. Based on literature review it was found that static pressure measurement error could occur when measuring antisymmetric flow based on the pressure ring configuration (including the pressure tap), which ASHRAE Standard 37 as it stands, does not prevent. It is recommended that the accuracy and reliability of the two methods be compared and

analyzed, especially when fluid maldistributions are present, which is the case for baseline, Scenario 1, and Scenario 2 tests.

CS-9: The Effects of Mounting an Elbow Downstream of the Static Pressure Measurement Point

Is the ASHRAE Standard 37 minimum-distance calculation for mounting an elbow downstream of the static pressure measurement point correctly specified?

ASHRAE Standard 37 specifies two equations that relate the cross-sectional dimensions of the unit to the static pressure measurement location in the outlet duct and to the overall length of the vertical outlet duct, which is marked by the flow entering an elbow. By definition, these two equations also relate the minimum distance between pressure measurement location and the downstream end of the vertical outlet duct. The possibility of reducing this distance has its advantages for the baseline tests and Scenario 2 tests because it reduces the height of the test apparatus. However, it is unknown whether this distance is too long, too short, or appropriate for either the baseline, Scenario 1, or Scenario 2 testing. Data from this project were analyzed to only a small degree with reference to this distance, and therefore, it would be beneficial to further investigate another possibility for reducing the test apparatus height.

CS-10: Positive Static Pressure Error for Scenario 1 Elbow Tests

Should the elbow and duct pressure drops for Scenario 1 always be greater than pressure drops for the baseline tests for the same duct length?

Static pressure measurements of the baseline and Scenario 2 tests were analyzed in detail, and it was determined that for matching airflows, the baseline pressure should always be larger than the Scenario 1 static pressure because of the additional elbow pressure drop, assuming the straight duct pressure drop is the same for both tests. However, this was not the case for tests done with the over-sized duct and tests done

with the 5 ton unit. It is thought that flow maldistribution caused by heat exchanger locations and by abrupt duct changes could create errors in the static pressure data; however, additional investigations may be required to arrive at a definitive answer and a solution, if in fact a problem exists.

CS-11: Baseline Test Results for Different Downstream Elbow Types and Orientations

Does the downstream elbow type and orientation affect the accuracy of ASHRAE Standard 37 in the baseline test measurements?

Normally, one would not expect geometry downstream of a static pressure measurement point to affect the pressure measurement itself. However, in the case of the smaller size units the distance from the measurement point to the elbow. Therefore, twelve baseline tests (three elbow types and four orientations) were performed in accordance with ASHRAE Standard 37 on the 2 ton unit in order to evaluate the effect that elbow type and orientation has on the power and airflow measurements. For all practical purposes, the different elbow types and orientations had only a negligible effect on the static pressure, power, and airflow measurements. However, this result may not be conclusive or universal because the 2 ton unit had an exit geometry with an aspect ratio of unity. Because most units have rectangular exit geometries, further investigations must be done to determine the effects of downstream elbow types and orientations on baseline test measurements performed according to ASHRAE Standard 37 specifications.

REFERENCES

AHRI. 2008. *Performance Rating of Unitary Air-Conditioning & Air-Source Heat Pump Equipment*. AHRI Standard 210/240-2008. Air-Conditioning, Heating, and Refrigeration Institute, Arlington, VA. Pg 20.

ASHRAE. 2005. *Methods of Testing for Rating Electrically driven Unitary Air-Conditioning and Heat Pump Equipment*. ANSI/ASHRAE Standard 37-2005. American Society of Heating, Refrigerating, and Air-Conditioning Engineers, Inc., Atlanta, GA.

ASHRAE. 2007. *Laboratory Methods of Testing Fans For Certified Aerodynamic Performance Rating.* ANSI/ASHRAE Standard 51-2007. American Society of Heating, Refrigerating, and Air-Conditioning Engineers, Inc., Atlanta, GA.

ASHRAE. 2009a. *2009 ASHRAE Handbook- Fundamentals*, I-P edition. American Society of Heating, Refrigerating, and Air-Conditioning Engineers, Inc., Atlanta, GA.

ASHRAE. 2009b. *2009 ASHRAE Handbook- Fundamentals*, I-P edition, Page 21.26, American Society of Heating, Refrigerating, and Air-Conditioning Engineers, Inc., Atlanta, GA.

Baines, W. D., & Peterson, E. G. 1951. An Investigation of Flow Through Screens. *Trans. Am. Soc. Mech. Engrs., 73*.

Bayomi, N. N., Abdel Hafiz, A., & Osman, A. M. 2006. Effect of Inlet Straighteners on Centrifugal Fan Performance. *Energy Conversion and Management, 47*(18), 3307-3318.

Blake, K. A. 1976. The Design of Piezometer Rings. *Journal of Fluid Mechanics, 78*(2), 415-428.

Bohanon, H. R. 1975. Fan Test Chamber-Nozzle Coefficients. *ASHRAE Transactions, 81*(Pt 1), 104-122.

Bommisetty, Ramakumar, Joshi, Dhanvantri, & Kollati, Vighneswara Rao. 2011. *Flow Loss in Screens: A Fresh Look at Old Correlation.* Paper presented at The 11th Asian International Conference on Fluid Machinery.

Bradshaw, P. 1965. The Effect of Wind-Tunnel Screens on Nominally Two-Dimensional Boundary Layers. *J. Fluid Mech, 22*(4), 679-687.

Brundrett, E. 1993. Prediction of Pressure Drop for Incompressible Flow through Screens. *Journal of Fluids Engineering, 115*(2), 239-242.

Churchill, Stuart W. 1977. Friction Factor Equation Spans all Fluid Flow Regimes. *Chemical Engineering, 84*(24), 91-92.

DOE. 2013. Uniform Test Method For Measuring the Energy Consumption of Central Air Conditioners and Heat Pumps. *10CFR430.2, Subpart b, Appendix M*. Code of Federal Regulations, U.S. National Archives and Records Administration, 8601 Adelphi Road, College Park, MD 20740-6001.

Fuchs, Ewald, & Masoum, Mohammad. 2008. *Power Quality in Power Systems and Electrical Machines*. Burlington: Elsevier Academic. 210-15.

Griggs, E. I., & Khodabakhsh-Sharifabad, F. (1992). Flow Characteristics in Rectangular Ducts. *ASHRAE Transactions, 98*(1), 116-127.

Huebscher, R. G. 1948. Friction Equivalents for Round, Square and Rectangular Ducts. *ASHVE Transactions (renamed ASHRAE Transactions), 54*, 101-144.

HVI. 2009. *HVI Airflow Test Procedure*. HVI Publication 916. Home Ventilating Institute, Wauconda, IL.

Idelchik, Isaak E, & Fried, Erwin. 1986. Handbook of Hydraulic Resistance. Mumbai: Jaico Publishing House.

King, J. Darrell, Cooperman, Alissa, Dieckmann. 2012. Induction or PM motors. *ASHRAE Journal*. October 2012. American Society of Heating, Refrigerating, and Air-Conditioning Engineers, Inc., Atlanta, GA.

Kline, S. J., & McClintock, F. A. 1953. Describing Uncertainties in Single-Sample Experiments. *Mechanical Engineering*, 75(1), 3-8.

Kwon, Eui-Yong, & Cho, Nam-Hyo. 2001. Experimental Study on the Mean Flow Characteristics of Forward-Curved Centrifugal Fans. *KSME International Journal, 15*(12), 1728-1738.

Lau, Y. L., & Baines, W. D. 1968. Flow of Stratified Fluid through Curved Screens. *Journal of Fluid Mechanics, 33*(04), 721-738.

Laws, E. M., & Livesey, J. L. 1978. Flow through Screens. *Annual Review of Fluid Mechanics, 10*(1), 247-266.

Mandal, Arindam, Bhattecharjee, Somnath, Debnath, Rabin, Roy, Debasish, & Majumder, Snehamoy. 2010. Experimental Investigation of Turbulent Fluid Flow through a Rectangular Elbow. *International Journal of Engineering Science and Technology, 2*(6), 1500-1506.

Moody, Lewis F. 1944. Friction Factors for Pipe Flow. *Trans. ASME, 66*(8), 671-684.

Montgomery, Douglas C., Runger, George C., Hubele, Norma Faris. 2007. *Engineering Statistics* (4 ed.). New York: John Wiley & Sons, Inc.

Moujaes, S. F., & Aekula, S. 2009. CFD Predictions and Experimental Comparisons of Pressure Drop Effects of Turning Vanes in 90° Duct Elbows. *Journal of Energy Engineering, 135*(4), 119-126.

Pinker, R. A., & Herbert, M. V. 1967. Pressure Loss Associated with Compressible Flow through Square-Mesh Wire Gauzes. *Journal of Mechanical Engineering Science, 9*(1), 11-23.

Roth, W. Kurt, Chertok, Allen, Dieckman, John. 2004. Electronically commutated permanent magnet motors. *ASHRAE Journal*. March 2004. American Society of Heating, Refrigerating, and Air-Conditioning Engineers, Inc., Atlanta, GA.

Shaw, R. 1960. The Influence of Hole Dimensions on Static Pressure Measurements. *J. Fluid Mech, 7*(4), 550-564.

Zhao, Zenghui, Peles, Yoav, & Jensen, Michael K. 2013. Properties of Plain Weave Metallic Wire Mesh Screens. *International Journal of Heat and Mass Transfer, 57*(2), 690-697.

APPENDIX A

The dimensional drawings of the damper-box and skirt are presented in this appendix. The dimensions are in reference to variables c and d which represent the inlet dimensions of the air handling unit. x and y are set to be larger than c and d as required by the DOE (DOE 2013).

A.1 Damper-Box Dimensions

For the damper-box utilized in the project x and y were 22 in. and 23 in., respectively.

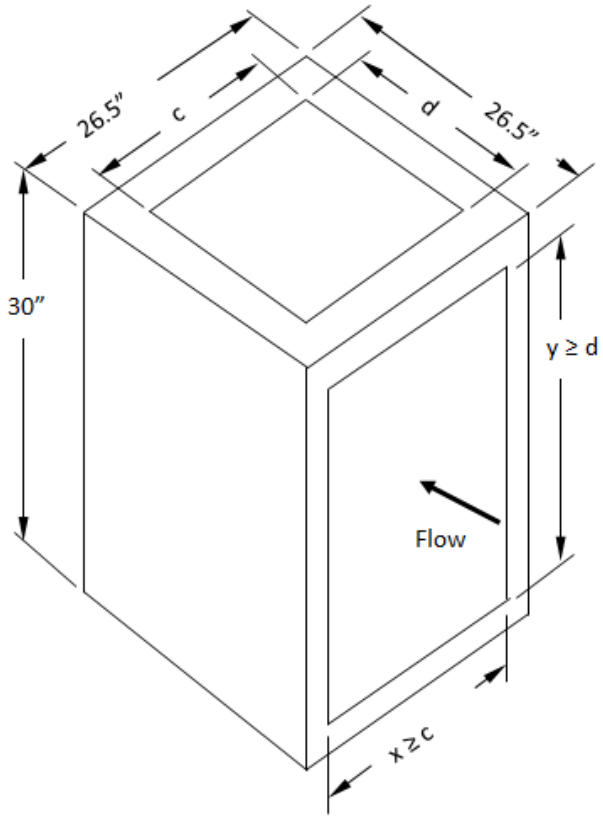

Figure 51: Dimensions of damper-box.

A.2 Skirt Dimensions

The skirt dimensions are also shown below. The skirt was made with 1.5 in. thick boards. c and d again were the inlet dimensions of the unit and therefore the outer edge dimensions were the addition of two times the thickness, t, to the unit inside dimensions. Pressure taps were placed in the center of each side. The height of the skirt was specified for all units as 6 in as shown in Figure 52.

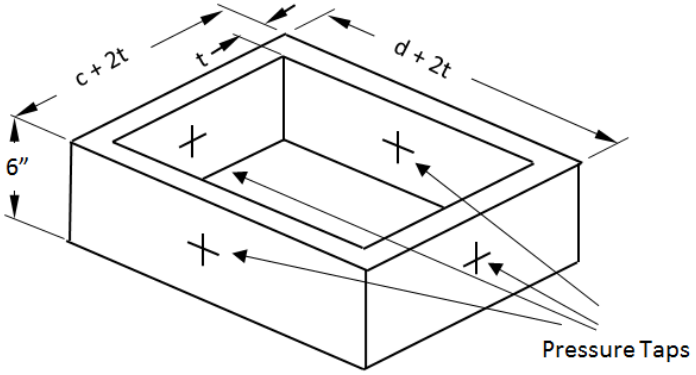

Figure 52: Dimensions of skirt.

APPENDIX B

Appendix A details the sample calculations that were referred to in the main report. They are organized in the order in which they are referenced.

B.1 Uncertainty Propagation

For a sample of uncertainty propagation, power measurements for the 2 ton unit were used as an example with the measurements and corresponding error shown in Table 37.

Table 37: Measurements for power uncertainty calculation.

Voltage	Error	Amperage	Error	Power Factor	Phase Angle Error
(V)	(V)	(A)	(A)		(Radians)
230	0.4103	1.05	0.0275	0.95	0.010297

The measured data included the voltage, current, and power factor. The error for each parameter was given in the instrument specifications. The power factor error was given in phase angle. The first use of the root sum of the squares (Equation 13, RSS) was for finding the power factor error related to phase angle error due to the relation shown in Equation 27.

$$PF = \cos(\varphi) \tag{27}$$

Converting the power factor of 0.95 to phase angle, resulted in a phase angle of 0.318 radians. The partial derivative of the Equation 27 and application of RSS can be seen below.

$$\frac{\partial \, \mathrm{P}}{\partial \, \varphi} = -\sin(\varphi)$$

$$\frac{\partial \, PF}{\partial \, \varphi} = -\sin(0.318) = 0.313$$

$$w_{PF} = \left[\left(\frac{\partial \, PF}{\partial \, \varphi} \, w_{\varphi}\right)^{2}\right]^{0.5}$$

$$w_{PF} = [(-0.313 * 0.010297)^2]^{0.5}$$

$$w_{PF} = 0.0032$$

Therefore the value for the power factor was 0.95 ± 0.0032.

The actual power was found from Equation 28.

$$\mathrm{P} = \mathrm{I\ V\ PF} \tag{28}$$

Similar to before, the error for the actual power was found by finding the partial derivatives of each parameter in the equation and applying RSS.

$$\frac{\partial\ \mathrm{P}}{\partial\ \mathrm{V}} = \mathrm{I\ PF} = (1.05\ \mathrm{A})(0.95) = 0.9975\ \mathrm{A}$$

$$\frac{\partial\ \mathrm{P}}{\partial\ \mathrm{I}} = \mathrm{V\ PF} = (230\ \mathrm{V})(0.95) = 218.5\ \mathrm{V}$$

$$\frac{\partial\ \mathrm{P}}{\partial\ \mathrm{PF}} = \mathrm{VI} = (230\ \mathrm{V})(1.05\ \mathrm{A}) = 241.5\ \mathrm{VA}$$

$$\mathrm{w_P} = \left[\left(\frac{\partial\ \mathrm{P}}{\partial\ \mathrm{V}}\ w_{\mathrm{V}}\right)^2 + \left(\frac{\partial\ \mathrm{P}}{\partial\ \mathrm{I}}\ w_{\mathrm{I}}\right)^2 + \left(\frac{\partial\ \mathrm{P}}{\partial\ \mathrm{PF}}\ w_{\mathrm{PF}}\right)^2\right]^{0.5}$$

$$\mathrm{w_P} = [(0.9975 * 0.4103)^2 + (218.5 * 0.0275)^2 + (241.5 * 0.0032)^2]^{0.5}$$

$$\mathrm{w_P} = 6.072\ \mathrm{W}$$

The actual power for the sample calculation was 229.425 ± 6.072 W.

This same process was used to find the error for airflow and pressure measurements. The complete table of instrument uncertainty was shown in Instrumentation Uncertainties.

B.2 Sample Calculations for Standardized Airflow and Static Pressure

The following parameters were used for calculating standardized airflow and static pressure as shown in Table 38. Many are self-explanatory, but some require mentioning. PF stands for the power factor and *P*, for the static pressure. T is for temperature and D and A are for diameter and area, respectively. The subscript n denotes parameters for the nozzle section. DB and WB stand for dry bulb and wet bulb, respectively. The subscript baro represents barometric.

Table 38: Sample parameters for standardized airflow and pressure calculations.

Voltage	Current	PF	P	P_n	T_{DB}	T_{WB}	P_{Baro}	D_n	A_n
(V)	(A)		(in w.c.)	(in w.c.)	(F)	(F)	(in Hg)	(ft)	(ft^2)
230	1.05	0.95	0.0993	1.045	67.09	56.49	29.78	0.490	.1886

With the above parameters from Table 38, it was possible to determine the density and airflow as shown in this sample calculation. Equation 14 is a polynomial equation that utilizes T_{WBr}(T_{WB} in rankine).

$$Pln = \frac{C8}{T_{WBr}} + C9 + C10(T_{WBr}) + C11(T_{WBr})^2 + C12(T_{WBr})^3 + C13\ln(T_{WBr}) \quad (14)$$

$$Pln = \frac{C8}{56.49 + 460.67} + C9 + C10(56.49 + 460.67) + C11(56.49 + 460.67)^2 + C12(56.49 + 460.67)^3 + C13\ln(56.49 + 460.67)$$

$$Pln = -1.45$$

Utilizing this result in Equation 15, the saturation pressure was found.

$$Pws = e^{Pln} \quad (15)$$

$$Pws = \mathrm{e}^{-1.45} = 0.2343\ [\text{in w.c.}]$$

Humidity ratio at saturation, Wxs, was then calculated using Equation 16.

$$Wxs = \frac{0.621945\ Pws}{0.491098\ P_{Baro} - Pws} \quad (16)$$

$$Wxs = \frac{0.621945\ (0.2343)}{0.491098\ (29.78) - (0.2343)} = 0.010126\ \left[\frac{lbm\ water}{lbm\ dry\ air}\right]$$

Assuming that the process of adding water to the air is adiabatic, enthalpy is conserved resulting in Equation 17, which finds the humidity ratio of the air.

$$W = \frac{(1093 - .556\ T_{WB})Wxs - .240\ (T_{DB} - T_{WB})}{1093 + .444T_{DB} - T_{WB}} \quad (17)$$

$$W = \frac{\big(1093 - .556\ (56.49)\big)(0.010126) - .240\ (67.09 - 56.49)}{1093 + .444(67.09) - 56.49}$$

$$W = 0.007695 \left[\frac{lbm\ water}{lbm\ dry\ air}\right]$$

The specific volume of moist air relative to dry air was found with Equation 18.

$$v = \frac{.370486\ T_{DBR}\ (1 + 1.607858\ W)}{.491098\ P_{Baro}} \tag{18}$$

$$v = \frac{.370486\ (67.09 + 460.67)\ (1 + 1.607858\ (0.007695))}{.491098\ (29.78)}$$

$$v = 13.53492\ [\text{ft}^3\ \text{lbmda}^{-1}]$$

Since viscosity also varies with temperature, the dynamic viscosity (lbm ft^{-1} s^{-1}) was calculated where Tn is the nozzle temperature.

$$\mu = (11.00 + .018\ T_{DB}) * 10^{-6} \tag{19}$$

$$\mu = (11.00 + .018\ (67.09)) * 10^{-6} = 1.2208E - 05\ [\text{lbm ft}^{-1}\ \text{s}^{-1}]$$

To find the specific volume of wet air, the below relation from ASHRAE Standard 37 was used.

$$v_{np} = \frac{v}{1 + W} \tag{20}$$

$$v_{np} = \frac{13.53492}{1 + 0.007695} = 13.43156\ [\ ft^3\ lbm^{-1}]$$

The Reynolds number was calculated by converting the differential pressure across the nozzles into an airflow measurement (Equation 21). The Reynolds number is dependent on the discharge coefficient, C, which is defined in Equation 22 (Bohanon 1975).

$$Re = 1.523\ \frac{D_n\ C1}{\mu}\sqrt{\Delta P * v_{np}} \tag{21}$$

$$C = .9986 - \frac{7.006}{\sqrt{Re}} - \frac{134.6}{Re} \tag{22}$$

An iterative process was used with these two equations where C1 was an old discharge coefficient and C a new discharge coefficient until the difference between C1 and C was less than 0.001 (ASHRAE 2007). For the first iteration, C1 was set to 0.95.

$$Re = 1.523\ \frac{0.4901\ (0.95)}{1.2208E - 05}\sqrt{1.045 * 13.43156}$$

$$Re = 217{,}619.9$$

$$C = .9986 - \frac{7.006}{\sqrt{217{,}619.9}} - \frac{134.6}{217{,}619.9} = 0.9830$$

$$C1 - C = 0.9830 - 0.95 = 0.0330 > 0.001$$

$$C1 = 0.9830$$

Since the difference between C1 and C was larger than 0.001 another iteration was completed below.

$$Re = 1.523\ \frac{0.4901\ (0.9830)}{1.2208E-05}\sqrt{1.045 * 13.43156}$$

$$Re = 225{,}170.9$$

$$C = .9986 - \frac{7.006}{\sqrt{225{,}170.9}} - \frac{134.6}{225{,}170.9} = 0.9832$$

$$C1 - C = 0.9832 - 0.9830 = 0.0002 < 0.001$$

$$C = 0.9832$$

In this particular case only two iterations were necessary as shown above. With the discharge coefficient found, the airflow could be calculated from Equation 23.

$$Q = 1097C\ A_n\ \sqrt{\Delta P * vnp} \tag{23}$$

$$Q = 1097(0.9832)\ (0.188618)\ \sqrt{1.045 * 13.43156}$$

$$Q = 762.2\ cfm$$

Density was found although one last step needed to be done to define it.

$$\rho = \frac{1}{v_{np}} = \frac{1}{13.43156}$$

$$\rho = 0.074452\ lbm\ ft^{-3}$$

The airflow was corrected to standard airflow to make tests independent of temperature and humidity. The correction following mass conservation is shown in Equation 25.

$$Q_s = Q\ \frac{\rho}{\rho_s} \tag{25}$$

$$Q_s = 762.2\ \frac{0.074452}{0.075}$$

$$Q_s = 756.62\ cfm$$

The standard density is defined as ρ_s = .075 lbm ft^{-3}. Applying the same principles for pressure one gets Equation 26.

$$P_s = P\,\frac{\rho_s}{\rho} \tag{26}$$

$$P_s = 0.0993\,\frac{0.075}{0.074452}$$

$$P_s = 0.100\ in\ w.c.$$

This calculation procedure was repeated for all of the tests during this project. The standard airflow and standard static pressure were tabulated in the results section so that all tests were comparable. Power was also calculated. This process was shown in Appendix B.2 and was standardized as well.

B.3 Calculating ASHRAE Straight Duct Height

From the ASHRAE Handbook-Fundamentals it can be found that to obtain fully developed flow at the outlet when discharging to atmosphere through a straight duct it is required to allow an outlet duct length, L_e to be at least

$$L_e = \frac{\sqrt{a\,b}}{4.3} \tag{39}$$

For The 5 ton unit this would be an effective length of four inches as shown below.

$$L_e = \frac{\sqrt{282}}{4.3} \approx 4\ in \tag{40}$$

This is not considering downstream effects. If one accounts for an elbow a distance of L away from the centrifugal fan with a safety factor, the following inequality applies (ASHRAE 2009b).

$$\frac{L}{L_e} \geq 10$$

Solving for L

$$L \geq 10\, L_e$$

$$L \geq 10\, \frac{\sqrt{a\, b}}{4.3}$$

$$\frac{10}{4.3} \approx 2.5$$

$$L \geq 2.5\sqrt{a\, b} \tag{29}$$

APPENDIX C

Appendix C displays all the passive resistive pieces used for Scenario 2 testing of the 2, 3, and 5 ton units as previously mentioned in Table 5.

C.1 Passive Resistive Pieces for the 2 Ton Unit

Figure 53: Metal mesh passive resistive piece for the 2 ton unit.

Figure 54: Plastic mesh passive resistive piece for the 2 ton unit.

Figure 55: Half plastic mesh passive resistive piece for the 2 ton unit.

Figure 56: Single bar passive resistive piece for the 2 ton unit.

Figure 57: Parallel rods passive resistive piece for the 2 ton unit.

C.2 Passive Resistive Pieces for the 3 Ton Unit

Figure 58: Metal mesh for the 3 ton unit.

Figure 59: Plastic mesh for the 3 ton unit.

Figure 60: Half plastic mesh for the 3 ton unit.

Figure 61: Double strip mesh for the 3 ton unit.

C.3 Passive Resistive Pieces for the 5 Ton Unit

Figure 62: Metal mesh for the 5 ton unit.

Figure 63: Parallel rod for the 5 ton unit.

Figure 64: Large mesh for the 5 ton unit.

Figure 65: Frame for the 5 ton unit.

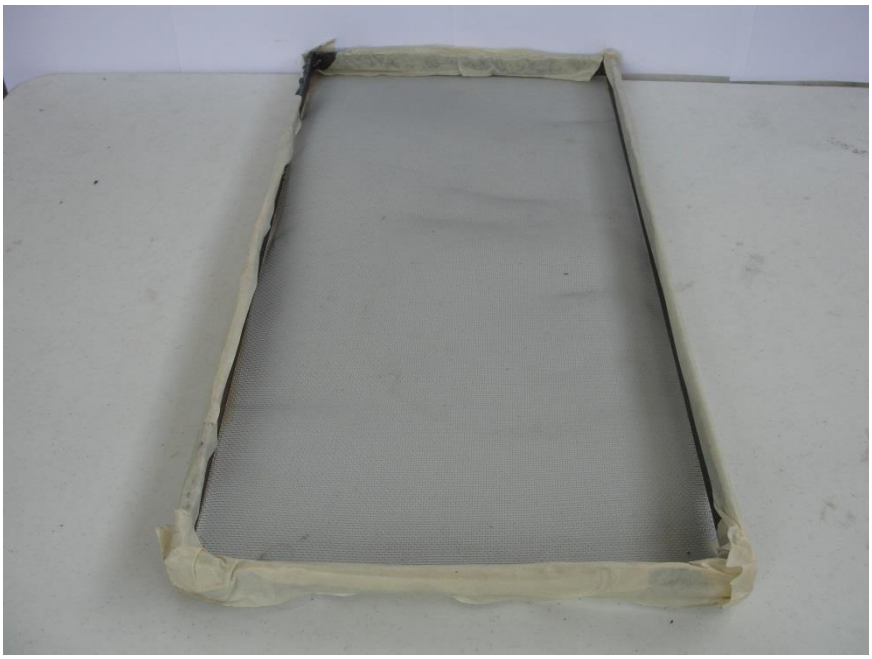

Figure 66: Metal mesh with a metal frame for the 5 ton unit.

APPENDIX D

D.1 Scenario 2 Raw Data

Table 39: Data for the 2 ton unit.

Metal Mesh	Location	P_{AS}	P_s	Q_s	P_s	ρ
Units	(in)	(in w.c)	(in w.c)	(cfm)	(W)	(lbm.ft-3)
	2.5	0.094	0.087	727	236	0.0757
	8	0.089	0.087	728	236	0.0757
	13	0.092	0.090	728	236	0.0757
	18	0.092	0.093	727	236	0.0757
	23	0.096	0.098	728	236	0.0757
	30	0.093	0.093	728	236	0.0757
Plastic Mesh	Location	P_{AS}	P_s	Q_s	P_s	ρ
Units	(in)	(in w.c)	(in w.c)	(cfm)	(W)	(lbm.ft-3)
	2.5	0.058	0.052	726	231	0.0738
	8	0.060	0.060	727	230	0.0739
	13	0.056	0.057	727	230	0.0742
	18	0.059	0.062	728	230	0.0739
	23	0.057	0.060	726	233	0.0738
	30	0.058	0.058	727	231	0.0739
Half Plastic Mesh	Location	P_{AS}	P_s	Q_s	P_s	ρ
Units	(in)	(in w.c)	(in w.c)	(cfm)	(W)	(lbm.ft-3)
	2.5	0.070	0.061	727	242	0.0739
	8	0.068	0.064	727	242	0.0739
	13	0.071	0.067	727	242	0.0739
	18	0.071	0.071	727	242	0.0739
	23	0.072	0.073	727	242	0.0739
	30	0.070	0.070	727	242	0.0739
1 Bar	Location	P_{AS}	P_s	Q_s	P_s	ρ
Units	(in)	(in w.c)	(in w.c)	(cfm)	(W)	(lbm.ft-3)
	2.5	0.098	0.077	728	237	0.0756
	8	0.096	0.086	727	237	0.0755
	13	0.096	0.086	727	237	0.0755
	18	0.102	0.090	727	237	0.0755
	23	0.101	0.099	728	236	0.0758
	30	0.099	0.099	727	237	0.0756

Table 39 Continued: Data for the 2 ton unit.

Parallel Rods	Location	P_{AS}	P_s	Q_s	P_s	ρ
Units	(in)	(in w.c)	(in w.c)	(cfm)	(W)	(lbm.ft-3)
	2.5	0.069	0.047	727	247	0.0738
	8	0.072	0.058	728	247	0.0739
	13	0.067	0.055	727	247	0.0739
	18	0.067	0.055	727	247	0.0739
	23	0.067	0.064	728	246	0.0739
	30	0.068	0.068	727	247	0.0739

Table 40: Scenario 2 data for the 3 ton unit.

Metal Mesh	Location	P_{AS}	P_s	Q_s	P_s	ρ
Units	(in)	(in w.c)	(in w.c)	(cfm)	(W)	(lbm.ft-3)
	2.5	0.142	0.126	1155	262	0.07464
	8.8	0.141	0.133	1154	267	0.07448
	13	0.144	0.141	1155	267	0.07453
	19.8	0.139	0.138	1155	266	0.07458
	25.3	0.142	0.144	1155	267	0.07440
	33	0.142	0.142	1155	266	0.07453
Plastic Mesh	Location	P_{AS}	P_s	Q_s	P_s	ρ
Units	(in)	(in w.c)	(in w.c)	(cfm)	(W)	(lbm.ft-3)
	2.5	0.144	0.143	1150	266	0.07438
	8.8	0.142	0.142	1151	264	0.07441
	13	0.136	0.139	1151	260	0.07463
	19.8	0.139	0.142	1152	264	0.07454
	25.3	0.142	0.146	1151	258	0.07434
	33	0.141	0.141	1151	262	0.07446
Half Plastic Mesh	Location	P_{AS}	P_s	Q_s	P_s	ρ
Units	(in)	(in w.c)	(in w.c)	(cfm)	(W)	(lbm.ft-3)
	2.5	0.152	0.139	1152	267	0.07418
	8.8	0.158	0.157	1153	267	0.07406
	13	0.153	0.153	1153	264	0.07404
	19.8	0.151	0.152	1153	262	0.07411
	25.3	0.149	0.151	1153	261	0.07427
	33	0.153	0.153	1153	264	0.07413
Double Strip	Location	P_{AS}	P_s	Q_s	P_s	ρ
Units	(in)	(in w.c)	(in w.c)	(cfm)	(W)	(lbm.ft-3)
	2.5	0.157	0.135	1154	262	0.07433
	8.8	0.157	0.148	1153	261	0.07432
	13	0.156	0.152	1153	264	0.07413
	19.8	0.158	0.155	1153	262	0.07408
	25.3	0.158	0.159	1154	262	0.07403
	33	0.157	0.157	1153	262	0.07418

Table 41: Scenario 2 data for the 5 ton unit.

Baseline	Location	P_{AS}	P_s	Q_s	P_s	ρ
Units	(in)	(in w.c)	(in w.c)	(cfm)	(W)	(lbm.ft-3)
	2.5	0.200	0.080	1961	717	0.0736
	8	0.200	0.052	1957	717	0.0737
	11.9	0.201	0.076	1955	727	0.0736
	14.7	0.199	0.096	1953	717	0.0734
	20.4	0.198	0.125	1956	724	0.0735
	33.8	0.200	0.200	1956	720	0.0736
Metal Mesh	Location	P_{AS}	P_s	Q_s	P_s	ρ
Units	(in)	(in w.c)	(in w.c)	(cfm)	(W)	(lbm.ft-3)
	2.5	0.141	0.041	1951	738	0.0737
	8	0.138	0.084	1953	739	0.0735
	11.9	0.115	0.051	1958	717	0.0736
	14.7	0.110	0.060	1959	741	0.0736
	20.4	0.105	0.068	1959	730	0.0735
	33.8	0.122	0.122	1956	733	0.0736
Parallel Rods	Location	P_{AS}	P_s	Q_s	P_s	ρ
Units	(in)	(in w.c)	(in w.c)	(CFM)	(W)	(lbm.ft-3)
	2.5	0.148	0.029	1953	726	0.0730
	8	0.149	0.041	1952	726	0.0730
	11.9	0.149	0.042	1954	726	0.0730
	14.7	0.150	0.056	1953	729	0.0730
	20.4	0.155	0.086	1952	730	0.0730
	33.8	0.150	0.150	1953	727	0.0730
Large Mesh	Location	P_{AS}	P_s	Q_s	P_s	ρ
Units	(in)	(in w.c)	(in w.c)	(CFM)	(W)	(lbm.ft-3)
	2.5	0.114	0.007	1950	716	0.0733
	8	0.067	0.001	1957	719	0.0728
	11.9	0.070	0.006	1957	719	0.0729
	14.7	0.073	0.016	1956	719	0.0729
	20.4	0.077	0.034	1956	723	0.0728
	33.8	0.080	0.080	1955	719	0.0729

Table 41 Continued: Scenario 2 data for the 5 ton unit

Frame	Location	P_{AS}	P_s	Q_s	P_s	ρ
Units	(in)	(in w.c)	(in w.c)	(CFM)	(W)	(lbm.ft-3)
	2.5	0.151	0.006	1956	718	0.0733
	8	0.152	0.028	1956	717	0.0733
	11.9	0.155	0.031	1953	717	0.0733
	14.7	0.153	0.048	1954	718	0.0733
	20.4	0.149	0.076	1959	717	0.0734
	33.8	0.152	0.152	1956	717	0.0733
Metal Frame	Location	P_{AS}	P_s	Q_s	P_s	ρ
Units	(in)	(in w.c)	(in w.c)	(CFM)	(W)	(lbm.ft-3)
	2.5	0.049	0.000	1954	753	0.0722
	8	0.054	0.000	1958	727	0.0724
	11.9	0.069	0.006	1952	724	0.0726
	14.7	0.068	0.011	1953	711	0.0727
	20.4	0.069	0.026	1956	722	0.0729
	33.8	0.062	0.062	1954	727	0.0726

D.2 Scenario 1 Velocity Profile Figures

The visual results for the 16 point velocity profile are displayed below. Each test is organized with baseline tests first and each consecutive row representing a different test orientation in the case of Scenario 1. A zero velocity boundary condition was applied for each profile due to the no slip condition. Since the velocity profile was simply a visualization tool, linear interpolation was used to fill in the contour plots. Intersecting gridlines represented points where actual data were taken. The rest of the data were interpretations of what would likely occur.

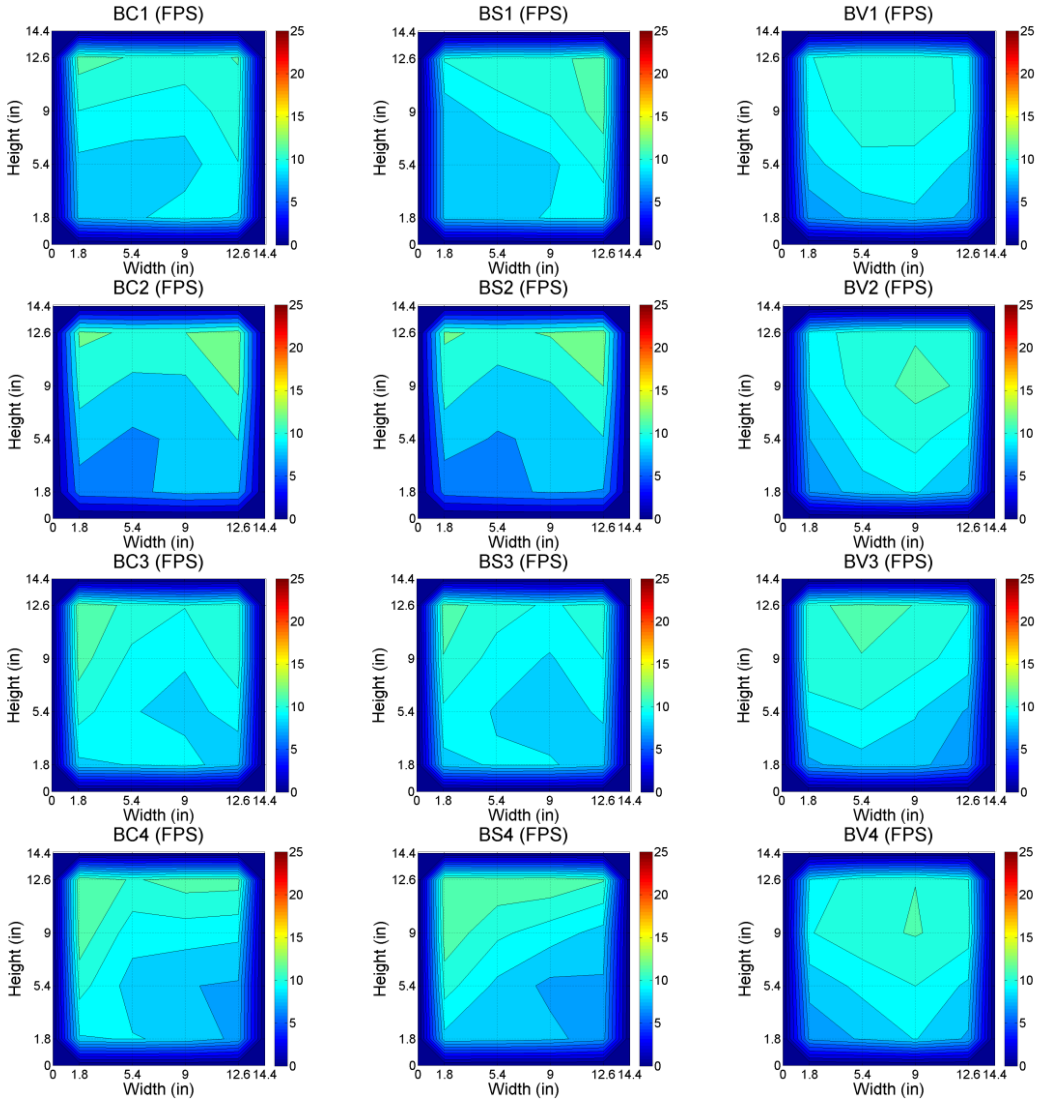

Figure 67: Velocity profiles for the baseline 2 ton unit.

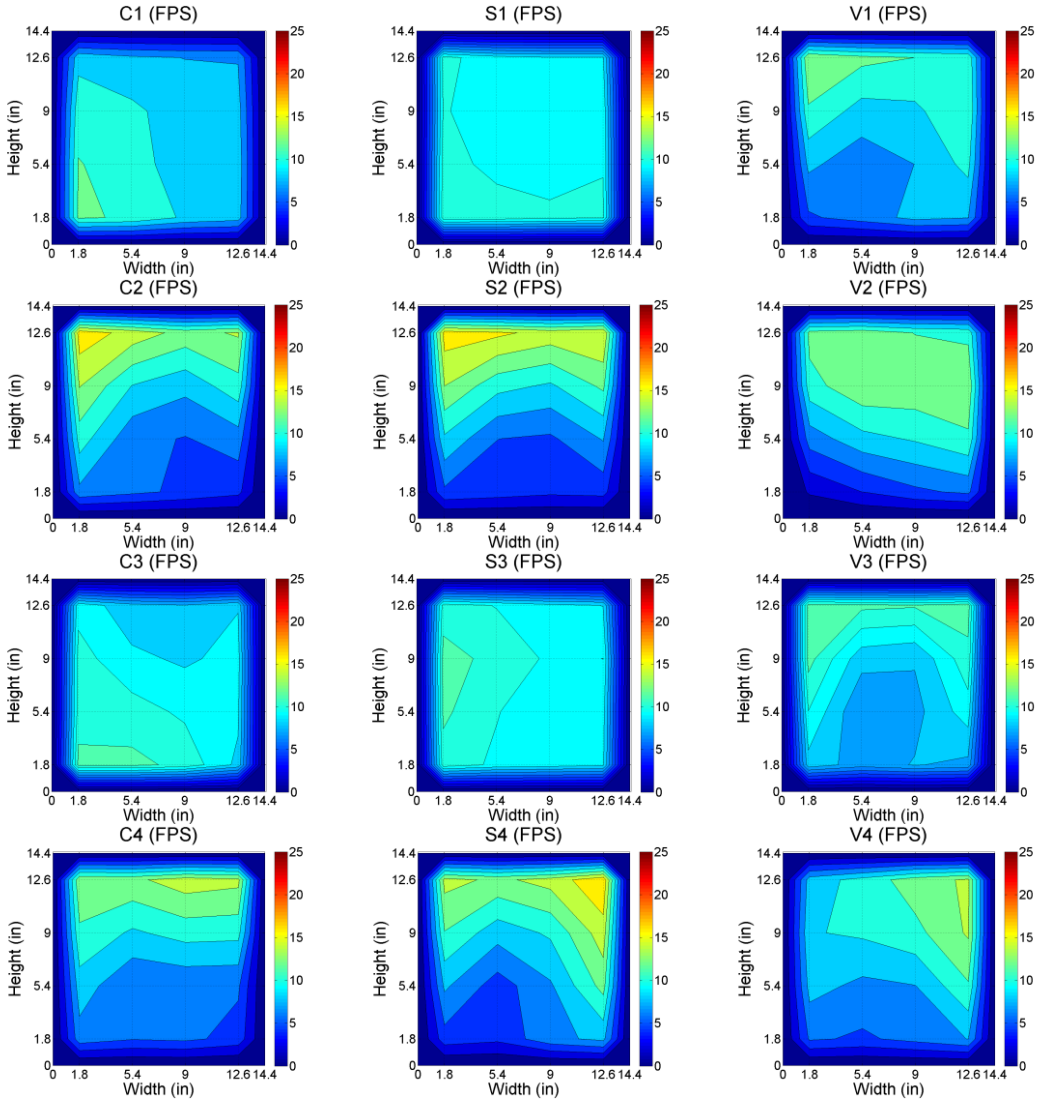

Figure 68: Velocity profiles for the 2 ton unit.

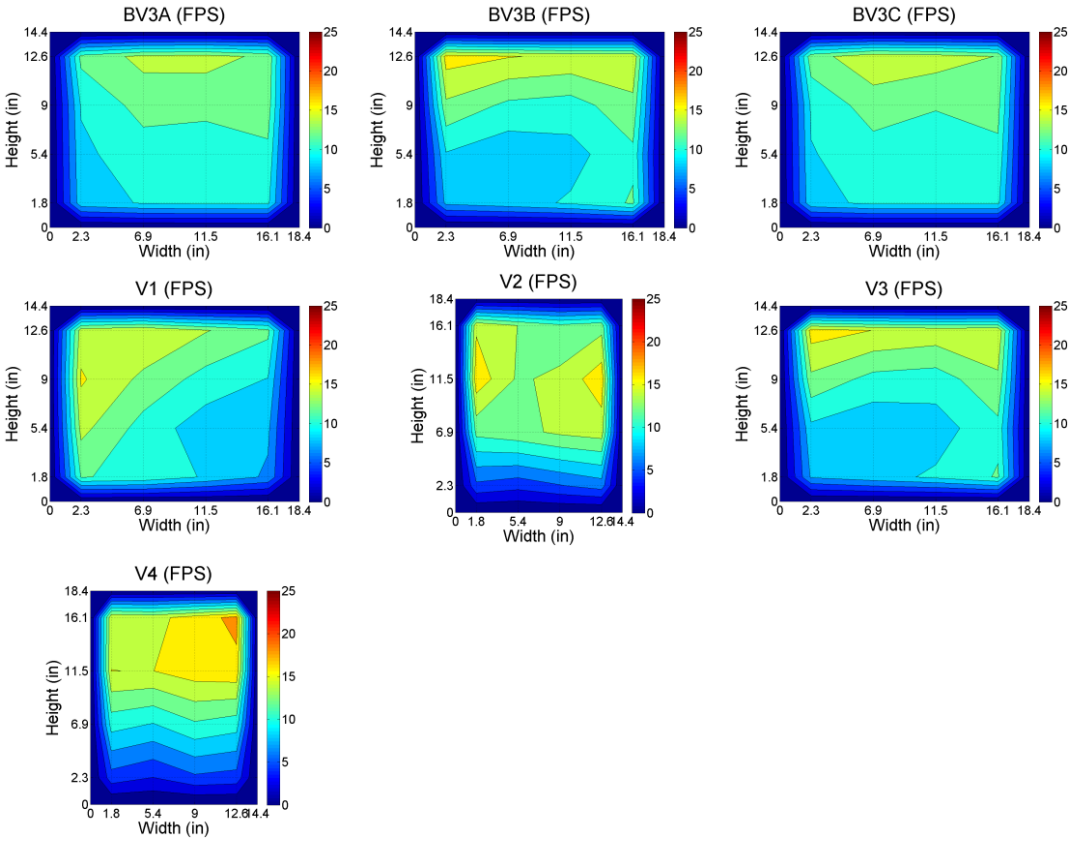

Figure 69: Velocity profiles for the 3 ton unit.

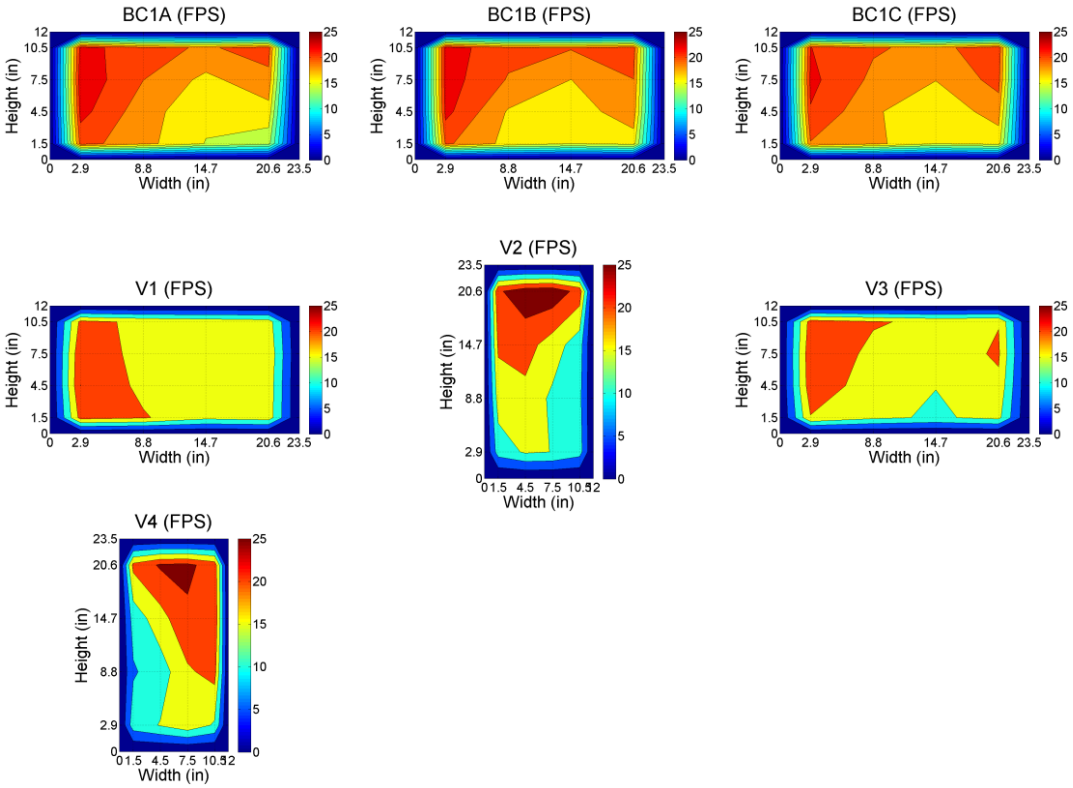

Figure 70: Velocity profiles for the 5 ton unit.

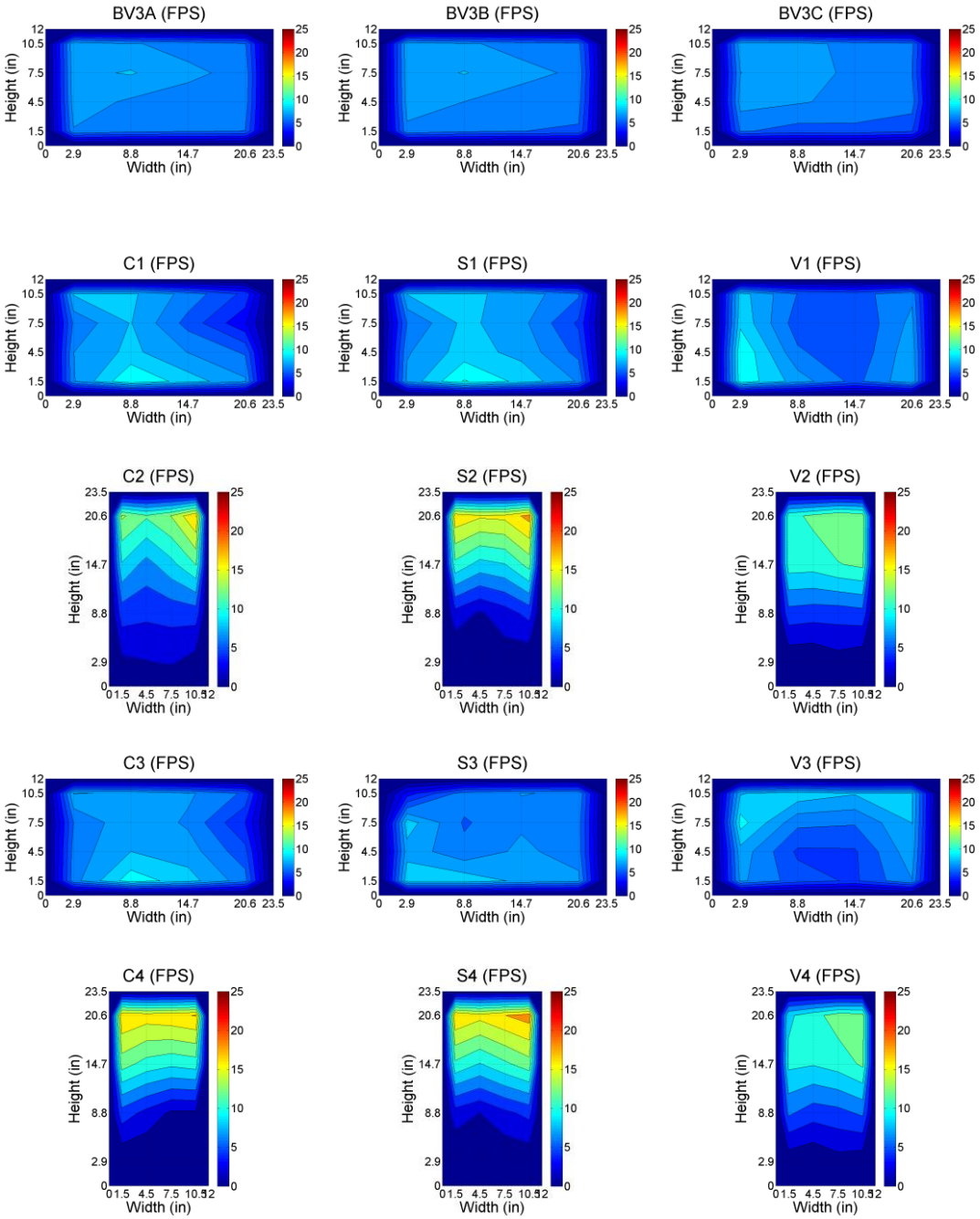

Figure 71: Velocity profile for the 2 ton unit with the oversized duct.

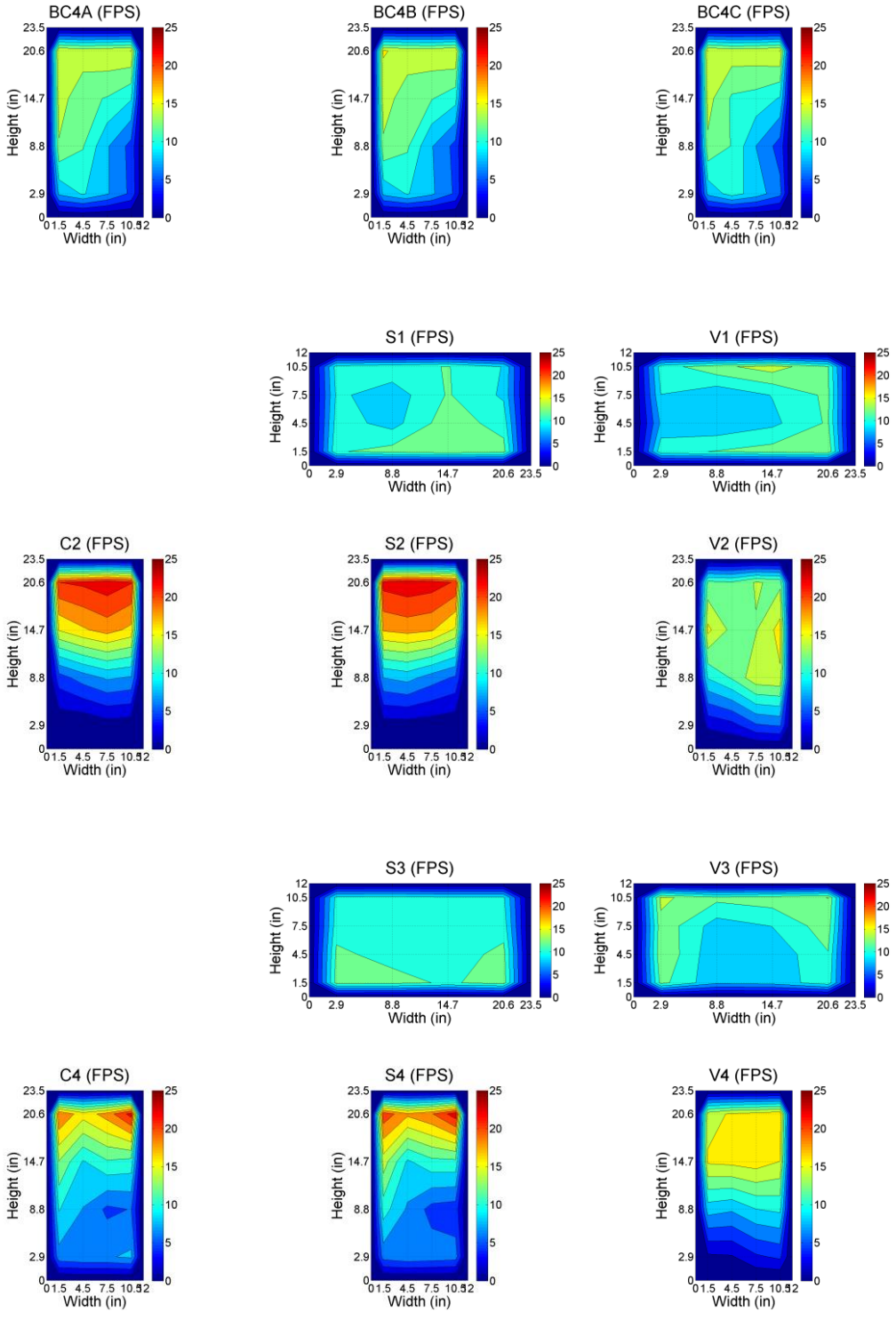

Figure 72: Velocity profiles for the 3 ton unit with the oversized duct.

D.3 Scenario 2 Velocity Profile Figures

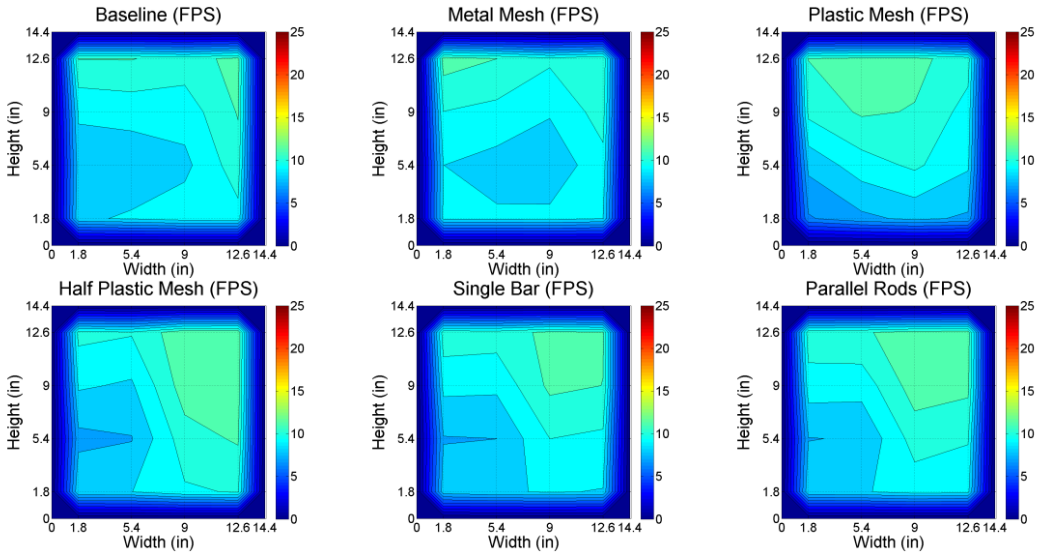

Figure 73: Scenario 2 velocity profiles for the 2 ton unit.

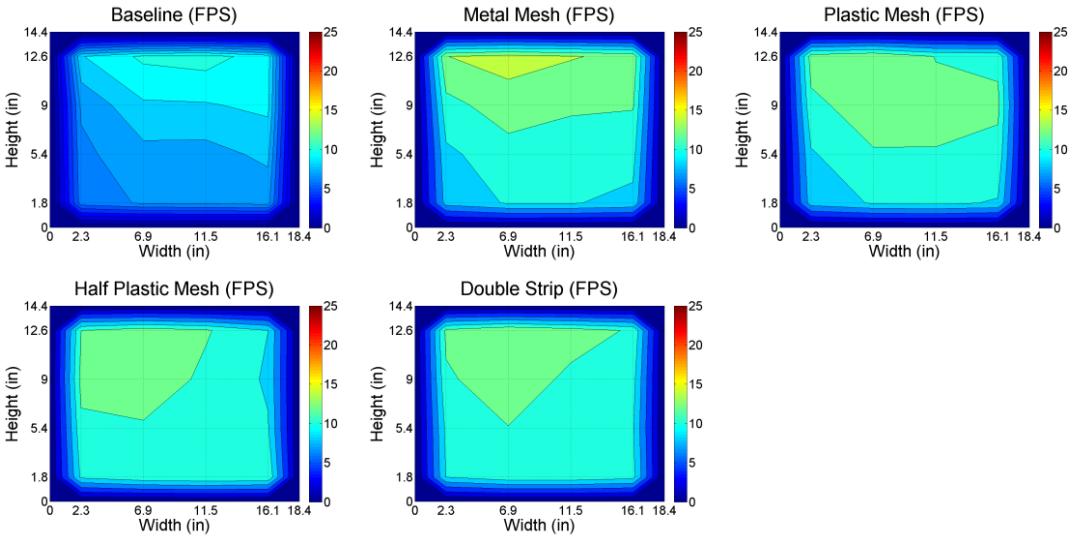

Figure 74: Scenario 2 velocity profiles for the 3 ton unit.

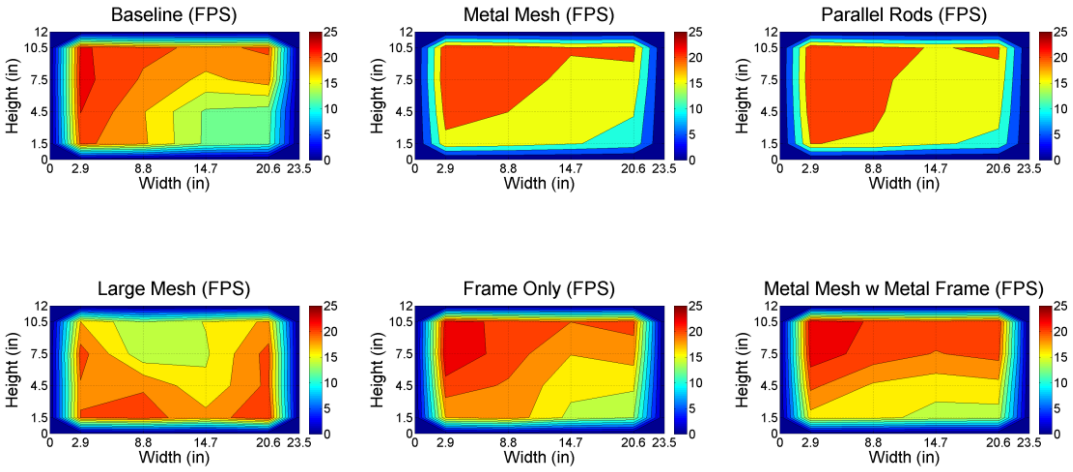

Figure 75: Scenario 2 velocity profiles for the 5 ton unit.

D.4 Set Pressure Velocity Profiles

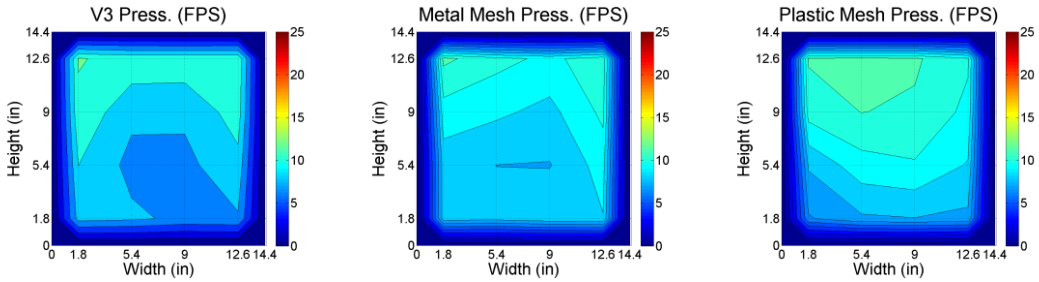

Figure 76: Set pressure velocity profiles for the 2 ton unit.

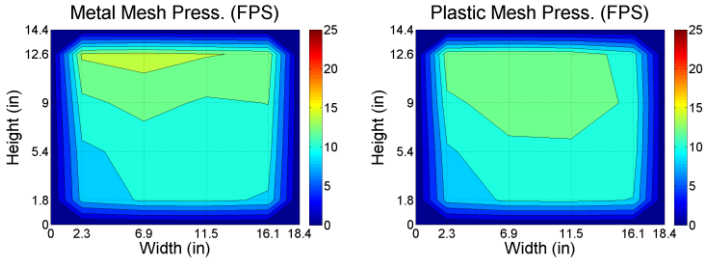

Figure 77: Set pressure velocity profiles for the 3 ton unit.

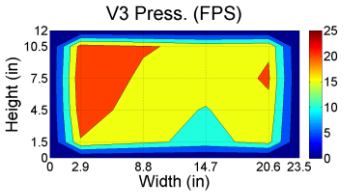

Figure 78: Set pressure velocity profile for the 5 ton unit.